THE ROLES OF MEMBRANE RAFTS IN CD32A MEDIATED PHAGOCYTOSIS

Timothy P. Tolentino[1]

Periasamy Selvaraj[2]

Cheng Zhu[3]

Department of Pediatrics, Division of Neonatology, Emory University School of Medicine, Atlanta, Georgia 30032

Department of Pathology and Laboratory Medicine, Emory University School of Medicine, Atlanta, Georgia 30032

Wallace H. Coulter Dept. of Biomedical Engineering, Georgia Institute of Technology, Atlanta, GA 30332-0535

Correspondence: Emory University School of Medicine, 2040 Ridgewood Dr. Atlanta, Georgia 30032. Tel: 404-727-3478; Fax: 404-727-9834;

TABLE OF ABBREVIATIONS

AOTF	-	Acoustic Optical Tuning filter
DRMs	-	Detergent resistant membranes
DIGs	-	Detergent-insoluble glycose sphingolipid-enriched membranes
DNP	-	Dinitrophenyl
DNP-Cap-PE	-	Dinitrophenylaminocaproyl Phosphatidylethanolamine
CD64	-	FcγRI
CD32	-	FcγRII
CD16	-	FcγRIII
FBS	-	Fetal bovine serum
FMM	-	Fluid Mosaic Model
FRAP	-	Fluorescence recovery after photobleaching
FCS2	-	Focht Chamber System 2
GSLB	-	Glass-supported lipid bilayer
GPI	-	Glycosylphosphatidylinositol
HBS	-	HEPES buffer saline solution
HA	-	Human albumin
HAS	-	Human serum albumin
IgG	-	Immunoglobulin G
IgSF	-	Immunoglobulin super family
Ig's	-	Immunoglobulins
ITAM	-	Immuno-receptor tyrosine-based activation motif
ITIM	-	Immuno-receptor tyrosine-based inhibition motif
IRM	-	Interference Refractive Microscopy
l_d	-	Liquid disordered
MβCD	-	Methyl-β-Cyclodextrin
MTOC	-	Microtubule organizing center
mAb	-	Monoclonal antibodies
NK	-	Natural killer
PTIC	-	Phosphatidylcholine
RBC	-	Red blood cells
TSA	-	Tris buffered saline

ABSTRACT

Membrane rafts are highly dynamic heterogeneous sterol- and sphingolipid-rich micro-domains on cell surfaces. They are generally believed to provide residency for cell surface molecules (e.g., adhesion and signaling molecules) and scaffolding to facilitate the functions of these molecules such as membrane trafficking, receptor transport, cell signaling, and endocytosis.

The governing, or overall hypothesis, for this project is that membrane rafts provide residency for FcγRIIA (CD32A) on K562 cells, and that by doing so they provide a platform from which FcRIIA initiate or carry out their functions, which include migration, signaling, phagocytic synapse formation, and internalization of IgG opsonized targets.

Using immuno-fluorescent laser scanning confocal microscopy and reflection interference microscopy (RIM), we studied the spatial and temporal distributions of membrane rafts and surface receptors, signaling molecules, and cell organelles during the formation of phagocytic contact areas. K562 cells, which naturally express CD32A, a cell surface receptor for the Fc portion of Immuno-globulin γ (IgG), was chosen as a model for neutrophils. An opsonized target was modeled using a glass supported lipid bilayer reconstituted with IgG. CD32A was found to cluster and co-localize with membrane rafts. Placing the K562 cells on the lipid bilayer triggered a process of contact area formation that includes binding between receptors and ligands, their recruitment to the contact area, a concurrent membrane raft movement to and concentration in the contact area, and transport of CD32A, IgG, and membrane rafts to the Golgi complex. Characterization of these processes was performed using agents known to disrupt detergent resistant membranes (DRMs), dissolve actin microfilaments, and inhibit myosin motor activity, which abolished the CD32A clusters and prevented the contact area formation.

The relevance to phagocytosis of contact area formation between K562 cells and lipid bilayers was demonstrated using micro-beads coated with a lipid bilayer reconstituted with IgG as the opsonized target instead of the glass supported planar lipid bilayer. Disruption of membrane rafts, salvation of the actin cytoskeleton, and inhibition of myosin II activity were found to inhibit phagocytosis.

These data suggest membrane rafts play several important roles in CD32A mediated phagocytosis including pre-clustering CD32A, transport of CD32A to the phagocytic cup, and transport of the opsonized target towards the Golgi complex. Here we have provided evidence that membrane rafts serve as platforms which are used to cluster CD32A and transport CD32A along the actin cytoskeleton to the site of phagocytic synapse formation thus allowing for the quick assembly of a phagocytic synapse.

BACKGROUND

Fcγ RIIA (CD32A)

The structures of FcγRs have been well characterized [2-5, 7-11], as have their signaling domains [7, 12-23]. CD32 isoforms are unique among the three classes of FcγRs in that their signaling domains are found within their cytosolic regions [18, 24,

25], whereas CD64 and CD16 associate with, but are segregated from, their signaling domains. CD32A is an activating receptor as it contains an immuno-receptor tyrosine-based activation motif (ITAM) in its cytoplasmic domain [12, 13, 15, 18] whereas CD32B is an inhibitory receptor containing an immuno-receptor tyrosine-based inhibition motif (ITIM [17]), also in it's cytoplasmic domain. ITAM becomes phosphorylated upon CD32A-IgG binding and initiates signaling which can activate antibody dependent phagocytosis [25-28]. This event sets off a signaling cascade which results in the initiation of the immune cells effector functions.

Membrane Rafts

Lipid rafts are highly dynamic heterogeneous cholesterol- and sphingolipid rich micro-domains on cell surfaces which compartmentalize cellular processes such as membrane trafficking, cell signaling, endocytosis, phagocytosis, lipid sorting [31, 33, 34, 37, 40, 45-49]. Due to the increasing body of evidence and certain discrepancies in ideas among scientists as to exactly what lipid rafts are, however, at the 1996 keystone symposium, researchers came together to resolve these issues. It was decided to rename lipid rafts to membrane rafts. These membrane rafts were defined as small (10 – 200 nm), heterogeneous, highly dynamic, sterol- and sphingolipid-enriched domains that compartmentalize cellular processes [50].

Despite the different opinions over the specifics of lipid rafts, there are a few generally accepted commonalities. Chief among these would be that membrane rafts are detergent-resistant; more specifically, they are not readily dissolved in non-ionic detergents[33, 34, 51]. This is a major defining characteristic of membrane rafts. This physical property led to the reference of certain micro-domains as detergent-resistant membranes (DRMs) and detergent-insoluble glycosphingolipid-enriched membranes (DIGs). Another commonality is that these micro-domains are highly concentrated in cholesterol and glycol-sphingolipids[33, 34, 37, 49, 50, 52, 53]. It is likely that the properties of sphingolipids are what gives these micro-domains their detergent-insolubility and causes them to be highly concentrated in cholesterol. The acyl chains of sphingolipids are saturated; therefore they have no double bonds which result in bends in acyl chains, as with the case of phospholipids. These long, straight acyl chains enable sphingolipids to pack together more tightly than phospholipids. Also, sphingolipid acyl chains tend to be longer than phospholipid acyl chains. Because their acyl chains are longer, sphingolipids have a larger non-polar region in which to pack cholesterol. Hence, thermodynamically, the packing of cholesterol within a sphingolipid bilayer is favored over the packing of cholesterol within a phospholipid bilayer. The sphingolipid bilayer alone still allows free movement throughout the bilayer in either direction. However, cholesterol molecules are inserted horizontally between the acyl chains, thus they restrict diffusion in one direction in their immediate vicinity. Furthermore, the sphingolipid bilayers preferentially sequester proteins that have a glycosylphosphatidylinositol (GPI) anchor[50, 52, 54-56]. These properties in this biochemical composition are the basis for the heterogeneity of these micro-domains, allowing them to exist as micro-domains that are separated from the phospholipid bilayer which forms the majority of a cell membrane.

These detergent-resistant cholesterol and sphingolipid-enriched micro-domains have been commonly associated with the actin cytoskeleton[57-61]. A great deal of research has shown that signaling which is initiated within these domains leads to a

reorganization and sometimes a polarization of the actin cytoskeleton[14, 54, 62]. Conversely, some cells also have the ability to send signals to rafts to activate them for a specific function, giving these cells a sort of inside-out signaling relationship with membrane rafts. It has also been shown that these domains can be transported along the actin cytoskeleton. The relationship between rafts and the cytoskeleton gives the cell a mechanism by which to control and use rafts. Clearly, there is a significant relationship between membrane rafts and the cell's actin cytoskeleton.

Because these structures are isolated from the phospholipid bilayers, anchored to the cytoskeleton, and can reorganize in response to cell signalling, they can serve as platforms for different cell processes. For example, membrane rafts can serve as platforms which enhance the process of cell signalling. It has been shown that signalling proteins involved in the process are either constitutively present in, or are recruited to, lipid rafts[15]. A cell can increase the local concentration of a surface receptor by using rafts to cluster the receptors. This increased concentration of receptors increases the probability of receptor-ligand binding, which can then initiate signalling. The transduction of a signal from outside the cell to inside is augmented by membrane rafts, as many signalling molecules have been shown to reside at the base of membrane rafts, making signal transduction more efficient[15].

Membrane rafts can also serve as platforms for pino- and endocytosis[63, 64]. On the membrane surface, rafts can cluster proteins required for engulfment of extra-cellular particles. Within the cytoplasm, a membrane raft's connection to the cytoskeleton in conjunction with the presence of motor proteins gives the cell a mechanism by which to internalize particles bound to the membrane surface receptors. Just as surface membrane rafts can be transported along the actin cytoskeleton to different locations on the cell membrane surface, within the cytosol a membrane raft can be transported along microtubule filaments[65, 66]. Like the saying "All roads lead to Rome", within the cell all microtubules lead to the microtubule organizing center (MTOC). Taking advantage of the ability to transport rafts along the actin cytoskeleton and along microtubules gives the cell a mechanism for the internalization of extra-cellular particles and also a path along which to do so. Membrane rafts have been shown to participate in FcγIIA–mediated phagocytosis.

By using rafts to cluster the appropriate receptors, adhesion molecules, and signaling molecules, the cell uses rafts as platforms for pre-assembled structures, which can be used to construct larger structures like the immunological synapse[66-69]. A plethora of evidence has been found suggesting that formation of immunological synapse requires membrane rafts. Within the construction of various types of immunological synapses, membrane rafts have been shown to sequester or exclude certain proteins, form boundaries at the edge of the synapse, and participate in signaling within the immunological synapse.

Membrane Rafts in CD32A Mediated Phagocytosis

One of the important functions commonly triggered by CD32A-IgG binding is phagocytosis of the opsonized target [15, 19, 21, 24]. In the past seven years attention has been focused on the relationship between membrane rafts and the cell surface receptors of immune cells. The results give a great deal of insight and it is clear that membrane rafts play significant roles in receptor signalling, receptor clustering, actin

cytoskeletal rearrangement, and phagocytic synapse formation. While the relationship between membrane rafts and Fc receptors have been the focus of many projects[70], very little investigation into the roles of membrane rafts in CD32A mediated phagocytosis have been done[71]. It is clear that Fc receptors in general associate with various types of immune cells to perform various functions. This research has provided the following findings not reported previously: 1) membrane rafts are required for proper signalling initiated by the FcR ligand binding; 2) they participate in Fc receptor clustering; 3) they have an inter-dependent relationship with the actin cytoskeleton, in that membrane rafts have been shown to depend on the actin cytoskeleton for migration, and the actin cytoskeleton requires the presence of membrane rafts to reorganize in response to the proper stimuli.

Unfortunately, virtually no attention has been focused on the relationship between membrane rafts and CD32A during CD32A mediated phagocytosis. Erick Garcia et al[72] investigated the association of CD32A with lipid rafts and found sound evidence CD32A-mediated responses can be modulated by lipid raft association of the ligated receptor.

Where different investigations have elucidated a role for membrane rafts in various parts of Fc receptor mediated phagocytosis, no project has yet followed the roles of membrane rafts through the entire process of phagocytosis. To date, there has been no investigation of the roles of membrane rafts in CD32A mediated phagocytosis.

While much can be inferred about membrane rafts / Fc receptor relationships, there is caveat in that these investigations have never used a human leukocyte cell line, which constitutively expresses the wild type form of Fcγ receptor, in which phagocytosis has been initiated by the binding of an Fcγ receptor to the Fc portion of IgG that is bound to an opsonized target. In addition, while previous data investigates spatial relationships they lack temporal information.

In this project we improve on previous research by: 1) Using K562 cells – a human leukocyte cell line that constitutively expresses the human form of WT CD32A, 2) Using lipid anchored IgG glass supported bilayer or an IgG opsonized micro-sphere to model opsonized targets, 3) Allow signaling to initiate as it does in vivo, by the binding of CD32A to the Fc portion of IgG bound to a target, rather than forcing signal initiation by using anti-CD32A IgG to crosslink CD32A receptors – a process which does not occur in vivo; 4) Monitoring the spatial relationship between membrane rafts, CD32A, and signaling molecules over time; 5) Investigating the role of membrane rafts through the entire process of CD32A mediated phagocytosis from receptor-ligand binding to the internalization, engulfment, of an opsonized target.

Experimental Model

In previous research, we modelled the formation of a contact area of an immunological synapse by placing a glass-supported lipid bilayer (GSLB) labelled with fluorescent ligand at the base of a flow chamber, into which we injected cells expressing the receptor for that ligand. When these cells are close enough to the labelled bilayer, receptor-ligand binding can begin. The depletion of free ligand creates a concentration gradient, which drives the diffusion of free ligand into the contact area[73, 74]. We used this model to investigate the roles of membrane rafts in CD32A mediated phagocytosis. We specifically modelled the formation of a *phagocytic* synapse between a CD32A expressing neutrophils and an opsonized target by replacing the opsonized target with a glass-supported phospholipid bilayer (GSLB) labelled with fluorescent or non-fluorescent IgG. We then replaced CD32A expressing neutrophils with K562 cells. K562 cells constitutively express CD32A.

Figure 1 illustrates the process of contact area formation between a CD32A expressing K562 cell and an anti-dnp IgG labeled GSLB. Panel A shows a K562 floating above the GSLB. In panel B the cell comes within binding proximity, and receptor-ligand bonds begin to form. This creates a concentration gradient of free IgG on the bilayer, since the receptor-ligand complex is considered a unique species. This concentration gradient drives diffusion of free IgG into the region of contact as seen in panel C. Accumulation of receptors and ligands into the area of contact continues until the system reaches a dynamic equilibrium.

By fluorescently labeling the appropriate protein, molecules, or structure, we were able to monitor the spatial relationship between membrane rafts, CD32A, signaling molecules, and the Golgi complex.

MATERIALS AND METHODS

Antibodies, Protein and Cells

Anti-CD32 monoclonal antibody (mAb) IV.3, purified from hybridoma (HB-217) culture supernatant, was provided by Dr. P. Selvaraj (Emory University School of Medicine). Alexa 488 conjugated rabbit anti-dinitrophenyl (DNP) IgG, non-conjugated rabbit anti-DNP IgG, Alexa 488 conjugated anti-mouse IgG, Alexa 555 and 633 conjugated cholera toxin subunit B, Alexa 488 donkey anti-goat, Alexa 647 donkey a-mouse, BODIPY® TR C5-ceramide were obtained from Molecular Probes (Eugene, OR). Goat anti-SYK IgG and mouse anti-PO4-Y were obtained from Upstate Cell Signaling (Charlottesville, VA).

K562 cells constitutively expressing $CD32A^{TM}$ and CHO cells transfected to express $CD32^{GPI}$ or $CD32A^{TM}$ were a kind gift of Dr. P. Selvaraj.

Cells were cultured in RPMI/10% fetal bovine serum (FBS) according to standard practices.

Colocalization of CD32A and Membrane Rafts in Cells Fixed after Labeling

Live $CD32A^{TM}$ expressing K562 cells, $CD32A^{TM}$ CHO cells, and $CD32A^{GPI}$ cells (1×10^6/ml) were fluorescently labeled by incubation in cold (4°) FACS buffer (PBS with 1% bovine serum albumin and 0.05% NaN3) with primary antibody mouse anti-CD32A (IV.3-Fab) IgG (5 μg/ml) for 30 minutes. Afterwards, the cells were washed in

50 ml cold FACS buffer. Next, the cells were incubated for 30 minutes in cold FACS buffer with secondary antibody mouse Alexa Fluor 488 goat-anti-mouse IgG (10 μg/ml). Next the cells were washed twice and re-suspended in cold FACS buffer (1 x 10^6/ml) with 5μg Alexa Fluor 647 cholera toxin subunit B conjugate and incubated at 4°C for ten minutes. Next the cells were washed twice with cold FACS buffer and fixed in a 4% formalin solution for ten minutes. After fixation, the cells were washed in PBS and then imaged with laser-scanning confocal microscopy.

Colocalization of CD32A and Membrane Rafts in Cells Labeled after Fixation

Live CD32A^{TM} expressing K562 cells, CD32A^{TM} CHO cells, and CD32A^{GPI} CHO cells (1 x 10^6/ml) were fixed by incubation in a cold 4% formalin solution for ten minutes. After the cells were washed once in 50 ml cold PBS, they were fluorescently labeled by incubation cold FACS buffer with primary antibody mouse anti-CD32A (IV.3-Fab) IgG (5 μg/ml) for 30 minutes. Afterwards, the cells washed in 50 ml cold FACS buffer. Next, the cells were incubated for 30 minutes in cold FACS buffer with secondary antibody Alexa Fluor 488 goat-anti-mouse IgG (10 μg/ml). Next the cells were washed twice and re-suspended in cold FACS buffer (1 x 10^6/ml) with 5μg Alexa Fluor 647 cholera toxin subunit B conjugate and incubated at 4°C for ten minutes. Next the cells were washed twice with PBS and then imaged with laser-scanning confocal microscopy.

Preparation of Lipid Bilayers Reconstituted with Ligands

Liposomes of Dinitrophenylaminocaproyl Phosphatidylethanolamine (DNP-Cap-PE) or L-a-Phosphatidylcholine (PTIC) were prepared via continuous extrusion of a 4.0 mM lipid solution containing PTIC solution with or without 0.2 mM DNP-Cap PE. PTIC and DNP-Cap-PE were purchased from Avanti-Polar Lipids (Alabaster, AL). Both lipids were dissolved in chloroform at a concentration of 10 mg/ml. PTIC alone or combined with DNP-Cap-PE in a 19/1 mixture (by mole fraction), and then dried under vacuum for 1 h. PTIC or DNP-liposomes were formed when the lipid was dissolved in 25 mM Tris, 150 mM NaCl, 0.02% NaN_3 to a concentration of 4.0 mM, and then extruded at 55°C through a 1μm filter. The resultant liposome were a 10x concentration and diluted to 1x with a 25 mM Tris, 150 mM NaCl, 0.02% NaN_3 solution (TSA).

Lipid bilayers were formed in a Focht Chamber System 2 (FCS2) from Bioptechs (Butler, PA) on glass cover-slips. The cover-slips were previously cleaned rigorously by boiling in piranha solution (70% reagent grade sulphuric acid, 30% concentrated (30%) hydrogen peroxide) for 1 h at 90°C followed by thorough rinses with de-ionized water and blown dry with argon gas. A 2-μl drop of liposome suspension was sandwiched between the micro-aqueduct slide and a 40 mm diameter circular cover-slip, separated by a 0.25-mm spacer. The liposomes fused on the hydrophilic glass surface to form a continuous bilayer [2]. The flow chamber was connected with two syringes; one filled with TSA containing 1% BSA and the other with HEPES buffer saline solution (HBS) containing 1% human serum albumin (HSA). After 15 minutes of liposome incubation on the cover slip, excess liposome solution was washed off by injecting 3 ml TSA/1% BSA. The solution was left for 15 minutes to block non-specific binding, after which the chamber was washed with 3 ml HBS/1% HSA. One ml of Alexa 488 rabbit anti-DNP

IgG (10 μg/ml) was injected into the flow chamber for incubation for 1 hour at room temperature, and then washed off with 3 ml HBS/1% HSA.

Colocalization after Cholesterol Extraction with MβCD

K562 cells (5 x 10^6/ml) were incubated in activation buffer (PBS + 5mM HEPES, pH 7.2) containing varying concentrations of MβCD (0.01-10mM) for 30 minutes at 37^0 C. The cells were immediately washed twice, checked for viability with trypan blue exclusion, and then fluorescently labeled as described in the Colocalization of CD32A and Membrane Rafts section. After two washes in cold PBS the cells were fixed by incubation in a cold 4% formalin solution for ten minutes. Z-stack images where then captured using laser-scanning florescence microscopy.

Contact Area Formation after Cholesterol Extraction with MβCD

K562 cells (5 x 10^6/ml) were incubated in activation buffer (PBS + 5mM HEPES, pH 7.2) containing varying concentrations of MβCD (0.01-10mM) for 30 minutes at 37^0 C. The cells were then washed twice, and fluorescently stained by incubation in cold FACS buffer with 5μg Alexa Fluor 647 cholera toxin subunit B conjugate and incubated at 4°C for ten minutes. The cells were immediately washed twice, checked for viability with trypan blue exclusion, and then used to form contact areas as previously described.

Colocalization after Cholesterol Oxidation

K562 cells (1 x 10^6/ml) were incubated at 4^0C for 30 minutes in PBS containing varying concentrations of cholesterol oxidase (1.4 units). The cells were immediately washed twice, checked for viability with trypan blue exclusion, and then fluorescently labeled as described in the Colocalization of CD32A and Membrane Rafts section.

Contact Area Formation after Cholesterol Oxidation

K562 cells (1 x 10^6/ml) were incubated at 4^0C for 30 minutes in PBS containing varying concentrations of cholesterol oxidase (1.4-0.014 uM). The cells were immediately washed twice, checked for viability with trypan blue exclusion, and then used to form contact areas as previously described.

Contact Area Formation after Sphingomyelin Hydrolysis

K562 cells (1 x 10^6/ml) were treated incubated at 4^0C for 30 minutes in PBS containing varying concentrations of sphingomyelinase (1-0.001 units). The cells were immediately washed twice, checked for viability with trypan blue exclusion, and then fluorescently labeled as described in the Colocalization of CD32A and Membrane Rafts section.

Disruption of Actin-cytoskeleton by Latrunculin A

Live K562 cells (1 x 10^6/ml) were incubated at 37^0C for 30 minutes in RPMI/10% FBS containing varying concentrations of Latrunculin A (0.01-100 μM). The cells were immediately washed twice in cold FACS buffer, checked for viability with trypan blue exclusion, re-suspended in 1 ml HBS/1% HSA containing Latrunculin A (0.01-100 μM), and then used to form contact areas as previously described.

Inhibition of Myosin II by Blebbistatin

K562 cells (1 x 10^6/ml) were incubated at 37^0C for 30 minutes in RPMI/10% FBS containing Blebbistatin (100 μM). The cells were immediately washed twice, checked for viability with trypan blue exclusion, re-suspended in 1 ml HBS/1% HSA, and then injected into a FCS2 flow chamber to form contact areas as previously described.

Signaling via ITAM

K562 cells were washed twice in FACS buffer, re-suspended in 1 ml HBS/1% HSA (10 x 10^6/ml), then injected into the FCS2 chamber and kept at 37°C, which was then mounted on a Zeiss LSM 500 confocal microscope. At 3, 9, 30, and 60 minutes, K562 cells were fixed with 4% formalin solution for 10 minutes. After two washes with HBS, the cells were fluorescently labeled.

At the 3 and 9 minute intervals, cells with strong contact areas to remain in the flow chamber were incubated in HBS with 10 μg/ml donkey anti-SYK IgG and 10 μg/ml mouse anti-PO4-Y. After washing, the cells were incubated in HBS with 10 μg/ml FITC anti-donkey and 10 μg/ ml Alexa 647 anti-mouse IgG.

For the 30 and 60 minute intervals, the cells were incubated at 23°C for 30 minutes in HBS with 10 μg/ml donkey anti-SYK IgG. After washing, the cells were incubated at 23°C for 30 minutes in HBS with 10 μg/ml FITC anti-donkey IgG. Thirty minutes later the chamber was washed 1 ml TBS and images were collected.

RESULTS

Colocalization of CD32A with membrane rafts

As the first step towards testing our overall hypothesis, we asked the following questions: 1) was CD32A expressed uniformly or formed clusters on the cell surface? 2) if CD32A did exist in clusters on the cell membrane, did those clusters associate with membrane rafts, and 3) if the CD32A clusters did associate with membrane rafts, did the disruption of membrane rafts also disperse CD32A?

For colocalization studies, three cell types were used: K562 cells constitutively expressing CD32A and CHO cells transfected to express either wild-type CD32A, or a chimeric molecule that fuses the extra-cellular domain of CD32A with a GPI anchor ($CD32A^{GPI}$). Comparison between results obtained using K562 cells and CD32A-expressing CHO cells would allow us to examine whether the observations are cell-specific or not. Comparison between results obtained using CD32A-expressing CHO cells and $CD32A^{GPI}$-expressing CHO cells would allow us to examine whether the observations depend on the membrane anchor of CD32A. The latter comparison is of interest because GPI-anchored proteins are known to concentrate in membrane rafts.

Live CD32A-expressing K562 cells (1 x 10^6/ml) were fluorescently labeled by incubation cold FACS buffer with primary antibody mouse anti-CD32A (IV.3-**Fab**) IgG (5 μg/ml) for 30 minutes. Afterwards, the cells washed in 50 ml cold FACS buffer and then incubated for 30 minutes in cold FACS buffer with secondary antibody Alexa Fluor 488 goat-anti-mouse IgG (10 μg/ml). Next, the cells were washed twice and re-suspended in cold FACS buffer (1 x 10^6/ml) with 5μg Alexa Fluor 647 cholera toxin subunit B conjugate and incubated at 4°C for ten minutes. After two washes in cold facs

buffer, the cells were fixed in a 4% formalin solution for ten minutes. After fixation, the cells were washed in PBS and then imaged with laser-scanning confocal microscopy. This experiment was run three times, and three z-stack series of fluorescent images were acquired from each experiment.

The first row of **Figure 2** contains a z-stack series captured from a K562 cell fluorescently stained for CD32A (pseudo colored green) and membrane rafts (pseudo colored red). The images begin at the bottom of the cell at 0.0 μm and go upwards along the z-axis through the cell to 15.5 μm. The individual panels represent the fluorescence from a single plane. Fluorescence from the membrane raft marker Alexa 647 was pseudo colored red; the fluorescence from the CD32A marker Alexa Fluor 488 goat anti-mouse was pseudo colored green. The yellow spots or patches seen on nearly every panel results from the merging of the two fluorophores that happen to be in the same space, thus indicating colocalization. The fluorophores are located at points on the cell surface; hence, the fluorescence of the individual planes should follow the same spatial pattern as a fluorescently labeled sphere. On the bottom plane only small areas of fluorescence can be seen. However, going upwards through the cell the areas of fluorescence increase in size and form a ring. The rings continue to grow in diameter until they reach a maximum at the center of the cell, after which they begin decreasing until there is only a small spot of fluorescence at the top of the cell.

The second row of **Figure 2** shows the profile view of a 3D image made by reconstructing the z-stack images. In the left and middle columns of row two, the positions of CD32A and membrane rafts are indicated by the green and red fluorescence, respectively. These images confirm what is seen in the z-stacks. The fluorophores form a spherical pattern as expected, and the merged image shows only red and yellow fluorescence. The absence of green in the merged image suggests CD32A is completely colocalized with membrane rafts.

Both CD32A and the membrane rafts appear to exist in clusters rather than being uniformly distributed. In addition, there appears to be a much more extensive staining for membrane rafts than for CD32A, suggesting the presence of more membrane rafts than CD32A.

Colocalization of CD32A with membrane rafts after fixation of K562 Cells

When labeling a cell with fluorophores, antibodies, or protein, there exists the possibility of the labeling molecule inducing a change in cell properties, phenotype, or structural rearrangement. Since cholera toxin is pentavalent, it is possible that labeling of cell membrane GM1 with cholera toxin could lead to clustering of GM1, which in turn could lead to clustering of membrane raft, or membrane raft formation altogether. Therefore, it was necessary to answer the question "Does cholera toxin B induce raft formation upon binding cell surface sphingolipids?"

To answer this question, the first set of experiments was repeated with one difference: the cells were fixed before being fluorescently labeled. The same microscope and laser settings from the previous experiment were used for each image acquisition.

Figure 3 shows a z-stack series (top row) and the profile view of an image made from its reconstruction (bottom row). The images begin at the bottom of the cell at 0.0 μm and go upwards through the cell to 14.5 μm. Once again, lone green fluorescence, representing the location of CD32A, is absent from every panel while red fluorescence,

representing the location of membrane rafts, is present in every panel. The yellow spots indicating colocalization are seen on nearly every panel. These panels show the same spatial relationship that is seen from cells which were fluorescently labeled prior to fixation.

Cell membranes are known to become rigid during fixation, making cross-linking by the binding of antibodies or any other multi-valent molecules impossible. The cells used in this set of experiments were fixed prior to being labeled with cholera toxin B or antibodies. The data here gives clear evidence that the size, location, and even the existence of either is unaffected by the binding of cholera toxin B to GM1 on sphingolipids or the by the binding of IV.3-Fab to CD32A.

Colocalization of CD32A and membrane rafts on CHO-CD32A^{TM} / CHO-CD32A^{GPI}

The previous protocol was repeated using CHO-CD32A^{TM}, and CHO-CD32A^{GPI} cells. These experiments were repeated three times, with three images being acquired for each experiment.

Figure 4 and **Figure** 5 show z-stack images (top row) and reconstructions of the z-stacks (bottom row) from CHO-CD32A^{TM}, and CHO-CD32A^{GPI} expressing-cells respectively.

These data show the same spatial patterns as the first two data sets, once again suggesting complete colocalization between CD32A and membrane rafts. They also suggest that these observations are not cell specific, as K562-CD32A^{TM} and CHO-CD32A^{TM} cells have the same patterns of fluorescence. Furthermore, the data suggest that the fluorescent patterns are not a function of the receptors anchor type as CHO-CD32A^{TM} and CHO-CD32A^{GPI} show identical patterns.

Colocalization of CD32A with membrane rafts after cholesterol extraction

While the previous data does suggest colocalization between the CD32A clusters and the membrane rafts, it must be noted that the strength of these data is limited in that the fluorophores are much smaller (~nm) than the spatial resolution of the microscope (hundreds of nanometers). Thus, while the overlapping of the green and red fluorescence *must* occur if there is colocalization, the mere *appearance* of colocalization is not enough to conclude that it actually exists. Therefore, to strengthen the suggestion of colocalization, MβCD was used to disrupt membrane raft structures via extraction of cholesterol.

K562 cells (5 x 10^6/ml) were incubated in activation buffer pH 7.2 (PBS + 5mM HEPES) for 30 minutes at 37^0 C containing varying concentrations of MβCD (0.01-10mM). The cells were immediately washed twice, checked for viability with trypan blue exclusion, fixed, and then fluorescently stained as previously described. The same microscope and laser settings as the four previous experiments were used. This experiment was repeated three times, with three images being acquired for each experiment.

The top row of **Figure 6** shows a z-stack series of images from a K562 cell treated with MβCD prior to fixation and fluorescent labeling. The images begin at the bottom of the cell where Z = 0.0 μm (top left corner) and go upwards through the cell to Z = 12.0 μm. Fluorescence from the membrane raft marker Alexa 647cholera toxin B

was pseudo colored red, and fluorescence from Alexa Fluor 488 goat anti-mouse / mouse anti-human CD32A was pseudo colored green. In the z-stack, yellow spots or patches indicating colocalization are present only at 3.0 and 4.0 μm and even then only in a very small area.. A quick inspection of the image reveals an almost complete absence of CD32A clusters. While red fluorescence is present in every panel, indicating the presence of sphingomyelin over the entire cell surface, it appears more dispersed than clustered.

These data suggest that the density of CD32A is much lower, and that membrane rafts have been disrupted. The decrease in CD32A density, although unexpected, could have resulted from CD32A being extracted from the cell surface along with the cholesterol molecules. The disruption or dispersal of membrane rafts is expected to occur when cholesterol is extracted from the cell surface.

Colocalization of CD32A with membrane rafts after cholesterol oxidation

The caveat to using MβCD is that the extraction of cholesterol via MβCD is not limited to the cell surface but can also occur in any part of the cell, an action which could affect any number of cell processes. To overcome this limitation, cholesterol oxidase was used to oxidize cholesterol to cholesterone. This oxidation results in a change in structure as the alcohol group, a polar molecule, becomes a carbonyl group, a non-polar molecule. Being polar, the carbonyl group must be hidden within the non-polar region of the cell membrane, which results in disruption of membrane rafts. There are four advantages of using cholesterol oxidase instead of MβCD: 1) only cholesterol present on the cell surface is affected; 2) the composition of the cell membrane does not change as no cholesterol is extracted; 3) since cholesterol is not extracted, there is little chance of CD32A being extracted; 4) the number of cell processes which could be affected are reduced significantly.

K562 cells (1 x 10^6/ml) cells were incubated at 37ºC in standard culture media, RPMI with 10% FBS, that contained 1.4 units/ml cholesterol oxidase. After washing and fixation, the cells were fluorescently labeled as previously described. This experiment was repeated three times, with two images being acquired for each experiment (n=6).

The top row of **Figure 7** shows z-stack images of a cell that is representative of the data set. The images begin at the bottom of the cell at 0.0 μm and go upwards through the cell to 14.0 μm. Fluorescence from the membrane raft marker Alexa 647 was pseudo colored red, and fluorescence from Alexa Fluor 488 goat anti-mouse / IV.3 Fab was pseudo colored green. There are four obvious differences from the positive control cell: 1) sphingomyelin appears to be ubiquitously dispersed; 2) CD32A is present in nearly every panel; 3) CD32A appears to be dispersed rather than clustered; 4) the absence of yellow, which of course suggests the absence of colocalization.

These results suggest that oxidation of cell surface cholesterol results in disruption of membrane rafts and CD32A.

Colocalization of CD32A with membrane rafts during contact area formation

What are the functional consequences of CD32A residing in membrane microdomains? Do membrane rafts play a role in CD32A mediated cellular functions? To address these questions, we studied the spatial relationship between CD32A and

membrane rafts in CD32A-mediated cellular processes, during which CD32A on the cell membrane is expected to be redistributed. Since a major function of CD32A is the binding of IgG-opsonized surfaces, we hypothesize that CD32A colocalizes with membrane rafts not only prior to but also *during* ligand binding and contact area formation. It would be difficult to fluorescently label CD32A prior to ligand binding without affecting its ability to bind ligand or transduce signals. Previous studies have shown that it is possible to monitor receptor binding to fluorescent ligand on a glass supported lipid bilayer (GSLB). We have shown this to be the case for Fcγ receptors CD16A, CD16B and CD32A, expressed on CHO and K562 cells, binding fluorescently labeled IgG bound to antigenic phospholipids in a glass supported lipid bilayer[73, 74]. It has been observed that after placing the cell on the bilayer, FcγR interacts with IgG Fc to initiate randomly isolated contact points of close proximity (observed as dark spots via IRM) where IgG ligands are concentrated (observed as fluorescent spots in confocal microscopy) due to the formation of FcγR-IgG bonds. Over time, these contact points not only increase in size and in number but also fuse together to form a large contact area with highly concentrated IgG. Given that IgG is the only ligand on the GSLB and that the receptor-ligand stoichiometry is 1:1, it is reasonable to assume the number of receptors within the contact area between the receptor-expressing cell and the ligand-coated GSLB is proportionate to the number of ligand within the contact area. The ligand concentration within the contact area is determined from the measured fluorescent intensity, where proportionality constant has been determined from a calibration curve of fluorescent intensity versus known ligand concentrations. It is important to note the lack of any other ligand for said receptor. Thus accumulation of ligand within the contact area suggests receptor accumulation within the contact area as well. This process of contact area formation is of interest -- such a contact area may be regarded as an immunological synapse-link functional structure capable of signaling for phagocytosis [21, 79-81].

Receptor-ligand binding creates a concentration gradient of free ligand on the bilayer. This gradient then drives diffusion of IgG into the area of contact. This accumulation of IgG ligand within the contact area drives receptor ligand kinetics forward. This process continues until receptor-ligand binding has reached a dynamic equilibrium. Since the IgG ligand is fluorescently labeled, and fluorescence intensity is proportional to the concentration of fluorophores, the accumulation of IgG results in a proportional increase in fluorescence intensity. Simply stated, the increase in fluorescence intensity indicates an increase in IgG concentration.

The discussion in the preceding paragraph indicates that a coupled kinetics-diffusion process provides a physical mechanism for the accumulation of a high concentration of IgG in the contact area. Increases in bound IgG concentration within the contact area require a parallel increase in the concentration of CD32A in the same contact area on the cell surface above the bilayer because these IgG were bound to CD32A. Is the same physical mechanism of coupled kinetics-diffusion responsible for the accumulation of CD32A, or is there a different biological mechanism that drives their accumulation in the contact area? To answer this question, let's first address a related question: regardless of whether the coupled kinetics-diffusion process was responsible for the accumulation of CD32A, would the concentration of CD32A also lead to accumulation of membrane rafts, or would it result in the departure of CD32A from their membrane raft's residence to the contact area?

To answer these questions, we investigated the effect of raft disruption on CD32A functions by monitoring contact area formation between an anti-dnp IgG-labeled glass-supported lipid bilayer (GSLB) and CD32A-expressing K562 cells with and without chemical treatments that disrupted membrane rafts, disrupted the actin cytoskeleton, or impaired the motor protein Myosin II.

Membrane rafts on live K562 cells (1×10^6/ml) were fluorescently stained with Alexa 647 cholera toxin B, as previously described, and then injected into an FCS2 flow chamber, the bottom surface of which is a glass supported lipid bilayer labeled with Alexa Fluor 488 rabbit-anti-dnp IgG. The chamber was maintained at 37°C and placed on a Zeiss LSM 510 confocal microscope. Contact area formation between the cell and the glass supported lipid bilayer, formed by the binding of the cell surface receptor CD32A and phospholipid-anchored anti-dnp IgG, was monitored over a range of time points covering both the transient phase of the process and steady-state in which receptor-ligand binding has reached equilibrium.

Fluorescence recovery after photobleaching (FRAP) was used to test the viability of the glass-supported lipid bilayer before cells were injected. The bilayer's quality was assessed by fluorescence microscopy and conventional FRAP; uniform fluorescence intensity and diffusion coefficients of ~ $1\mu m^2/s$ were used as the criteria for a good bilayer. For all bilayer FRAPs, a circular region with a radius of 5 μm was bleached to below 20% initial fluorescence intensity; afterwards, fluorescence recovery was monitored for one minute. Only bilayers with at least 90% recovery were used for contact area formation experiments.

The top row of **Figure 8** shows a z-stack series of a K562 cell three minutes into contact area formation. The images begin at the bottom of the cell at 0.0 μm and go upwards through the cell to 11.25 μm. Fluorescence from the membrane raft marker Alexa 647 was pseudo colored red, and fluorescence from Alexa Fluor 488 goat anti-mouse / IV.3 Fab was pseudo colored green.

The first panel of the z-stack series, Z = 0.0 μm, shows an area of intense green fluorescence indicating the accumulation of Alexa 488 anti-dnp IgG within the initial area of contact. The first panel also shows the presence of red fluorescence, indicating the presence of membrane rafts within the same region. This is significant in that it suggests the presence of membrane rafts within the contact area at three minutes. Most of the rafts still appear on the surface of the cell. There is, however, a slight but noticeable decrease at the top of the cell.

As previously stated, the area of intense green fluorescence in the plane at 0.0 μm is the result of IgG accumulation within the contact area. It should be noted that the presence of IgG suggests the presence of CD32A, as CD32A is the only cell surface protein present which is a receptor for the Fc portion of IgG.

Row II of **Figure 9** shows a profile view of an image made by reconstruction of the z-stack series. The image reflects what is found in the z-stack series in four ways: 1) there is an intense area of green fluorescence whose size correlates well with that found in the first plane of the z-stack, 2) membrane rafts appear to cover most of the cell's surface, 3) the concentration of membrane rafts is significantly reduced in the top plane of the cell, 4) membrane rafts are present within the contact area. In the profile view, the cell appears to be leaning to the right and gives the impression that the area of depleted rafts is more or less on one side of the cell. This leaning of the cell was caused by sheer

force, resulting from the injection of formalin, applied over the surface of the cell. At the three minute time point, the phagocytic synapse has not yet acquired the rigidity, size, or strength necessary to stabilize the cells against sheer force created by the formalin injection. In row three of **Figure 9**, the cell image is rotated back to an upright position. It then becomes easier to see the decreased raft density at the top of the cell.

This contact area formation experiment was repeated under identical conditions with various times of fixation, including 9, 12, 15, 45, and 60 minutes.

Figure 10 shows a z-stack series from a K562 cell imaged 9 minutes into contact area formation. Contact areas imaged at 9 and 12 minutes showed slight but not significant differences and, for the purpose of analysis, were grouped together. Again, there is an area of intense green fluorescence in the plane at Z = 0.0 μm indicating the accumulation of a high concentration of anti-dnp IgG within the contact area, although most of the green is difficult to see in the merged images. However, the yellow indicates colocalization between the anti-dnp IgG and membrane rafts. This accumulation of membrane rafts within the contact area is significant. Casual inspection of the z-stack images reveals a higher concentration of membrane rafts within the contact area. Furthermore, the majority of rafts are in the lower half of the cell, with most of those being in the lowest quarter of the cell.

The second row of **Figure 10** shows a profile view of an image reconstructed from the z-stack. The image of CD32A fluorescence supports what is found in the z-stack in three noticeable ways: 1) the increase in size of the contact area as indicated by the increased area of bright green fluorescence; 2) the decrease in membrane raft from the cell surface, in particular from the upper part of the cell surface, away from the contact area; 3) the increase in membrane rafts within the contact area. Note that the brightest red fluorescence occurs below 4.0 μm.

The data suggests that membrane rafts and CD32A are moving towards the contact area over time.

Membrane Cholesterol Extraction or Oxidation Impairs Contact Area Formation

The colocalization and concurrent accumulation of CD32A and membrane rafts within the contact area during its formation may be coincidental or due to a role membrane rafts play in this process. If the coupled kinetics-diffusion were responsible for the concentration of CD32A, and an affinity of CD32A and membrane rafts were responsible not only for the residence of CD32A in membrane raft but also for bringing the membrane raft along with CD32A as it diffused towards the contact area, then the same physical mechanism should be operative with or without membrane rafts. Thus, one would predict that the contact area formation and the accumulation of CD32A alone would not be affected by the disruption of membrane rafts. To test this prediction, contact formation experiments were performed using cells treated with or without agents that would disrupt membrane rafts.

Cholesterol, a major component of membrane rafts, is necessary for the proper formation and function of membrane rafts. High concentrations of cholesterol within a phospholipid bilayer have a profound effect on the physical properties of the bilayer. Cholesterol is a long, rigid, and wide molecule with an acyl chain at one end. In a phospholipid bilayer, it causes the acyl chains of the phospholipids to become more

tightly packed, which reduces the bilayer permeability. A cholesterol molecule lies perpendicular to the phospholipid bilayer; its effect is directional in that the cholesterol can block mobility in one direction but has virtually no effect on the lateral mobility of phospholipids and protein. This effect tends to create a certain amount of order within the bilayer.

Without cholesterol to maintain order, a membrane raft tends to dissolve or become dispersed. Ergo, removal of cholesterol or altering of its molecular structure leads to disruption of the membrane raft, a fact which can be exploited to investigate the function of rafts.

Cholesterol was extracted from live K562 cells (5 x 10^6/ml) by incubation in activation buffer pH 7.2 (PBS + 5mM HEPES) for 30 minutes at 37^0 C containing varying concentrations of MβCD (0.01-10mM). The cells were then washed twice and fluorescently stained by incubation in cold FACS buffer (1 x 10^6/ml) with 5μg Alexa Fluor 647 cholera toxin subunit B conjugate for ten minutes. The cells were immediately washed twice, checked for viability with trypan blue exclusion, and then used to form contact areas as previously described.

MβCD cholesterol extraction from K562 cells had the effect of diminishing the size of contact areas formed between the cells and the GSLB. This effect was inversely proportionate to the concentration of MβCD used. The data is summarized in **Figure 11**.

MβCD treatment diminished the size of the contact area in a concentration-dependant manner. 100 μM of MβCD was sufficient to completely abrogate contact area formation, whereas a concentration of 0.01 μM had no visible effect on contact area size.

Other attributes of contact area formation were also observed to diminish in parallel to the reduced size of contact area formed by the MβCD-treated cells. These included lower membrane raft concentration as indicated by lower intensity in the GM1-conjugated red fluorescence and the concurrently reduced accumulation of IgG and membrane rafts in the smaller contact area.

Cholesterol Oxidation Contact Area Formation

As mentioned previously, the caveat to using MβCD is that extraction of cholesterol via MβCD is not limited to the cell surface but also has the potential to extract cholesterol from any other part of the cell, an action which could affect any number of cell processes. Once again, to overcome this limitation, cholesterol oxidase was used to oxidize cholesterol to cholesterone. This oxidation results in a structural change in the molecule which disrupts the membrane raft.

K562 cells (1 x 10^6/ml) were incubated at 4^0C for 30 minutes in PBS containing varying concentrations of cholesterol oxidase (1.4 -0.014 units/ml). The cells were immediately washed twice, checked for viability with trypan blue exclusion, and then used to form contact areas as previously described.

Like MβCD treatment, cholesterol oxidase treatment also affected contact area size, but more dramatically. A concentration of 1.4 units/ml cholesterol oxidase was found to completely abrogate contact area formation. However, a decrease of just one order of magnitude in concentration of 0.14 units/ml did allow contact areas to form, but they were very small (~12 μm^2). And yet, another decrease in concentration by one order of magnitude had no visible effects on contact area formation. Oxidation of cell-surface cholesterol by cholesterol oxidase affected contact area formation in a concentration-

dependent manner, but these changes were more dramatic. While cholesterol oxidase treatment affected the contact area formation in a concentration-dependant fashion like MβCD, the range of concentrations which actually allowed contact areas to form was very narrow.

Sphingomyelin hydrolysis abrogates Contact Area Formation

It is the high concentration of sphingomyelin which gives membrane rafts their ability to separate from the rest of the cell membrane as their long straight acyl chains pack tightly together. It is reasonable to assume that the hydrolysis of sphingomyelin would cause a membrane raft to lose its cohesion and simply fall apart. Thus, the enzyme sphingomyelinase provides another mechanism by which to disrupt membrane rafts. To add strength to the observations gathered from the previous experiment involving cholesterol oxidase disruption of membrane rafts, we repeated the previous experiments but replaced cholesterol oxidase with sphingomyelinase.

K562 cells (1 x 10^6/ml) were incubated at 4^0C for 30 minutes in PBS containing varying concentrations of sphingomyelinase (1.0 - 0.0014 units/ml). The cells were immediately washed twice, checked for viability with trypan blue exclusion, and then used to form contact areas as previously described.

Like cholesterol oxidase, sphingomyelinase also affected contact area size, but more dramatically. A concentration of 0.014 units/ml sphingomyelinase abrogated contact area formation. However, decreasing the concentration just one order of magnitude (0.0014 units/ml) allows the formation of very small contact areas (< 12 μm^2). A decrease in concentration of just one order of magnitude had no visible effects on contact area formation. Hydrolysis of sphingomyelin via sphingomyelinase drastically affected contact area formation.

Cholesterol Oxidation has no effect on CD32A Concentration or Binding Kinetics

While oxidation of cell surface cholesterol by cholesterol oxidase clearly affects contact area formation, it is possible that this effect comes from a mechanism other than raft disruption. Two major factors that affect contact area formation are the receptor-ligand binding kinetics and cell surface concentration of CD32A. To determine whether cholesterol oxidase affected either of these processes, the micropipette experiment and flow-cytometry analysis were used to measure receptor-ligand binding kinetics and cell surface concentration of CD32A, respectively.

Live K562 cells (1x10^6/ml), were incubated with or without cholesterol oxidase (1.4 mM), washed twice, and then immuno-fluorescently stained by incubation with primary antibody mouse anti-CD32A IgG, and secondary antibody Alexa 488 labeled anti-mouse IgG. For the negative control, a non-relevant mouse IgG was used as the primary antibody. Flow cytometry analysis was performed to determine CD32A expression level.

For each sample, ten thousand events were collected. The data collected is summarized in **Figure 12**. The data shows no significant differences in CD32A expression level between positive control and cholesterol oxidase treated K562 cells.

K562 cells from the same group as the flow-cytometry analysis were used to perform the micropipette experiment[82], which measured the binding frequency between CD32A-expressing K562 cells and IgG opsonized red blood cells. The data

collected is summarized in **Figure 13**. The data shows no significant difference between the positive control K562 cells and the chemically treated K562 cells.

These data suggest that the decrease in contact area size as a function of cell surface cholesterol oxidation by cholesterol oxidase has no effect on CD32A expression or its binding kinetics, thereby supporting the hypothesis that the effect on contact area size caused by oxidation of cell surface cholesterol by cholesterol oxidase results from the disruption of membrane rafts.

Disruption of actin microfilament

The data from the preceding section suggest a role for membrane rafts in contact area formation between K562 cells and a GSLB, as they are required for the process to occur. Given that membrane rafts have been shown to facilitate protein transport and that the disruption of membrane rafts diminishes or abrogates contact area formation, it is not unreasonable to assume that membrane rafts play a role in the transport of CD32A to the contact area, which of course contradicts the CD32A coupled kinetics-diffusion process described earlier. Membrane rafts are associated with the actin cytoskeleton through a number of possible anchor proteins. It is logical to assume the actin cytoskeleton could affect the mobility of membrane rafts which are anchored to it. Studies have shown that the actin cytoskeleton is involved in membrane rafts signaling, trafficking, and clathrin-dependant endocytosis. Furthermore, it has been suggested that membrane rafts are transported along the actin cytoskeleton. To investigate the relationship between the actin cytoskeleton and the membrane rafts that colocalized with CD32A, varying concentrations of Latrunculin A were used to dissolve the actin cytoskeleton.

Live K562 cells (1 x 10^6/ml) were incubated at 37^0C for 30 minutes in RPMI/10% FBS containing varying concentrations of Latrunculin A (0.01 - 100 μM). The cells were immediately washed twice, checked for viability with trypan blue exclusion, re-suspended in 1 ml HBS/1% HA containing Latrunculin A (0.01 - 100 μM), and then used to form contact areas as previously described. The results from these experiments are summarized in **Figure 14**.

Latrunculin A treatment had the effect of diminishing the size of the established contact area, and this effect was found to be concentration dependant, where the size of the contact area decreasing with an increase in the concentration of Latrunculin A. One μM Latrunculin A was sufficient to completely abrogate contact area formation, whereas a concentration of 0.01 μM had no visible effect on contact area size, suggesting that contact area formation is dependent on the actin cytoskeleton.

Because Latrunculin A has the potential to affect contact area size by altering CD32A expression level and binding kinetics, it was necessary to perform flow cytometry analysis and the micropipette experiment on K562 cells treated with Latrunculin A. Latrunculin A treatment had no effect on the expression level or binding frequency of CD32A on K562 cells (**Figure 12** and **Figure** 13).

Blebbistatin inhibition of myosin II activity abrogates contact area formation

Myosin II is an actin based molecular motor protein which uses energy from the hydrolysis of ATP to perform its various functions. One such function is the transport of membrane rafts along F-actin cytoskeleton. Based on this and the previous data, we

predicted that the presence and viability of Myosin II were necessary for contact area formation.

To test this hypothesis, we monitored contact area formation between K562 cells and a GSLB in the presence of Blebbistatin, a specific Myosin II inhibitor. Myosin II molecules bind to ATP and upon hydrolysis of ATP generate the force needed for movement. Blebbistatin specifically inhibits the hydrolysis of ATP by Myosin II, thus eliminating force generation within Myosin II.

Live K562 cells (1 x 10^6/ml) were incubated at 37^0C for 30 minutes in RPMI/10% FBS containing Blebbistatin (100 μM). Afterwards, the cells were washed twice in cold FACS buffer, checked for viability with trypan blue exclusion, re-suspended in 1 ml HBS/1% HA containing Blebbistatin (100 μM), and then used to form contact areas as previously described.

Blebbistatin treatment completely abrogated contact area formation. This protocol was repeated twice to verify this finding.

Flow cytometry analysis and the micropipette experiment were used to determine if the abrogation of contact area formation caused by Blebbistatin was due to it affecting either CD32A binding kinetics or CD32A expression levels (**Figure 12** and **Figure** 13**)**. The data indicates no significant difference in binding kinetics or CD32A expression for cells treated with Blebbistatin.

This data lends credence to the idea that the motor protein Myosin II moves membrane rafts along the actin cytoskeleton to the site of contact area formation, and that active movement of the membrane rafts, rather than passive diffusion of CD32A, is required for contact area formation between K562 cells and an IgG labeled GSLB.

ITAM signaling is required for contact area formation

Can the coupled kinetics and diffusion process be a physical mechanism responsible for contact area formation? Previous experiments were performed using human red blood cells reconstituted with GPI-anchored CFD16 molecules to form contact area on IgG-coated lipid bilayer (Zarnitsina, V. Tolentino, T. data not shown). Although membrane rafts also exist in red blood cells, active transport by actin-myosin interaction was unlikely in that study, suggesting a physical mechanism to be responsible for contact area formation, which may be the coupled kinetics and diffusion process. However, the data from the present thesis have provided strong evidence to disprove the coupled kinetics and diffusion process as the physical mechanism responsible for contact area formation. Thus, accumulation of CD32A into the contact area is presumably due to active transport by Myosin II along actin microfilaments of membrane rafts, which carry with them CD32A that resides in membrane rafts. Initiation of active transport requires signaling. We therefore studied signaling triggered by engagement of CD32A with IgG-opsonized surfaces.

Binding to or cross-linking by ligand of some members of the Fcγ receptor group is known to initiate signaling through an ITAM signaling motif. With FcγI (CD64) and FcγIIIA (CD16A) ITAM is present only in an associated γγ, ζζ, or γζ subunit, whereas in FcγIIA (CD32A) it is a part of the cytoplasmic region of the receptor itself.

Cross-linking or ligand binding leads to the phosphorylation of ITAM by a member of the Src family of kinases[23, 83]. Phosphorylation of ITAM is the first easily detected stage of FcγR signaling. Phosphorylation of ITAM converts it into a docking

site for the SH2-containing protein SYK, which leads to the recruitment of SYK to the region of phosphorylated ITAM. Recruitment of SYK initiates signaling pathways, resulting in phosphorylation of downstream proteins. While different signaling pathways can be initiated depending on the cell type and effector function, they are similar to those found in all ITAM containing receptors. To test the hypothesis that signaling was triggered in CD32A-mediated contact area formation, we used anti-SYK mAb to visualize the spatial and temporal distribution of SYK. In addition, we used an anti-phosphorylated tyrosine mAb to visualize other proteins that were phosphorylated during the process of contact area formation.

K562 cells (1×10^6/ml) were washed and re-suspended in 1 ml HBSS with 1% HSA and then injected into an FCS2 flow chamber with a glass supported lipid bilayer labeled with non-fluorescent mouse-anti-dnp IgG, and kept at 37°C.

At 3, 9, 30, and 60 minute intervals, cells with contact areas were fixed for ten minutes by injecting 1 ml 4% formalin into the chamber. After washing the flow chamber, cells were stained for SYK by incubation with primary antibody donkey anti-SYK IgG (5 μg/ml), followed by washing and then incubation with secondary antibody FITC anti-donkey (10 μg/ml) at 4 °C for 30 minutes. At the 3 and 9 minute intervals, cells were also stained for Phosphorylated tyrosine (PO_4-Y) by incubation with primary antibody mouse anti-PO4-Y (5 μg/ml) at 4 °C for 30 minutes, followed by a wash and then incubation with Alexa 647 secondary antibody anti-mouse IgG (10 μg/ml) at 4°C for 30 minutes. After one hour, images were collected via Immuno-fluorescent confocal microscopy. Fluorescence from FITC anti-donkey (SYK indicator) and Alexa 647 anti-mouse IgG (anti-PO_4-Y indicator) were pseudo colored green and red, respectively.

Figure 16 shows representative images captured from cells that were fixed at three minutes into contact area formation. The top row shows the z-stack of images captured while the bottom row shows the profile view of a 3D image generated by reconstruction of the z-stack images. A casual inspection of the z-stack images reveals the presence of SYK from 0.0 μm to 4.2 μm. Also, PO_4-Y is fond to be present from 0.0 μm to 5.6 μm. The presence of these proteins in and above the contact area suggests that signaling begins within the contact area, which of course is the site of initial CD32A-IgG binding.

While both signaling molecules are present at 0.0 μm, in the contact area, the plane of brightest fluorescence is at 0.70 μm, still very near the contact area but just slightly above it.

Figure 17 shows representative images captured from cells that were fixed at nine minutes into contact area formation. The top row shows the z-stack of images captured while the bottom row shows a profile view of a 3D image formed by reconstruction of the z-stack.

The z-stack images clearly show fluorescence from both fluorophores from 0.65 μm to 11.05 μm, with the brightest region of fluorescence being between 3.25 μm and 7.15 μm. The absence of fluorescence at 0.0 μm and only light fluorescence apparent until 2.60 μm is significant in that it indicates a movement of SYK and PO_4-Y from the contact area to the interior of the cell.

Taken together, the data collected at 3 and 9 minutes suggest the following: 1) CD32A signaling begins within the contact area, 2) the signaling increases from 3 to 9 minutes, 3) the signaling molecules migrate inwards.

The previous procedure was repeated with fixation at 30 minutes and no PO_4-Y staining. **Figure 18** shows representative images of a cell with an established contact area that was fixed at 30 minutes into contact area formation and stained for SYK. The right column contains a z-stack series with the brightfield image of the cell included. The left column shows a profile and a bottom view of a 3D image generated by reconstruction of the z-stack series.

The profile and bottom views of the 3D image show SYK present in a very high concentration within the contact area and extending roughly 10 μm into the cell. Interestingly, the SYK present at the bottom plane (0.0 μm) is void of fluorescence in a circular region in the center of the contact area, resulting in a bulls-eye like appearance. Every sample is the data set had a very similar shape.

The data strongly suggests that SYK accumulates within the contact area, and that SYK from the central circular region of the contact area is internalized.

The previous procedure was repeated with fixation at sixty minutes. **Figure 19** shows representative images of a cell with an established contact area, fixed at 60 minutes into contact area formation. This experiment was performed three times under identical conditions. A total of fifteen images were collected (n = 15).

The right column shows z-stack images of the cell. The left column shows a profile and a bottom view of a 3D image generated by reconstructing the z-stack series. The bulls-eye pattern of SYK present in the bottom plane at 30 minutes is still present. However, the long band of SYK that extends inward is gone. Small clusters of SYK can be seen scattered randomly throughout the cell.

It is possible that SYK is internalized and possibly sorted into lysosomes. Given that SYK is binds to PO_4-Y after CD32A – IgG binding, and that PO_4-Y is a part of the ITAM, and furthermore, that ITAM is a part of the CD32A protein, it is reasonable to assume that this data not only supports the idea of SYK accumulation within the contact area, followed by internalization of SYK, but it also suggests CD32A accumulation within the contact area followed by its internalization, which strongly supports the main hypothesis of this project.

Internalization of Membrane Rafts from the Contact Area

The signaling events observed in the preceding section, revealed by the presence of SYK and PO_4-Y at the site of contact area formation, are likely triggered by the initial engagement of CD32A with IgG and required for the active transport of CD32A and membrane rafts to the contact area and their accumulation within it. However, they may also trigger other cellular processes, such as phagocytosis. This hypothesis is supported by the following observations.

In the experiments in which colocalization and accumulation of CD32A and membrane rafts were studied, observations were made after stable contact areas had been fully established, and fluorescent IgG appeared to have been internalized. From the colocalization experiments during contact area formation, the data shows red fluorescence of Alexa 647 cholera toxin B, the membrane raft marker, inside the cell appearing between nine and twelve minutes (**Figure 10**) indicating the internalization of membrane rafts.

Images collected 30 minutes into contact area formation (**Figure 20**) showed that the red fluorescence had disappeared from the contact area and nearly 100% of the

membrane raft staining was found inside the cell rather than on the cell membrane. It is at this point that the data begins to show a de-localization of membrane rafts and anti-dnp IgG as the membrane rafts moved inward and away from the contact area (**Figure 21**).

By 60 minutes, there was no colocalization between the membrane rafts and anti-dnp IgG, suggesting no colocalization between the membrane rafts and CD32A.

Colocalization of membrane rafts and the Golgi complex

Internalization of the membrane rafts raised the question of whether or not the membrane rafts were internalized to a specific organelle. To answer this question, internalized membrane rafts were tracked by fluorescent staining of the cells Golgi complex and lipid rafts prior to contact area formation.

The Golgi complex of K562 cells (1×10^6/ml) were fluorescently stained by incubation for 30 minutes at 4 °C with 5 mM Bodipy TR labeled Ceramide-BSA (a known Golgi marker[75, 84, 85]) in HBSS/HEPES. After washing with HBSS, GM1 was labeled by incubation for 10 minutes at 4 °C with 2 μg/ml Alexa Fluor 633 Cholera toxin B in HBSS, washed with HBSS with 1% HSA, re-suspended in HBSS with 1% HBS and then injected into a FCS2 flow chamber in which a glass supported lipid bilayer labeled with Alexa Fluor 488 rabbit-anti-dnp IgG, maintained at 37 °C, and then left to form established contact areas between the cell and the glass supported lipid bilayer, after which images were captured via immuno-fluorescent confocal microscopy. For these images, the Golgi marker Bodipy TR Ceramide and the membrane raft marker Alexa 555 cholera toxin B were pseudo-colored green, and red, respectively. These images are shown in **Figure 22**.

Colocalization of membrane rafts, Golgi, and ER

The previous experiment was repeated with the addition of labeling the ER with Concanavalin A by incubation in HBSS/HEPES with 50 μg/ml Concanavalin A for 30 minutes at 4°C.

As with the previous experiment, fluorescence images of a cell with an established contact area, labeled with the Golgi marker Bodipy TR Ceramide, the membrane raft marker Alexa 555 cholera toxin B, and the ER marker Concanavalin A[86-88], are shown in row one of **Figure 23** pseudo-colored green, red, and blue, respectively. The merged image of all three markers is shown in the last panel. Once again, there is strong colocalization between the Golgi complex and the membrane rafts but no suggestion of colocalization between membrane rafts and the ER. These data suggest membrane rafts are internalized to the Golgi complex via a non-ER related route.

The 3D images from **Figure 23** (top row) are presented again in **Figure 24** in a manner which makes colocalization more apparent. In each row, one of the fluorescent markers is removed to allow for detection of colocalization between two markers without the presence of a third color obscuring the process. Furthermore, the fluorescent markers being observed are pseudo-colored either green or red. This was done to make colocalization more apparent, as the yellow resulting from the overlap of red and green is easier to see than the pink or purple which results from the over lap of blue with either green or red.

Rows I through IV examine the colocalization between the following: I) Golgi, rafts and ER, II) Golgi and rafts, III) rafts and ER, and IV) Golgi and ER, respectively.

In rows II, III, and IV, the structures being compared are pseudo colored green and red to make colocalization more apparent.

In row II, the Golgi and membrane rafts are pseudo colored green and red, respectively. The merged image shows a spherical region of intense yellow at the location of the Golgi, suggesting that the Golgi is colocalized with some membrane rafts.

In row III, the membrane rafts and ER are pseudo colored red and green, respectively. The absence of yellow in the merged image suggests there is no colocalization between the ER and membrane rafts.

In row IV, the Golgi and ER are pseudo colored green and red, respectively. The absence of yellow in the merged image suggests there is no colocalization between the Golgi and the ER.

This data suggests that colocalization between the membrane rafts and the Golgi complex exists. However, there is no real evidence that the ER colocalizes with either membrane rafts or the Golgi. It is possible that the membrane rafts are being internalized to the Golgi complex via a non-ER route.

CD32 Mediated Phagocytosis of Opsonized Micro-beads

The data to this point suggests that contact area formation between K562 cells expressing CD32A and an IgG labeled GSLB is diminished or abrogated by the disruption of membrane rafts, disruption of the actin cytoskeleton, inhibition of the actin based motor protein Myosin II, and inhibition of cell signaling. These data led us to hypothesize that CD32A mediated phagocytosis of an opsonized target is diminished or abrogated by the disruption of membrane rafts, disruption of the actin cytoskeleton, inhibition of the actin based motor protein Myosin II, and inhibition of cell signaling.

To test this hypothesis, K562 cells and opsonized fluorescent micro-beads (diameter = 2 μm) were incubated together in standard culture media, RPMI 1640 with 10% FBS, for one hour at 37°C. The cells and beads were washed once, and then fixed for ten minutes in a cold 4% formalin solution. Afterwards, the cells and beads were washed, re-suspended in FBS, and imaged using laser-scanning confocal microscopy. All experiments were run in parallel with a positive control sample, in which all conditions were kept the same with the exception of chemical treatments. All experiments were run twice with a total of four images collected from each.

The results of these experiments are summarized in Table 1 with a sample image from each dataset shown in **Figure 27** through **Figure** 30.

From the positive control image (**Figure 25)** it can be seen that K562 cells are well capable of phagocytizing the opsonized fluorescent micro-beads. In fact, the cells engulfed so many beads that they nearly burst. Latrunculin A, cholesterol oxidase, Sphingomyelinase, and PTK treatment significantly diminish the quantity of micro-beads phagocytosed by the K562 cells, while Blebbistatin completely inhibited phagocytosis of the micro-beads.

Table 1 A summary of CD32A – mediated phagocytosis of opsonized μ-beads

Reagent	Action	Effect on contact area formation	Effect on phagocytosis
-	Positive Control	-	-
IV.3 (anti-CD32)	Negative Control	Inhibits	Inhibits
Latrunculin A	Dissolve the actin-cytoskeleton	Concentration dependent decrease in contact area size	Significantly decreased.
Cholesterol Oxidase	Disruption of membrane rafts by oxidation of cholesterol in the outer membrane	Concentration dependent decrease in contact area size	Significantly decreased
Sphingomyelinase	Disruption of membrane rafts by hydrolysis Sphingomyelin	Concentration dependent decrease in contact area size	Significantly decreased
Blebbistatin	Prevent transport of membrane rafts by inhibition of the F-actin motor protein, Myosin II	Abrogates	Abrogates
PTK inhibitor	Inhibits cell signaling	Abrogates	Significantly decreased

Cholesterol oxidase, sphingomyelinase, Latrunculin A, Blebbistatin, and PTK inhibitor impaired the K562 cells' ability to carry out CD32A mediated phagocytosis, in a manner similar to the effect it had on contact area formation between CD32A-expressing K562 cells and a GSLB labeled with anti-dnp IgG.

DISCUSSION

While the size, composition, and even the existence of *membrane rafts* remain the topic of much controversy, there can be little doubt that detergent-resistant cell surface micro-domains, that are highly concentrated in sterols and sphingolipids which are more ordered than the liquid-disordered state described in the fluid mosaic model proposed by Singer and Nicholson, actually exist. Furthermore, the fact that these heterogeneic micro-domains exist within the expanse of a cell membrane's homogeneity provides these micro-domains with the ability to sequester or exclude membrane proteins based on protein structure and anchor-type. In addition, these micro-domains have been shown to be anchored to the cell's actin-cytoskeletal network and that they are actively transported along these networks by molecular motor proteins. Simply stated, these structures provide a cell with a tool to cluster, bind, and transport protein. With this in mind, it is not surprising that a plethora of evidence has been provided to show that membrane rafts are involved in many different cell processes, including signal transduction,

immunological synapse formation, t-cell activation, membrane trafficking, and endocytosis.

In this study we have investigated the roles of these micro-domains, which we believe are membrane rafts, in CD32A mediated phagocytosis of an opsonized target.

Colocalization of CD32A with membrane rafts

We began our investigation by examining the spatial relationship between CD32A and membrane rafts on K562 cells, by using laser-scanning confocal microscopy to acquire 3D images of K562 whose membrane rafts and CD32A proteins had been fluorescently labeled with Alexa 647-conjugated Cholera toxin B and Alexa 488-conjugated goat anti-mouse bound to Fab anti-CD32A mAb (IV.3). CD32A was found to exist in clusters rather than being randomly distributed ubiquitously on the cell surface membrane. Each of these clusters was found to colocalize with membrane rafts, which were present in a much higher density. In the first set of experiments, cells were labeled prior to being fixed. While FAB anti-CD32A was used to avoid cross-linking of the Fcγ receptors, the use of Cholera toxin B, a pentavalent ion, left open the possibility of membrane raft cross-linking. To eliminate this possibility, these protocols were repeated but with cell fixation prior to fluorescent labeling. The images captured were identical to those from the previous data set. Since cell fixation with formalin leaves the cell membrane rigid, cell surface proteins become immobilized, thus eliminating the possibility that labeling of membrane rafts with Cholera toxin B could induce cross-linking.

In an effort to determine if this colocalization was a function of cell type or CD32A anchor type, we repeated the previous protocol using CHO cells that were transfected to express either $CD32A^{TM}$ or $CD32A^{GPI}$. CHO-$CD32A^{TM}$ expressed the WT form of CD32A, the same as that expressed on the K562 cells used in this investigation, whereas CHO-$CD32A^{GPI}$ expresses a form of CD32A, in which the transmembrane segment of the receptor has been replaced with a GPI molecule which anchors the protein by inserting into the cell membrane. CD32A clusters and membrane rafts on both cell types were found to have the same spatial relationship as those on K562 cells, suggesting that the colocalization of the two are not a function of cell type or protein anchor type.

Our results appear to agree with previous data as the experimental protocol and cell types may be responsible for differences in findings. In 2001, Katsumata et al[71] measured the colocalization of CD32A with DRM before and after cross-linking the Fcγ receptors. In their protocol they labeled CD32A with $^{I\text{-}125}$IV.3 in two groups of K562 cells. One group was activated by cross-linking, the other was not. Afterwards, membrane components were separated via cell lysis followed by sucrose gradient separation. Their results did not provide evidence that uncross-linked FcγRIIA did not associate with DRMs. They did, however, find an association between FcγRIIA and DRMs in the cross-linked group. They concluded that FcγRIIA was recruited to DRMs after cross-linking. So while their data provides clear evidence of colocalization after cross-linking it does leave open the question of whether or not colocalization exists prior to cross-linking.

We did not use cross-linking in this project. Any and all activation of cells as a result of FcγRIIA binding was from the binding of FcγRIIA to its natural ligand the Fc

portion of IgG. Hence, our results do agree with their findings from K562 cells that were cross-linked.

Kwiatkowska et, al[14] used immunoprecipitation to investigate colocalization between DRMs and CD32A in U937 cells. Like the Katsumata group they also Kwiatkowska used cross-linking. A major difference in their protocol is that they used CD55, a gpi anchored protein, as a raft marker. They found CD32A and CD55 association in both cross-linked and non-cross-linked U937 cell groups, however in the cross-linked group most of the CD55 associated with CD32A. Their conclusion was the same as Kwiatkowska. There is no clear evidence that CD55 resides solely within DRM. If CD55 exist both in DRM and outside the DRM it could convolute the data by creating the impression of DRMs being located where they are not. As yet, there is no data which compares the consequences of cross-linking Fc receptors to the consequences of ligand binding of Fc receptors, and as such it is impossible to say whether or not the differences in our results to theirs are due experimental protocol. However, it is fair to point out the fact that cross-linking is an event which does not occur in vivo, whereas Fc receptors binding to the Fc portion of IgG does occur in vivo – a task it has evolved to perform.

It is important to note, that the data collected here was acquired via laser-scanning confocal microscopy. Fluorescent images are only suggestive of colocalization, they are not what one might considered *hard* evidence. Molecular biology techniques such as gradient separation, immunoprecipitation, and western blotting are far more convincing.

Membrane rafts and CD32A colocalize during contact area formation

Having found that CD32A clusters colocalize with membrane rafts, and knowing from previous work that CD32A accumulated within the contact area formed between K562 cells and glass-supported lipid bilayers (GSLB), we then hypothesized that membrane rafts would also accumulate within the contact area formed between K562 cells and GSLB. To test this hypothesis, we labeled the membrane rafts of live K562 cells with Alexa 647 Cholera toxin B and then monitored the contact area formation between these cells and an Alexa 488 anti-dnp IgG labeled GSLB. Cells with contact areas, fixed at varying time points, all showed accumulation of membrane rafts within the contact area.

To our knowledge, based on an extensive article search in pubmed, there have been no attempts to measure colocalization between CD32A, or any other Fcγ receptor, and membrane rafts. However, if we assume that cross-linking of FcγRIIA ultimately affects DRMs in a similar fashion as contact area formation, they it is fair to say our data is in good agreement with previous findings as both Katsumata and Kwiatkowska found FcγRIIA associated with DRMs after cross-linking.

Cholesterol extraction impaired contact area formation

These findings led us to hypothesize that membrane rafts were used by the cell to transport CD32A clusters to the site of contact area formation. We first tested this hypothesis by monitoring contact area formation using K562 cells which had been treated with varying concentration of MβCD. MβCD was used to disrupt membrane rafts by extraction of cholesterol from the cell surface. Cholesterol extraction diminished the size of the contact areas established, and did so in a concentration-dependent manner. While this effect was expected as a result of membrane raft disruption, it was necessary to

eliminate the possibility that cholesterol extraction diminished contact area size by a mechanism other than raft disruption. Since contact area formation is driven by receptor-ligand binding, alteration of either adhesion frequency or receptor concentration could also diminish the size of contact areas formed. Therefore, a micropipette binding assay was used to measure the adhesion frequency between K562 cells treated with MβCD and red blood cells coated with IgG. The results of assay were compared to a micropipette binding assay of non-treated K562 cells. The data showed no significant difference in adhesion frequency, suggesting that receptor-ligand binding kinetics had not been affected by cholesterol extraction. However, the concentration of CD32A was decreased by cholesterol extraction.

Disruption of membrane rafts impaired contact area formation

Since cholesterol extraction had affected receptor concentration, and since MβCD has the potential to affect many cell processes by extraction of cholesterol from within the cell, the previous data lacked strength. Next, cholesterol oxidase treatment was used to overcome the limitations of cholesterol extraction by MβCD. Where MβCD has the potential to extract cholesterol from virtually every part of the cell, cholesterol oxidase affects cholesterol found only on the cell surface membrane. Also, where MβCD alters the cell composition by removing cholesterol, cholesterol oxidase leaves the membrane composition unaffected, but rather only changes the structure of cholesterol to cholesterone. Cell surface cholesterol oxidation also diminished the size of contact areas but did not affect receptor-ligand adhesion probability, as determined by a micropipette binding assay, nor did it affect CD32A concentration. These data strongly support the idea of membrane rafts being used to transport CD32A to the site of contact area formation.

Sphingomyelinase catalyzes the hydrolysis of sphingomyelin. Since cell surface sphingomyelin is only found within membrane rafts, its hydrolysis has the effect of disrupting membrane rafts. Therefore, we used sphingomyelinase as a secondary method of membrane raft disruption. Hydrolysis of cell surface sphingomyelin also diminished the size of contact areas without affecting receptor-ligand adhesion probability or CD32A concentration, with the only difference being that the effect was more dramatic. These data further support the idea of membrane rafts being used to transport CD32A to the site of contact area formation.

Disruption of the actin cytoskeleton impaired contact area formation

Previous research has shown that membrane rafts are transported along the actin cytoskeleton. It was therefore reasonable to assume that if CD32A was transported to the site of contact area formation by membrane rafts, it was transported by these rafts along the actin cytoskeleton. If so, disruption of the actin cytoskeleton would impair the transport of CD32A clusters and in turn impair contact area formation, itself. We tested this idea by monitoring contact area formation between Alexa 488 anti-dnp IgG labeled GSLB and K562 cells treated with various concentrations of Latrunculin A. The disruption of the cells' actin cytoskeleton with Latrunculin A also had the effect of decreasing the size of the contact area formed in a concentration-dependent manner. In fact, with a high enough concentration of Latrunculin A, contact area formation was completely abrogated. These data suggest that the stability as well as the amount of

cytoskeletal networks present affect contact area formation. Simply stated, the ability to use membrane rafts to transport CD32A depends on the number of paths upon which they can do so.

Again, a direct comparison to previous data isn't possible, however there is an abundance of data which shows that lipid rafts are attached to the actin cytoskeleton in many different cell types[57, 58, 61, 62, 89, 90]. Lipid rafts are not only linked to the actin cytoskeleton but are necessary for actin rearrangement in such processes as immunological synapse formation. Disruption of the actin cytoskeleton has also been shown to impair lipid raft coalescence. These findings correlate extremely well with ours as we found the disruption of the actin cytoskeleton impaired contact area formation. In both cases there is the implication of raft immobilization.

Inhibition of ATP cleavage in Myosin II abrogates contact area formation

While the membrane rafts provide residency for CD32A to cluster within, and while the rafts are transported along the actin cytoskeleton, it is the molecular motor protein Myosin II which anchors the membrane rafts to the actin cytoskeleton and generates the force required for movement. Myosin II must cleave ATP to generate this force. Blebbistatin specifically inhibits ATP cleavage within Myosin II, thus rendering the protein inert. To test the theory that membrane rafts are moved along the actin cytoskeleton by Myosin II, we monitored contact area formation between Alexa 488 anti-dnp IgG labeled GSLB and K562 cells treated with 100 μM Blebbistatin. Myosin II ATP inhibition by treatment with Blebbistatin completely abrogated contact area formation.

Blebbistatin has been shown to inhibit phagocytosis, hence our data is in good agreement with findings from previous studies involving Blebbistatin inhibition of phagocytosis[91-93].

Signaling begins at the initial site of contact

Previous work in our lab has shown that cell signaling is necessary for proper contact area formation between K562 cells expressing Fcγ receptors and IgG labeled GSLB. Here, we confirmed our previous findings by attempting contact area formation with the presence of protein kinase inhibitors. Given that the data thus far suggests that membrane rafts transport CD32A to the site of contact area formation and that cell signaling is required for proper contact area formation, we hypothesize that membrane rafts transport CD32A to the site of initial signaling.

To test this idea, we allowed contact area formation to occur between K562 cells and a GSLB labeled with non-fluorescent anti-dnp IgG, and fixed the cells with contact areas at various time intervals. Afterwards, we fluorescently labeled phosphorylated tyrosine and the signaling protein Syk. CD32A binding leads to phosphorylation of tyrosine within the Immuno-tyrosine-activation-motif (ITAM). The phosphorylation of tyrosine on ITAM leads to the recruitment of Syk, which binds with the phosphorylated tyrosine. Ergo, both PO_4-Y and Syk are expected to be present at the site of CD32A-IgG binding. Our data shows PO_4-Y colocalized with Syk at the site of initial receptor-ligand binding. Early in contact area formation (3 minutes), the region in which signaling occurs is very small, but it increases in both area and height over time. The increase in signaling correlates well with the growth in contact area size. At 15 minutes, Syk is present in a circular pattern immediately over the contact area. However, by 30 minutes,

the Syk disappeared from the centroid of that circular region, forming the bulls-eye pattern that is familiar within the immunological synapse. More interestingly, Syk also extended from the ring of Syk inward toward the center of the cell, thus forming one large structure that resembled a ring at the bottom of the cell with a column extending inward several microns. Syk at this point is bound to the ITAM portion of CD32A. It is likely that the position of CD32A at this point and time mirrors the position of Syk, suggesting that the accumulation of CD32A within the contact area is followed by its internalization. In previous research, we have observed fluorescent IgG from the bilayer being internalized into the cell. These two observations taken together suggest that CD32A and its bound ligand, IgG, are internalized together. At the one-hour time point, the portion of Syk which extended from the contact area to the cell is gone, and Syk appears randomly distributed within the cytosolic portion of the cell. Since K562 is a phagocytic cell, it is likely that the internalized Syk by the one-hour time point has been sorted into lysosomes.

Between zero to 15 minutes, membrane rafts appear to migrate from the cell surface down to the site of contact area formation, where they accumulate and appear to form one large structure, roughly equal in size to that of the contact area. Between 15 and 30 minutes, very few membrane rafts are present on the cell surface, and most have been internalized and accumulate in a spherical pattern within the cell. In an effort to determine the location to which these rafts were being internalized, we fluorescently labeled the Golgi and endoplasmic reticulum of live K562 cells, which were then used to form contact areas with a GSLB labeled with non-fluorescent IgG. The spherical structure formed by internalized membrane rafts was found to colocalize with the Golgi, but not with the endoplasmic reticulum, suggesting that the membrane rafts were internalized to the Golgi via non-ER route.

Taken together, the data seems to suggest that membrane rafts serve several functions in the contact area formation of a phagocytic synapse, these functions being pre-clustering of CD32A, cell signal transduction, and transport of CD32A to the contact area. Furthermore, the data provides evidence of a role for membrane rafts in the internalization of an opsonized target during CD32A mediated phagocytosis.

These findings are in excellent agreement with what is known about cell signaling initiated by the binding of CD32A to the Fc portion of IgG. Phosphorylation of ITAM followed by recruitment of SYK to the phosphorylated ITAM is known to be the first to steps in the signaling cascade of CD32A. Furthermore, inhibition of signaling involving ITAM has been shown to inhibit raft coalescence, phagocytosis,[15, 60] and actin cytoskeletal reorganization[14].

Phagocytosis of opsonized micro-spheres

To summarize, our findings provide evidence that membrane rafts provide residency for CD32A and that these rafts are moved by Myosin II along the actin cytoskeleton to the contact area, thus allowing for the quick assembly of a phagocytic synapse. Furthermore, membrane rafts appear to coalesce into one huge super-raft, which provides a scaffold to which the cell can apply a force and internalize. As this structure is internalized, the CD32A must also be internalized with it and, in turn, so must the IgG, bound to the CD32A. Assuming this is correct, it is not unreasonable to assume that the opsonized target would be internalized as well. Thus, we hypothesized that K562

cells incubated in the presence of opsonized micro-spheres would phagocytize the micro-spheres. Furthermore, this phagocytosis would be impaired by cholesterol oxidase, sphingomyelinase, Latrunculin A, and Blebbistatin in the same manner that these chemicals impaired contact area formation. To investigate this possibility, we repeated the contact area formation experiments but replaced the GSLB with opsonized fluorescent micro-spheres. These experiments were run under the same conditions as the contact area formation experiment.

The results of the K562-CD32A mediated phagocytosis of opsonized micro-spheres strongly supported our hypothesis. Cholesterol oxidase, sphingomyelinase, Latrunculin A, and PTK all significantly impaired phagocytosis of the opsonized micro-spheres while Blebbistatin completely abrogated phagocytosis. These results mirror those of the contact area formation.

BIBLIOGRAPHY

1. Tolentino, T.P., *The Roles of Membrane Rafts in CD32A Mediated Formation of a Phagocytic Contact Area*, in *Biomedical Engineering*. 2007, Georgia Institute of Technology: Atlanta.
2. Sondermann, P., et al., *The 3.2-A crystal structure of the human IgG1 Fc fragment-Fc gammaRIII complex.* Nature, 2000. **406**(6793): p. 267-73.
3. Sondermann, P., et al., *Characterization and crystallization of soluble human Fc gamma receptor II (CD32) isoforms produced in insect cells.* Biochemistry, 1999. **38**(26): p. 8469-77.
4. Sondermann, P., J. Kaiser, and U. Jacob, *Molecular basis for immune complex recognition: a comparison of Fc-receptor structures.* J Mol Biol, 2001. **309**(3): p. 737-49.
5. Sondermann, P. and V. Oosthuizen, *X-ray crystallographic studies of IgG-Fc gamma receptor interactions.* Biochem Soc Trans, 2002. **30**(4): p. 481-6.
6. Ravetch, J.V. and S. Bolland, *IgG Fc receptors.* Annu Rev Immunol, 2001. **19**: p. 275-90.
7. Nagarajan, S., et al., *Ligand binding and phagocytosis by CD16 (Fc gamma receptor III) isoforms. Phagocytic signaling by associated zeta and gamma subunits in Chinese hamster ovary cells.* J Biol Chem, 1995. **270**(43): p. 25762-70.
8. Krapp, S., et al., *Structural analysis of human IgG-Fc glycoforms reveals a correlation between glycosylation and structural integrity.* J Mol Biol, 2003. **325**(5): p. 979-89.
9. Mimura, Y., et al., *The molecular specificity of IgG-Fc interactions with Fc gamma receptors.* Adv Exp Med Biol, 2001. **495**: p. 49-53.
10. Mimura, Y., et al., *Role of oligosaccharide residues of IgG1-Fc in Fc gamma RIIb binding.* J Biol Chem, 2001. **276**(49): p. 45539-47.
11. Sondermann, P. and V. Oosthuizen, *The structure of Fc receptor/Ig complexes: considerations on stoichiometry and potential inhibitors.* Immunol Lett, 2002. **82**(1-2): p. 51-6.
12. Cambier, J.C., *Antigen and Fc receptor signaling. The awesome power of the immunoreceptor tyrosine-based activation motif (ITAM).* J Immunol, 1995. **155**(7): p. 3281-5.

13. Isakov, N., *Immunoreceptor tyrosine-based activation motif (ITAM), a unique module linking antigen and Fc receptors to their signaling cascades.* J Leukoc Biol, 1997. **61**(1): p. 6-16.

14. Kwiatkowska, K., J. Frey, and A. Sobota, *Phosphorylation of FcgammaRIIA is required for the receptor-induced actin rearrangement and capping: the role of membrane rafts.* J Cell Sci, 2003. **116**(Pt 3): p. 537-50.

15. Mansfield, P.J., et al., *Phagocytic signaling molecules in lipid rafts of COS-1 cells transfected with FcgammaRIIA.* Biochem Biophys Res Commun, 2005. **331**(1): p. 132-8.

16. Sandor, M., et al., *Developmentally regulated Fc gamma receptor expression in lymphopoiesis Fc gammaR III (CD16) provides an ITAM motif for pro-T and pro-B-cells.* Immunol Lett, 1996. **54**(2-3): p. 123-7.

17. Selvaraj, P., et al., *Functional regulation of human neutrophil Fc gamma receptors.* Immunol Res, 2004. **29**(1-3): p. 219-30.

18. Van den Herik-Oudijk, I.E., et al., *Functional differences between two Fc receptor ITAM signaling motifs.* Blood, 1995. **86**(9): p. 3302-7.

19. Aman, M.J., A.C. Tosello-Trampont, and K. Ravichandran, *Fc gamma RIIB1/SHIP-mediated inhibitory signaling in B cells involves lipid rafts.* J Biol Chem, 2001. **276**(49): p. 46371-8.

20. Canetti, C., et al., *Differential regulation by leukotrienes and calcium of Fc gamma receptor-induced phagocytosis and Syk activation in dendritic cells versus macrophages.* J Leukoc Biol, 2006. **79**(6): p. 1234-41.

21. Chuang, F.Y., M. Sassaroli, and J.C. Unkeless, *Convergence of Fc gamma receptor IIA and Fc gamma receptor IIIB signaling pathways in human neutrophils.* J Immunol, 2000. **164**(1): p. 350-60.

22. Coxon, P.Y., et al., *Differential mitogen-activated protein kinase stimulation by Fc gamma receptor IIa and Fc gamma receptor IIIb determines the activation phenotype of human neutrophils.* J Immunol, 2000. **164**(12): p. 6530-7.

23. Matsuda, M., et al., *Abrogation of the Fc gamma receptor IIA-mediated phagocytic signal by stem-loop Syk antisense oligonucleotides.* Mol Biol Cell, 1996. **7**(7): p. 1095-106.

24. Fanger, N.A., et al., *Type I (CD64) and type II (CD32) Fc gamma receptor-mediated phagocytosis by human blood dendritic cells.* J Immunol, 1996. **157**(2): p. 541-8.

25. Sanders, L.A., et al., *Human immunoglobulin G (IgG) Fc receptor IIA (CD32) polymorphism and IgG2-mediated bacterial phagocytosis by neutrophils.* Infect Immun, 1995. **63**(1): p. 73-81.

26. Worth, R.G., et al., *CR3 (alphaM beta2; CD11b/CD18) restores IgG-dependent phagocytosis in transfectants expressing a phagocytosis-defective Fc gammaRIIA (CD32) tail-minus mutant.* J Immunol, 1996. **157**(12): p. 5660-5.

27. Salmon, J.E., et al., *Allelic polymorphisms of human Fc gamma receptor IIA and Fc gamma receptor IIIB. Independent mechanisms for differences in human phagocyte function.* J Clin Invest, 1992. **89**(4): p. 1274-81.

28. Tuijnman, W.B., P.J. Capel, and J.G. van de Winkel, *Human low-affinity IgG receptor Fc gamma RIIa (CD32) introduced into mouse fibroblasts mediates phagocytosis of sensitized erythrocytes.* Blood, 1992. **79**(7): p. 1651-6.

29. Grendel, G.a., *ON BIMOLECULAR LAYERS OF LIPOIDS ON THE CHROMOCYTES*

OF THE BLOOD. Journal of Experimental Medicine, 1925. **41**(4): p. 439 - 443.

30. Singer, S.J. and G.L. Nicolson, *The fluid mosaic model of the structure of cell membranes.* Science, 1972. **175**(23): p. 720-31.

31. Somerharju, P., J.A. Virtanen, and K.H. Cheng, *Lateral organisation of membrane lipids. The superlattice view.* Biochim Biophys Acta, 1999. **1440**(1): p. 32-48.

32. Vereb, G., et al., *Dynamic, yet structured: The cell membrane three decades after the Singer-Nicolson model.* Proc Natl Acad Sci U S A, 2003. **100**(14): p. 8053-8.

33. Brown, D.A. and E. London, *Functions of lipid rafts in biological membranes.* Annu Rev Cell Dev Biol, 1998. **14**: p. 111-36.

34. Brown, D.A. and E. London, *Structure of detergent-resistant membrane domains: does phase separation occur in biological membranes?* Biochem Biophys Res Commun, 1997. **240**(1): p. 1-7.

35. Damjanovich, S., et al., *Dynamic physical interactions of plasma membrane molecules generate cell surface patterns and regulate cell activation processes.* Immunobiology, 1992. **185**(2-4): p. 337-49.

36. Douglass, A.D. and R.D. Vale, *Single-molecule microscopy reveals plasma membrane microdomains created by protein-protein networks that exclude or trap signaling molecules in T cells.* Cell, 2005. **121**(6): p. 937-50.

37. Edidin, M., *Lipid microdomains in cell surface membranes.* Curr Opin Struct Biol, 1997. **7**(4): p. 528-32.

38. Kusumi, A., K. Suzuki, and K. Koyasako, *Mobility and cytoskeletal interactions of cell adhesion receptors.* Curr Opin Cell Biol, 1999. **11**(5): p. 582-90.

39. Ryan, T.A., et al., *Molecular crowding on the cell surface.* Science, 1988. **239**(4835): p. 61-4.

40. Harder, T., et al., *Lipid domain structure of the plasma membrane revealed by patching of membrane components.* J Cell Biol, 1998. **141**(4): p. 929-42.

41. Harder, T. and K. Simons, *Clusters of glycolipid and glycosylphosphatidylinositol-anchored proteins in lymphoid cells: accumulation of actin regulated by local tyrosine phosphorylation.* Eur J Immunol, 1999. **29**(2): p. 556-62.

42. Janes, P.W., S.C. Ley, and A.I. Magee, *Aggregation of lipid rafts accompanies signaling via the T cell antigen receptor.* J Cell Biol, 1999. **147**(2): p. 447-61.

43. Cherukuri, A., M. Dykstra, and S.K. Pierce, *Floating the raft hypothesis: lipid rafts play a role in immune cell activation.* Immunity, 2001. **14**(6): p. 657-60.

44. Cheng, P.C., et al., *Floating the raft hypothesis: the roles of lipid rafts in B cell antigen receptor function.* Semin Immunol, 2001. **13**(2): p. 107-14.

45. Ikonen, E., *Roles of lipid rafts in membrane transport.* Curr Opin Cell Biol, 2001. **13**(4): p. 470-7.

46. Magee, A.I. and I. Parmryd, *Detergent-resistant membranes and the protein composition of lipid rafts.* Genome Biol, 2003. **4**(11): p. 234.

47. Martin, R.E., et al., *Detailed characterization of the lipid composition of detergent-resistant membranes from photoreceptor rod outer segment membranes.* Invest Ophthalmol Vis Sci, 2005. **46**(4): p. 1147-54.

48. Babiychuk, E.B. and A. Draeger, *Biochemical characterization of detergent-resistant membranes: a systematic approach.* Biochem J, 2006. **397**(3): p. 407-16.

49. Edidin, M., *The state of lipid rafts: from model membranes to cells.* Annu Rev Biophys Biomol Struct, 2003. **32**: p. 257-83.

50. Pike, L.J., *Rafts defined: a report on the Keystone Symposium on Lipid Rafts and Cell Function.* J Lipid Res, 2006. **47**(7): p. 1597-8.

51. Brown, D.A., *Lipid rafts, detergent-resistant membranes, and raft targeting signals.* Physiology (Bethesda), 2006. **21**: p. 430-9.

52. Macdonald, J.L. and L.J. Pike, *A simplified method for the preparation of detergent-free lipid rafts.* J Lipid Res, 2005. **46**(5): p. 1061-7.

53. Pike, L.J. and L. Casey, *Localization and turnover of phosphatidylinositol 4,5-bisphosphate in caveolin-enriched membrane domains.* J Biol Chem, 1996. **271**(43): p. 26453-6.

54. Moran, M. and M.C. Miceli, *Engagement of GPI-linked CD48 contributes to TCR signals and cytoskeletal reorganization: a role for lipid rafts in T cell activation.* Immunity, 1998. **9**(6): p. 787-96.

55. Brown, D.A. and E. London, *Structure and function of sphingolipid- and cholesterol-rich membrane rafts.* J Biol Chem, 2000. **275**(23): p. 17221-4.

56. Pike, L.J., *Lipid rafts: heterogeneity on the high seas.* Biochem J, 2004. **378**(Pt 2): p. 281-92.

57. Oliferenko, S., et al., *Analysis of CD44-containing lipid rafts: Recruitment of annexin II and stabilization by the actin cytoskeleton.* J Cell Biol, 1999. **146**(4): p. 843-54.

58. Valensin, S., et al., *F-actin dynamics control segregation of the TCR signaling cascade to clustered lipid rafts.* Eur J Immunol, 2002. **32**(2): p. 435-46.

59. Sukow, C. and D.J. DeRosier, *Order, disorder, and perturbations in actin-aldolase rafts.* Biophys J, 2003. **85**(1): p. 525-36.

60. Bodin, S., et al., *Integrin-dependent interaction of lipid rafts with the actin cytoskeleton in activated human platelets.* J Cell Sci, 2005. **118**(Pt 4): p. 759-69.

61. Simpson-Holley, M., et al., *A functional link between the actin cytoskeleton and lipid rafts during budding of filamentous influenza virions.* Virology, 2002. **301**(2): p. 212-25.

62. Wickstrom, S.A., K. Alitalo, and J. Keski-Oja, *Endostatin associates with lipid rafts and induces reorganization of the actin cytoskeleton via down-regulation of RhoA activity.* J Biol Chem, 2003. **278**(39): p. 37895-901.

63. Sandgren, S., et al., *The human antimicrobial peptide LL-37 transfers extracellular DNA plasmid to the nuclear compartment of mammalian cells via lipid rafts and proteoglycan-dependent endocytosis.* J Biol Chem, 2004. **279**(17): p. 17951-6.

64. Pietiainen, V., et al., *Echovirus 1 endocytosis into caveosomes requires lipid rafts, dynamin II, and signaling events.* Mol Biol Cell, 2004. **15**(11): p. 4911-25.

65. Heino, S., et al., *Dissecting the role of the golgi complex and lipid rafts in biosynthetic transport of cholesterol to the cell surface.* Proc Natl Acad Sci U S A, 2000. **97**(15): p. 8375-80.

66. Marwali, M.R., et al., *Lipid rafts mediate association of LFA-1 and CD3 and formation of the immunological synapse of CTL.* J Immunol, 2004. **173**(5): p. 2960-7.

67. Tavano, R., et al., *CD28 interaction with filamin-A controls lipid raft accumulation at the T-cell immunological synapse.* Nat Cell Biol, 2006. **8**(11): p. 1270-6.

68. Tavano, R., et al., *CD28 and lipid rafts coordinate recruitment of Lck to the immunological synapse of human T lymphocytes.* J Immunol, 2004. **173**(9): p. 5392-7.

69. Burack, W.R., et al., *Cutting edge: quantitative imaging of raft accumulation in the immunological synapse.* J Immunol, 2002. **169**(6): p. 2837-41.

70. Dykstra, M., et al., *Location is everything: lipid rafts and immune cell signaling.* Annu Rev Immunol, 2003. **21**: p. 457-81.

71. Katsumata, O., et al., *Association of FcgammaRII with low-density detergent-resistant membranes is important for cross-linking-dependent initiation of the tyrosine phosphorylation pathway and superoxide generation.* J Immunol, 2001. **167**(10): p. 5814-23.

72. Garcia-Garcia, E., E.J. Brown, and C. Rosales, *Transmembrane mutations to FcgammaRIIA alter its association with lipid rafts: implications for receptor signaling.* J Immunol, 2007. **178**(5): p. 3048-58.

73. Tolentino, T., Zarnitsin, V., Selvarah, P., Dustin, M., Zhu,C., *Measuring ligand diffusivity and receptor binding kinetics within a cell membrane contact area*, in *Bioengineering*. 2002, Georgia Institute of Technology: Atlanta.

74. Jianhua Wu, Y.F., Veronika I. Zarnitsyna, Timothy P. Tolentino, Michael L. Dustin, and Cheng Zhu., *A coupled diffusion-kinetics model for analysis of contact area frap experiment.* Submitted to biophysical journal, 2007).

75. Badizadegan, K., et al., *Floating cholera toxin into epithelial cells: functional association with caveolae-like detergent-insoluble membrane microdomains.* Int J Med Microbiol, 2000. **290**(4-5): p. 403-8.

76. Blank, N., et al., *Cholera toxin binds to lipid rafts but has a limited specificity for ganglioside GM1.* Immunol Cell Biol, 2007.

77. Shogomori, H. and A.H. Futerman, *Cholera toxin is found in detergent-insoluble rafts/domains at the cell surface of hippocampal neurons but is internalized via a raft-independent mechanism.* J Biol Chem, 2001. **276**(12): p. 9182-8.

78. Janes, P.W., et al., *The role of lipid rafts in T cell antigen receptor (TCR) signalling.* Semin Immunol, 2000. **12**(1): p. 23-34.

79. Bainton, D.F., et al., *Rapid fragmentation and reorganization of Golgi membranes during frustrated phagocytosis of immobile immune complexes by macrophages.* Am J Pathol, 1989. **134**(1): p. 15-26.

80. Kato, T., et al., *Influence of staphylococcal lipoteichoic acid on the frustrated phagocytosis of neutrophils against opsonized corneocytes.* Exp Dermatol, 1993. **2**(4): p. 171-4.

81. Takemura, R., et al., *Rapid redistribution of clathrin onto macrophage plasma membranes in response to Fc receptor-ligand interaction during frustrated phagocytosis.* J Cell Biol, 1986. **102**(1): p. 55-69.

82. Chesla, S.E., P. Selvaraj, and C. Zhu, *Measuring two-dimensional receptor-ligand binding kinetics by micropipette.* Biophys J, 1998. **75**(3): p. 1553-72.

83. Yanaga, F., et al., *Syk interacts with tyrosine-phosphorylated proteins in human platelets activated by collagen and cross-linking of the Fc gamma-IIA receptor.* Biochem J, 1995. **311 (Pt 2)**: p. 471-8.

84. Sofer, A. and A.H. Futerman, *Cationic amphiphilic drugs inhibit the internalization of cholera toxin to the Golgi apparatus and the subsequent elevation of cyclic AMP.* J Biol Chem, 1995. **270**(20): p. 12117-22.

85. Rosenwald, A.G. and R.E. Pagano, *Inhibition of glycoprotein traffic through the secretory pathway by ceramide.* J Biol Chem, 1993. **268**(7): p. 4577-9.

86. Baggiolini, M., M.E. Feigenson, and H.P. Schnebli, *Ricin- and concanavalin A-binding sites on the surface of polymorphonuclear leukocytes have no receptor function in phagocytosis.* Schweiz Med Wochenschr, 1976. **106**(40): p. 1371-2.

87. Feigenson, M.E., M. Baggiolini, and H.P. Schnebli, *Capping of concanavalin A- or ricin-binding sites does not influence phagocytosis in polymorphonuclear leukocytes.* Experientia, 1976. **32**(10): p. 1264-6.

88. Matsumoto, I., et al., *Derivatization of epoxy-activated agarose with various carbohydrates for the preparation of stable and high-capacity affinity adsorbents: their use for affinity chromatography of carbohydrate-binding proteins.* Anal Biochem, 1981. **116**(1): p. 103-10.

89. Holowka, D. and B. Baird, *Fc(epsilon)RI as a paradigm for a lipid raft-dependent receptor in hematopoietic cells.* Semin Immunol, 2001. **13**(2): p. 99-105.

90. Holowka, D., E.D. Sheets, and B. Baird, *Interactions between Fc(epsilon)RI and lipid raft components are regulated by the actin cytoskeleton.* J Cell Sci, 2000. **113 (Pt 6)**: p. 1009-19.

91. Koenigsknecht, J. and G. Landreth, *Microglial phagocytosis of fibrillar beta-amyloid through a beta1 integrin-dependent mechanism.* J Neurosci, 2004. **24**(44): p. 9838-46.

92. Rosenblatt, J., et al., *Myosin II-dependent cortical movement is required for centrosome separation and positioning during mitotic spindle assembly.* Cell, 2004. **117**(3): p. 361-72.

93. Shu, S., X. Liu, and E.D. Korn, *Blebbistatin and blebbistatin-inactivated myosin II inhibit myosin II-independent processes in Dictyostelium.* Proc Natl Acad Sci U S A, 2005. **102**(5): p. 1472-7.

LIST OF FIGURES

FIGURE LEGEND

Figure 1 Experimental Model

A: A K562 cell floats about the IgG labeled glass-supported lipid bilayer.
B: After the cell comes within binding proximity, receptor-ligand binding begins.
C: The depletion of free IgG within the area of contact creates a concentration gradient which drives the diffusion of free IgG into the contact area.
D: As more free-IgG accumulates, receptor-ligand binding continues until the system reaches a dynamic equilibrium.

Figure 2 CD32A Colocalizes With Membrane Rafts

CD32A on live K562 cells (1 x 10^6/ml) were fluorescently stained with mouse anti-CD32A (IV.3-**Fab**) IgG and Alexa Fluor 488 goat-anti-mouse IgG. Next, membrane rafts were labeled with Alexa 647 cholera toxin B. After fixation, laser-scanning confocal microscopy was used to collect fluorescent images, in 3D, of the cells. The emission of Alexa 488 and 633 were pseudo colored green and red, respectively.

From the z-stack series three observations are worth noting: 1) red fluorescence appears on every plane, 2) lone green fluorescence is not seen at all, 3) the pattern of fluorescence acquired is as expected from a sphere with a fluorescently labeled surface.

A 3D image made from reconstructing the z-stack series (row II) shows the position of CD32A in the left panel, membrane rafts as indicated by red in the middle panel, and the merged image in the right panel. As inferred from the z-stack, there are more membrane rafts than clusters of CD32A, and there appears to be complete colocalization of CD32A with membrane rafts.

This experiment was performed three times under identical conditions. Three images were collected from each trial (n = 9).

Figure 3 CD32A Colocalizes With Membrane Rafts in Pre-fixed K562 Cells

K562 cells (1 x 10^6/ml) cells were fixed and fluorescently labelled as previously described.

As before, the data shows: 1) red fluorescence appears on every plane, 2) lone green fluorescence is not seen at all, 3) The pattern of fluorescence acquired is as expected from a sphere with a fluorescently labelled surface.

As before, the 3D image made from reconstructing the z-stack series (row II) shows the position of CD32A in the left panel, membrane rafts as indicated by red in the middle panel, and the merged image in the right panel. Once again, there are more membrane rafts than clusters of CD32A, and there appears to be complete colocalization of CD32A with membrane rafts.

Given that cell membranes become rigid during fixation and that the CD32A clusters and membrane rafts on K562 cells fixed prior to fluorescent labelling have the same spatial relationship as those on K562 cells that were fixed after fluorescent labelling, it is evident that the size, location and existence of CD32A clusters and membrane rafts were unaffected by cholera toxin B binding.

This experiment was performed three times under identical conditions. Three images were collected from each trial (n = 9).

Figure 4 CD32A Colocalizes With Membrane Rafts CHO-CD32A^{TM} Cells

CHO-CD32A^{TM} cells (1 x 10^6/ml) cells were prepared for colocalization measurements as previously described, with fixation before fluorescent staining.

As with the K562 cells, the CD32A clusters and membrane rafts of CHO-CD32A^{TM} cells appear to have the same spatial relationships as those found on the K562 cells, which is to say:

1) red fluorescence appears on every plane, 2) lone green fluorescence is not seen at all, 3) the pattern of fluorescence acquired is as expected from a sphere with a fluorescently labelled surface.

As before, the 3D image made from reconstructing the z-stack series (row II) shows the position of CD32A in the left panel, membrane rafts as indicated by red in the middle panel, and the merged image in the right panel. Once again, there are more membrane rafts than clusters of CD32A, and there appears to be complete colocalization of CD32A with membrane rafts.

This experiment was performed three times under identical conditions. Three images were collected from each trial (n = 9).

Figure 5 CD32A Colocalizes With Membrane Rafts on CHO-CD32AGPI Cells

CHO CD32A^{GPI} cells (1 x 10^6/ml) cells were prepared for colocalization measurements as previously described, with fixation before fluorescent staining.

As with the K562 cells, the CD32A clusters and membrane rafts of CHO-CD32A^{GPI} cells appear to have the same spatial relationships as those found on the K562 cells, which is to say:

1) red fluorescence appears on every plane, 2) lone green fluorescence is not seen at all, 3) the pattern of fluorescence acquired is as expected from a sphere with a fluorescently labelled surface.

As before, the 3D image made from reconstructing the z-stack series (row II) shows the position of CD32A in the left panel, membrane rafts as indicated by red in the middle panel, and the merged image in the right panel. Once again, there are more membrane rafts than clusters of CD32A, and there appears to be complete colocalization of CD32A with membrane rafts.

This experiment was performed three times under identical conditions. Three images were collected from each trial (n = 9).

Figure 6 Cholesterol depletion disrupts CD32A Clusters and Membrane Rafts

K562 cells (5 x 10^6/ml) were incubated in PBS with 5mM HEPES containing 10 mM_MβCD for 30 minutes at 37^0 C. After washing, the cells were fixed and fluorescently stained as previously described.

The z-stack series (row 1) shows the presence of red fluorescence, indicating the position of sphingomyelin, its presence in every panel suggesting that sphingomyelin is present over the entire surface of the cell. However, there is a near complete absence of the color yellow, indicating colocalization between CD32A and membrane rafts. The image (row 2) mirrors this data and furthermore shows the near complete absence of CD32A from the cell surface. It also appears that sphingomyelin is more dispersed rather than clustered.

It is possible that MβCD extracted the CD32A clusters along with the cholesterol, which would explain both the absence of CD32A and the dispersion of sphingomyelin.

This experiment was performed three times under identical conditions. Three images were collected from each trial (n = 9).

Figure 7 Oxidation of Cholesterol Disperses CD32A Clusters and Membrane Rafts

K562 cells (1 x 10^6/ml) cells were incubated at 37ºC in standard culture media, RPMI with 10% FBS, that contained 1.4 units/ml cholesterol oxidase. After washing, the cells were fixed and fluorescently labeled as previously described.

The effect of membrane raft disruption via oxidation of cell surface cholesterol to cholesterone is readily apparent in the z-stack series. Both the red and the green fluorescence are apparent in every tile, and more importantly there is no sign of colocalization as evident by the lack of yellow clusters or patches.

The image (row II) mirrors these findings as both green and red fluorescence are present, but the merged image suggests only a sparse amount of colocalization.

This experiment was performed three times under identical conditions. Two images were collected from each trial (n = 6).

Figure 8 Colocalization of Membrane Rafts and anti-DNP IgG at 3 Minutes

Live K562 cells were stained with Alexa Fluor 633 Cholera Toxin B and injected into an FCS2 flow chamber in which the base was a GSLB labeled with Alexa 488 anti-dnp IgG. At 3 minutes, formalin was injected to wash out non-adherent cells and fix those with contact areas. After 10 minutes, z-stack series of fluorescent images were acquired. Fluorescent emission of Alexa 647 and Alexa 488 were pseudo colored red and green, respectively.

The area of intense green indicates accumulation of anti-dnp IgG within the area of contact between the cell and the GSLB. While membrane rafts are present in every tile of the z-stack series, it is apparent that their concentration at 9.75, 10.50, and 11.25 μm points are very low, as indicated by the low intensity of red fluorescence. Of significant note is the presence of membrane rafts on the bottom plane, Z =0.0 μm. In the profile view of the image, the cell appears to be tilted. At three minutes, the contact area is not well established and lacks the strength to hold the cell firmly in place. In **Figure 9** the cell position is adjusted.

This experiment was performed three times under identical conditions. A total of seven images were collected (n = 7).

Figure 9 Colocalization of Membrane Rafts and anti-DNP IgG at 3 Minutes w/o Tilt

Live K562 cells were stained with Alexa Fluor 633 Cholera Toxin B as previously described and injected into an FCS2 flow chamber in which the base was a GSLB labeled with Alexa 488 anti-dnp IgG. At 3 minutes, formalin was injected into the chamber to fix cells with contact areas.

In row II the 3D reconstruction is adjusted. The cell image has been rotated back to the upright position, making it easier to see that the top of the cell, rather than the side, has a low concentration rafts, confirming the observation made in the z-stack series - the top of the cell has a lower concentration of rafts as indicated by the significantly diminished red fluorescence.

Figure 10 Colocalization of Membrane Rafts and anti-DNP IgG at 9 to 12 Minutes

Live K562 cells were stained with Alexa Fluor 633 Cholera Toxin B and injected into an FCS2 flow chamber in which the base was a GSLB labeled with Alexa 488 anti-dnp IgG. At 9 minutes, formalin was injected into the chamber to fix cells with contact areas. A z-stack series of fluorescent images was then collected via laser-scanning fluorescent confocal microscopy. Fluorescence from the membrane raft marker Alexa 647 was pseudo colored red, and fluorescence from Alexa Fluor 488 goat anti-mouse / IV.3 Fab was pseudo colored green.

By 9 to 12 minutes into contact area formation, it is easy to see the significantly diminished presence of membrane rafts from the cell surface, with a proportionate increase in the concentration of membrane rafts within the contact area. The 3D view reflects what is seen in the z-stack series: 1) the increase in size of the contact area as indicated by the increased area of bright green fluorescence; 2) the decrease in membrane raft from the cell surface, in particular from the upper part of the cell surface, away from the contact area; 3) the increase in membrane rafts within the contact area. Note that the brightest red fluorescence occurs below 4.0 μm.

The data suggest that membrane rafts and CD32A are moving towards the contact area over time.

For both time points, the experiment was performed three times under identical conditions. Three images were collected from each trial.

Figure 11 Cholesterol Extraction by MβCD Treatment Affects Contact Area Size

K562 cells were treated with different concentrations of MβCD (0.0 -10 μM) before being used to form contact areas as previously described.

As can be seen from the data, the size of the contact area decreases as the concentration of MβCD used to treat the cells increases. This data supports the idea that membrane rafts are required for contact area formation.

For each data set, experiments were run a minimum of three times. All experimental trials were run in parallel with a positive control using the same protocol, preparation, and cell group. With the exception of MβCD treatment all other conditions were kept constant.

Figure 12 Flow Cytometry Analysis of Chemically Treated K562 Cells

K562 cells ($1x10^6$/ml) were chemically treated with or without cholesterol oxidase (1.4 mM), washed twice, and then immuno-fluorescently stained by incubation with primary antibody mouse anti-CD32A IgG and secondary antibody Alexa 488 labeled anti-mouse IgG. For the negative control, a non-relevant mouse IgG was used as the primary antibody. Flow cytometry analysis was performed to determine CD32A expression level. For each sample, ten thousand events were collected.

No significant differences in CD32A expression level are apparent.

Figure 13 Adhesion Frequencies of K562 Cells to RBCs

Micropipette experiments were run with K562 cells with and without chemical treatment. These experiments were all run simultaneously. For each category, the experiment was run five times, each with a sample size of fifty. Ergo, n = 250 for each experimental data set.

Figure 14 Latrunculin A Treatment Affects Contact Area Size

K562 cells (1×10^6/ml) were incubated in RPMI/10% FBS containing various concentrations of Latrunculin A (0.0 - 100 μM) for 30 minutes at 37 ^{0}C. Cells were washed and allowed to form contact areas as previously described, with the only difference being the presence of Latrunculin A in the HBSS, in which the cells were re-suspended.

Contact area size was measured at the one hour time-point. The contact area's size decreased in proportion to the increase in concentration of Latrunculin A.

For each data set, experiments were run a minimum of four times. Trials with Latrunculin A treatment were run in parallel with a positive control using the same protocol, preparation, and cell group. With the exception of Latrunculin A treatment all other conditions were kept constant.

Figure 15 Blebbistatin Inhibition Abrogates Contact Area Formation

These experiments were repeated three times simultaneous with a positive control using the same protocol, preparation, and cell group. With the exception of Blebbistatin treatment all other conditions were kept constant.

Figure 16 PO_4-Y and SYK in Contact Area Formation at Three Minutes

Contact area formation was carried out as previously described, but with non-fluorescent anti-dnp IgG. The signaling protein SYK was labeled with primary donkey anti-SYK IgG and secondary mouse FITC anti-donkey. Phosphorylated tyrosine (PO_4-Y) was labeled with primary antibody mouse anti-PO_4-Y and secondary antibody Alexa 647 anti-mouse IgG.

The z-stack images (row I) show the presence of SYK, indicated by yellow patches, from 0.0 μm to 2.8 μm. It also shows the presence of PO_4-Y from 0.0 μm to 5.6 μm. The fluorescence is brightest at 0.70 μm, at which point it begins to decrease until it fades altogether around 7.0μm.

The presence of these molecules in and above the contact area is significant in that it suggests that signaling begins at the initial site of contact.

This experiment was performed three times under identical conditions. Three images were collected from each trial (n = 9).

Figure 17 PO_4-Y and SYK in Contact Area Formation at Nine Minutes

Contact area formation and fluorescent labeling were accomplished as described in **Figure 8**. The z-stack images clearly show fluorescence from both fluorophores from 0.65 μm to 11.05 μm, with the brightest region of fluorescence being between 3.25 μm and 7.15 μm. The absence of fluorescence at 0.0 μm and only light fluorescence apparent until 2.60 μm is significant in that it indicates a movement of SYK and PO4-Y from the contact area to the interior of the cell.

At 9 minutes, SYK and PO4-Y are present in a much larger region than they are at 3 minutes. Furthermore, they appear to be moving inwards.

This experiment was performed three times under identical conditions. Three images were collected from each trial (n = 9).

Figure 18 SYK in Contact Area Formation at Thirty

K562 cells were used to form contact areas as previously described, using non-fluorescent anti-dnp IgG in place of its fluorescent version. The cells were fixed at 30 minutes and then stained for SYK by incubation with primary antibody donkey anti-SYK IgG and secondary antibody mouse FITC anti-donkey IgG.

The right column shows a z-stack series of fluorescent images captured from a cell fixed at thirty minutes into contact area formation. The middle column shows a profile view (top row) and a bottom view (second row) of an image made by reconstruction of the z-stack.

From the profile and bottom view of the image, we can discern that SYK is accumulated to a high concentration in the region of the contact area. A very interesting find is the straight and narrow band of SYK which extends from the contact area to roughly 10 μm into the cell. Also of note is the bulls-eye like pattern consisting of a ring of SYK around a circular space void of fluorescence.

From the profile and bottom view of the image, we can discern that SYK is accumulated to a high concentration in the region of the contact area. A very interesting find is the straight and narrow band of SYK which extends from the contact area to roughly 10 μm into the cell. Also of note is the bulls-eye like pattern consisting of a ring of SYK around a circular space void of fluorescence.

The images in the z-stack give a more precise description, however it does indeed confirm what is observed in the image. At 0.0 and 1.0 μm the ring of SYK fluorescence is not only visible but very intense. At 2 μm approximately a quarter of the ring is visible but still intense. Beginning at 3.0 μm we see a dot of fluorescence over what would be the upper left-hand side of the ring. This dot of fluorescence is present all the way up the z-axis and is clearly what appears in the profile view as a straight and narrow band of SYK. This was observed in every sample.

Figure 19 SYK in Contact Area Formation at Sixty Minutes

K562 cells were used to form contact areas as previously described, using non-fluorescent anti-dnp IgG in place of its fluorescent version. The cells were fixed at 60 minutes and then stained for SYK by incubation with primary antibody donkey anti-SYK IgG and secondary antibody mouse FITC anti-donkey

The right column shows a z-stack series of fluorescent images captured from a cell that were fixed at thirty minutes into contact area formation. The middle column shows a profile view (top row) and a bottom view (second row) of a image made by reconstruction of the z-stack

The right column shows a z-stack of fluorescent images captured from cells that were fixed at sixty minutes into contact area formation. The middle column shows a profile view (top row) and a bottom view (second row) of a 3D image made by reconstruction of the z-stack

The bulls-eye pattern is still present at 0.0 and 1.0 μm.

Of significant note is the disappearance of straight band of SYK which previously extended inwards from the contract area. Furthermore, the appearance of small clusters of SYK randomly scattered throughout the cell. This was observed in every sample. A possible explanation for the disappearance of the SYK band is that it was sorted into lysosomes, a part of the process of phagocytosis.

This experiment was performed three times under identical conditions. A total of fifteen images were collected (n =15).

Figure 20 Internalization of Membrane Rafts From Fifteen to Thirty Minutes

Contact areas formation was monitored as described in **Figure 20**. Again, the area of intense green indicates the accumulation of anti-dnp IgG into the contact area. The profile view of the 3D images, row two, shows the almost complete absence of rafts from the cell surface and the presence of rafts inside the cell, extending from the contact area upward. This is well supported by the images in the z-stack, which show the brightest regions of red fluorescence from 0.0 to 3.0 μm, in an area not much larger than the contact area.

For both 15 and 30 minute time points, this experiment was performed three times under identical conditions. A total of 9 and 14 images were collected, respectively.

Figure 21 Internalization of Membrane Rafts from Forty-five to Sixty Minutes

Live K562 cells were stained with Alexa Fluor 633 Cholera Toxin B and injected into an FCS2 flow chamber in which the base was a GSLB labeled with Alexa 488 anti-dnp IgG. At 3 minutes, formalin was injected into the chamber to fix cells with contact areas. A z-stack series of fluorescent images was then collected via laser-scanning fluorescent confocal microscopy. Fluorescence from the membrane raft marker Alexa 647 was pseudo colored red, and fluorescence from Alexa Fluor 488 goat anti-mouse / IV.3 Fab was pseudo colored green.

The profile view of the 3D image, row II, shows the absence of rafts from the cell surface and a high concentration of rafts inside the cell. This is confirmed in the z-stack, which shows the brightest regions of red fluorescence from 8.0 to 14.0 μm from the contact area, but in an area about the same size as the contact area.

For both 45 and 60 minute time points, this experiment was performed three times under identical conditions. A total of 7 and 15 images were collected, respectively.

Figure 22 Membrane Rafts Colocalize with the Golgi Complex

The Golgi complex and membrane rafts of live K562 cells (1×10^6/ml) were fluorescently stained with Bodipy TR labeled Ceramide-BSA (a Golgi marker), Alexa Fluor 555 Cholera toxin B (a membrane raft marker), respectively. The cells were used to form contact areas as previously described.

Row I shows the profile view of 3D images reconstructed from the z-stack series shown in Row II.

Fluorescence from Bodipy TR, pseudo-colored green, is shown in the top row left panel, in which the area of intense green fluorescence clearly marks the Golgi complex. The middle panel shows fluorescence from membrane rafts. The right panel shows the merged image which clearly suggests colocalization of the membrane rafts with the Golgi complex.

The suggestion of colocalization is stronger in the z-stack series as the area of intense yellow is not only circular on the x-y plane, but also that it is limited on the z-axis within the cell, strongly suggesting colocalization within a spherical region.

Two important observations can be made from this data: 1) membrane rafts are internalized, 2) internalized membrane rafts colocalize with the Golgi complex.

This experiment was performed twice under identical conditions. A total number of seven images were collected (n=7).

Figure 23 Membrane Rafts Colocalize with the Golgi Complex but not the ER

The Golgi complex, membrane rafts, and ER of K562 cells (1×10^6/ml) were fluorescently stained with Bodipy TR labeled Ceramide-BSA (a Golgi marker), Alexa Fluor 555 Cholera toxin B, and Concanavalin A (an ER marker), respectively. The cells were then used to form contact areas as previously described

Both the 3D view and the z-stack images suggest colocalization between the Golgi and the membrane rafts, however there is no real suggestion of colocalization between the membrane rafts and the ER.

This experiment was performed three times under identical conditions. A total number of seven images were collected (n=6).

Figure 24 Colocalization between Membrane Rafts and the Golgi Complex

The 3D images from **Figure 24** are examined for colocalization between only two structures at a time. The following are structures are examined for colocalization: I) Golgi, rafts and ER, II) Golgi and rafts, III) rafts and ER, and IV) Golgi and ER, respectively.

Colocalization is apparent between the Golgi and membrane rafts, but not between the ER and either of those structures.

Figure 25 (+) Control – Phagocytosis of Opsonized μ-spheres

K562 cells and opsonized fluorescent micro-beads (diameter = 2 μm) were incubated together in standard culture media, RPMI 1640 with 10% FBS, for one hour at 37°C. The cells and beads were washed once then fixed for ten minutes in 4% formalin. After fixation, the cells and beads were washed, re-suspended in FBS, and imaged using laser-scanning confocal microscopy.

Row I shows the profile view of a 3D image made by re-constructing the fluorescent images from a z-stack. This image shows two cells that are near full to bursting. This is clear evidence that K562 cells are capable of performing phagocytosis of the opsonized fluorescent μ-spheres.

Row II shows a z-stack with the brightfield and fluorescent images merged to show the presence of μ-spheres within the cells.

This experiment as performed twice under identical conditions. A total of four images were collected (n=4).

Figure 26 (-) Control – Phagocytosis of Non-opsonized μ-spheres

The previous experiment, positive control, was repeated but with non-opsonized μ-spheres.

Both the z-stack and the 3D image show that the cell is void of μ-spheres, giving clear evidence that the target must be opsonized with IgG before phagocytosis by K562 cells is possible.

This experiment as performed twice under identical conditions, in parallel with the positive control. A total of four images were collected (n=4).

Figure 27 Phagocytosis of opsonized μ-spheres – Latrunculin A

A quick inspection of the 3D image reveals a significantly diminished concentration of micro-beads within the cell, while the z-stack image gives an even clearer idea of how few micro-beads have actually been internalized.

This data provides clear evidence that disruption of the cell's actin cytoskeleton by treatment with Latrunculin A significantly impairs phagocytosis.

This experiment as performed twice under identical conditions, in parallel with the positive control. A total of four images were collected (n=4).

Figure 28 Phagocytosis of Opsonized μ-spheres – Cholesterol Oxidase

A quick inspection of the 3D image reveals a significantly diminished concentration of micro-beads within the cell.

The z-stack image gives an even clearer idea of how few micro-beads have actually been internalized.

This data provides clear evidence that oxidation of cell surface cholesterol by treatment with cholesterol oxidase significantly impairs phagocytosis, most likely due to the disruption of membrane rafts.

This experiment as performed twice under identical conditions, in parallel with the positive control. A total of four images were collected (n=4).

Figure 29 Phagocytosis of Opsonized μ-spheres – Sphingomyelinase

The z-stack image shows the absence of fluorescent micro-beads within the cell. The only noticeable fluorescence is outside of the cell against its surface. The profile view of the 3D image confirms what is shown in the z-stack as there is only one spot of fluorescence which comes from the fluorescent micro-bead on the outside of the cell.

This provides clear evidence that hydrolysis of cell-surface sphingomyelin by treatment with sphingomyelinase drastically impairs phagocytosis, most likely due to the disruption of membrane rafts.

This experiment as performed twice under identical conditions, in parallel with the positive control. A total of four images were collected (n=4).

Figure 30 Phagocytosis of opsonized μ-spheres – PTK Inhibitor

The z-stack image indicates the presence of sparse but scattered fluorescent μ-spheres within the cell. The profile view of the 3D image confirms what is shown in the z-stack.

This provides clear evidence that inhibition of cell signaling, within K562 cells, with PTK significantly reduces phagocytosis.

This experiment as performed twice under identical conditions, in parallel with the positive control. A total of four images were collected (n=4).

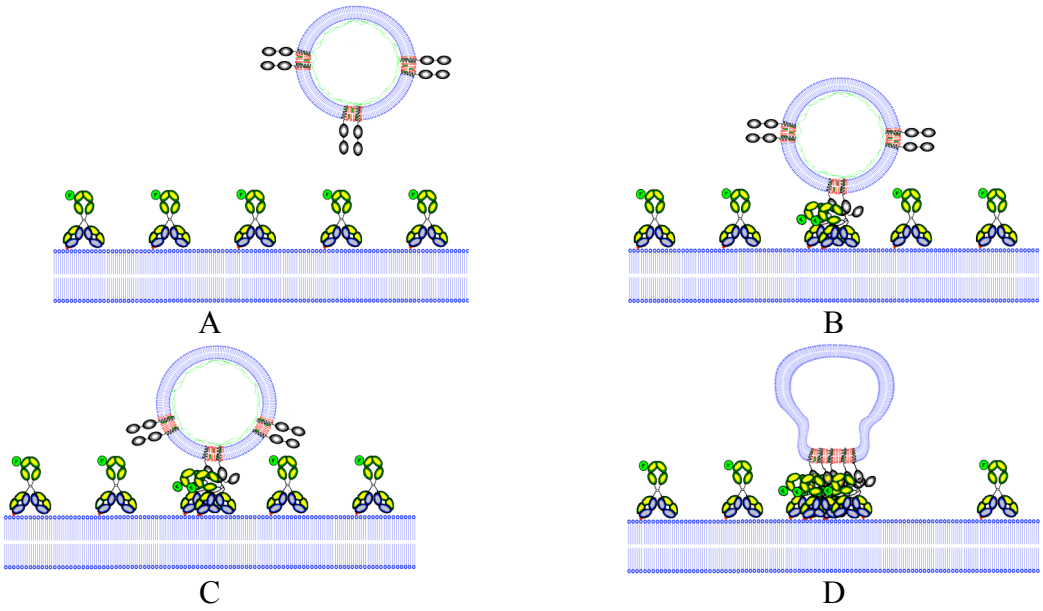

Figure 1 Experimental Model

Z-Stack of K562 cells with fluorescently labeled membrane rafts and CD32A

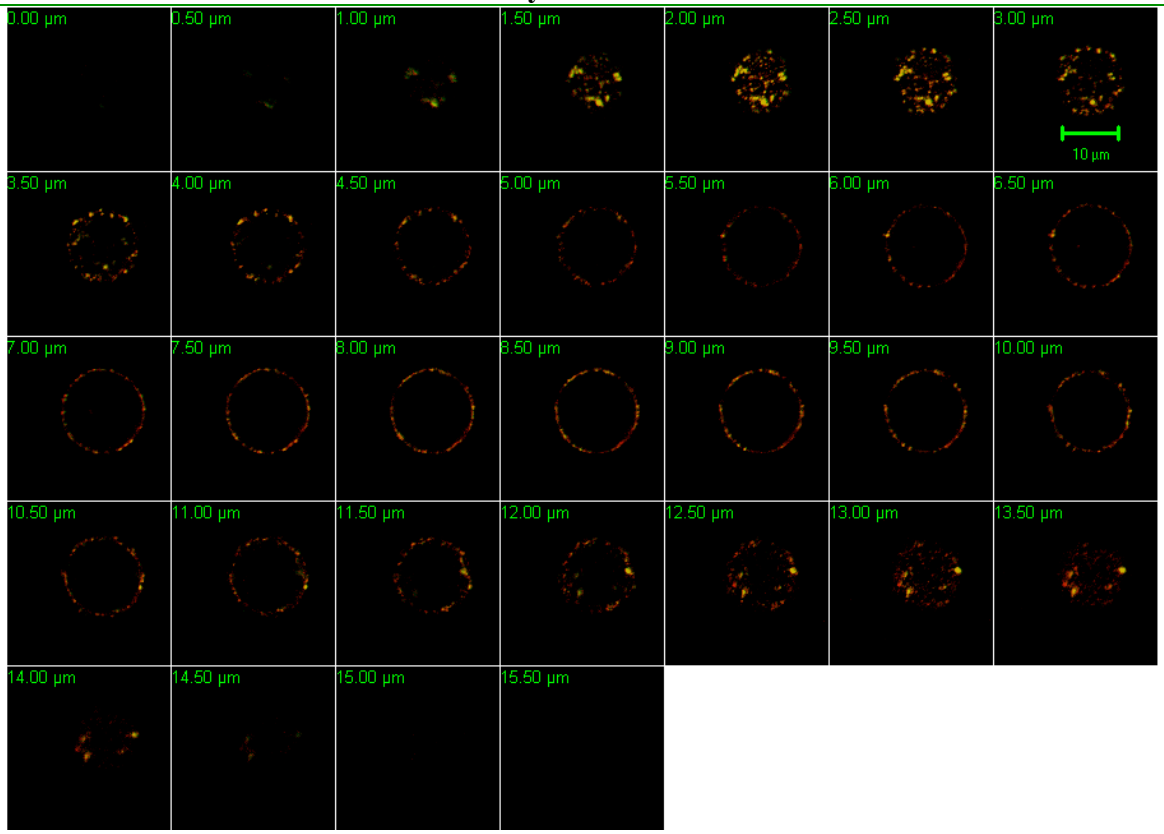

Alexa Fluor 488 goat anti-mouse IgG **Alexa 647 cholera toxin B** **Merged**

K562 CD32A

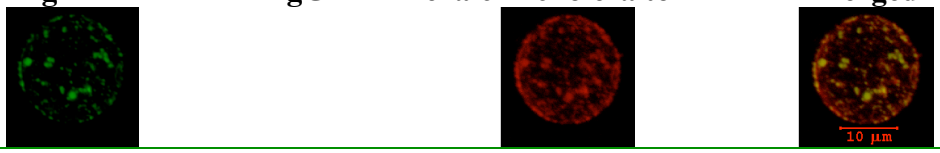

Figure 2 CD32A Colocalizes With Membrane Rafts

Z-Stack of Pre-fixed K562 cells with fluorescently labeled membrane rafts and CD32A

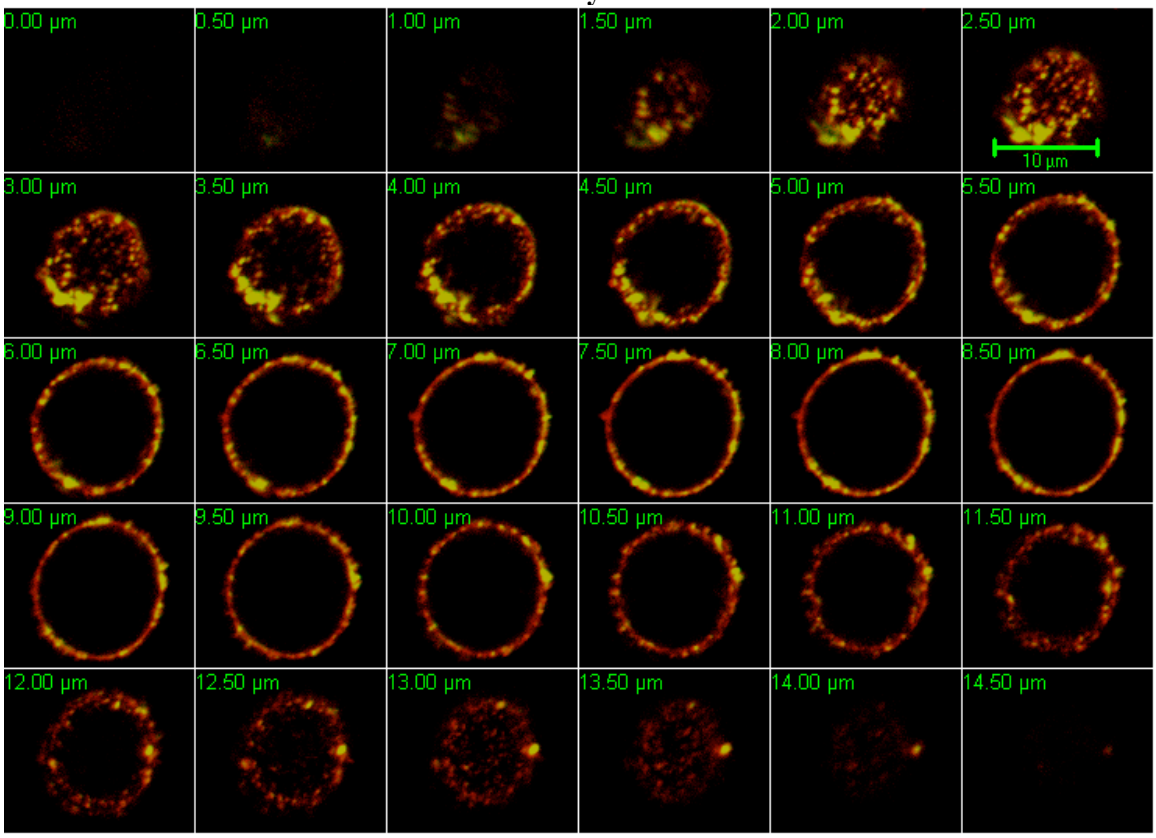

Alexa Fluor 488 goat anti-mouse IgG **Alexa 647 cholera toxin B** **Merged**

K562 CD32A

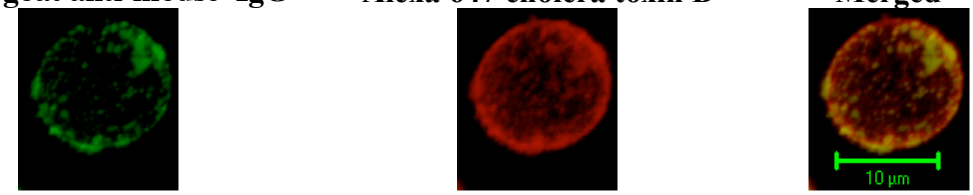

Figure 3 CD32A Colocalizes With Membrane Rafts in Pre-fixed K562 cells

Z-stack of CHO CD32A™ with fluorescently labeled membrane rafts and CD32A

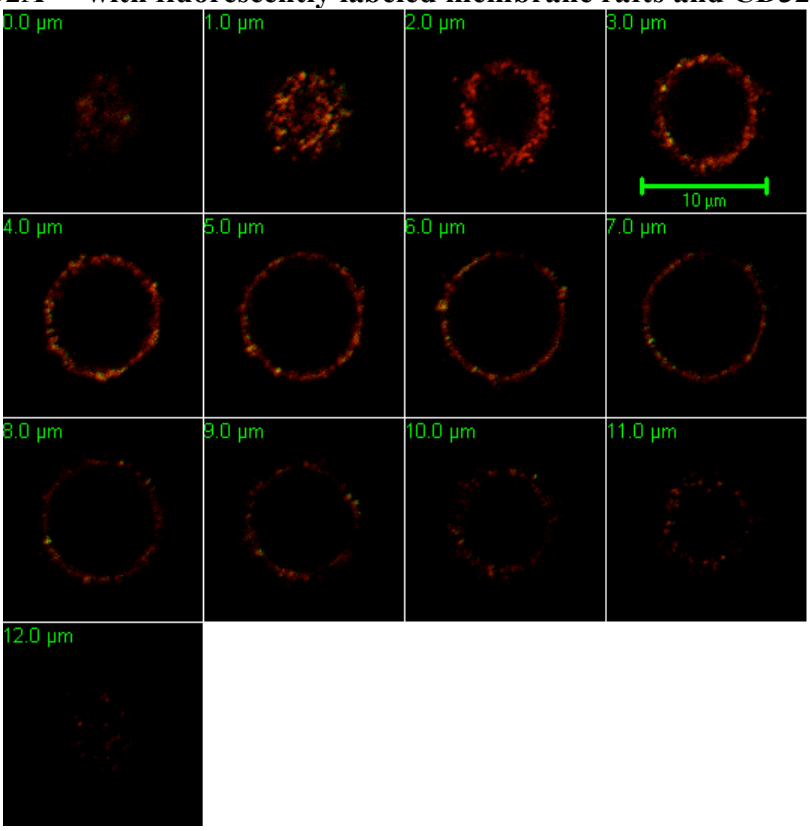

Alexa Fluor 488 goat anti-mouse IgG **Alexa 647 cholera toxin B** **Merged**

CHO-CD32A™

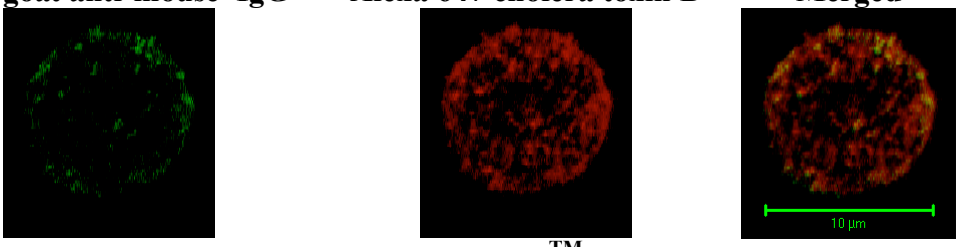

Figure 4 CD32A Colocalizes With Membrane Rafts CHO-CD32A™ cells

Z-stack of CHO CD32ATM with fluorescently labeled membrane rafts and CD32A

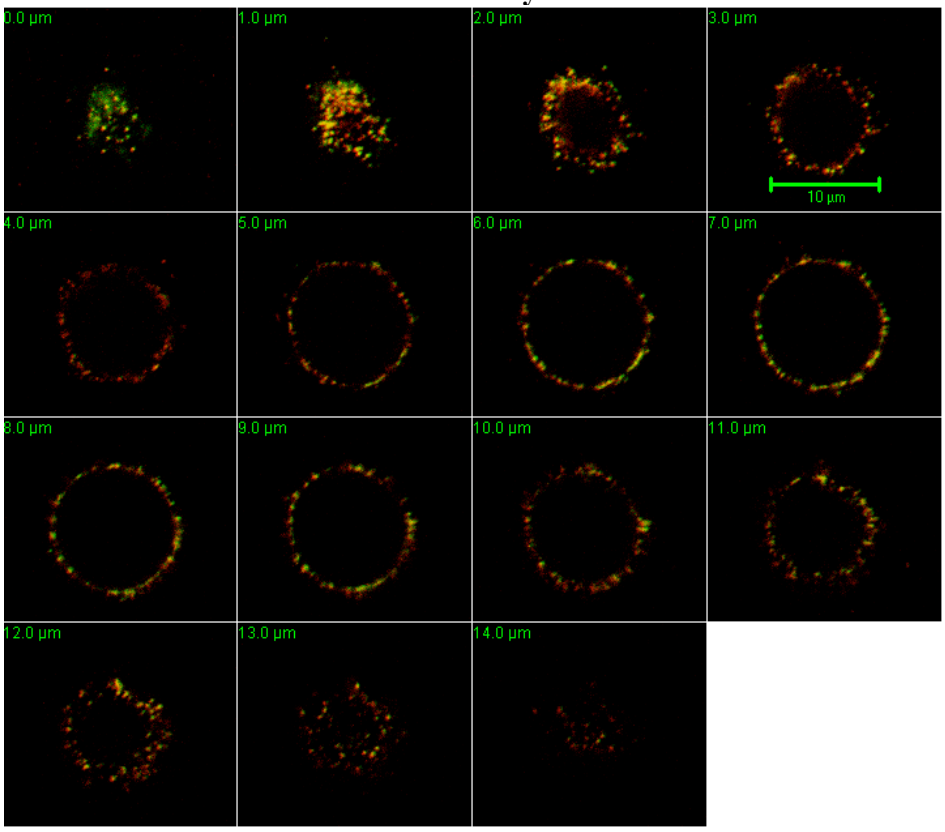

Alexa Fluor 488 goat anti-mouse IgG **Alexa 647 cholera toxin B** **Merged**

CHO-CD32A^{GPI}

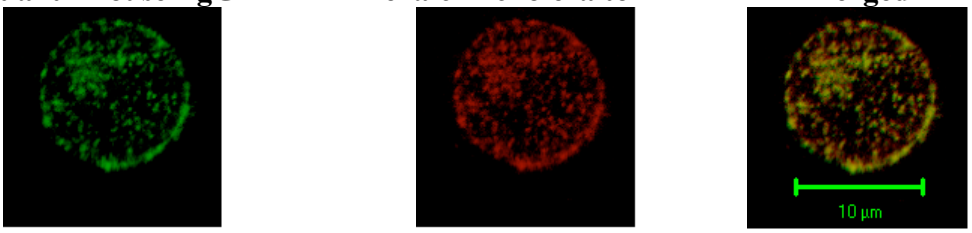

Figure 5 CD32A Colocalizes With Membrane Rafts on CHO-CD32A^{GPI} cells

Z-Stack of pre-fixed K562 cells with fluorescently labeled membrane rafts and CD32A

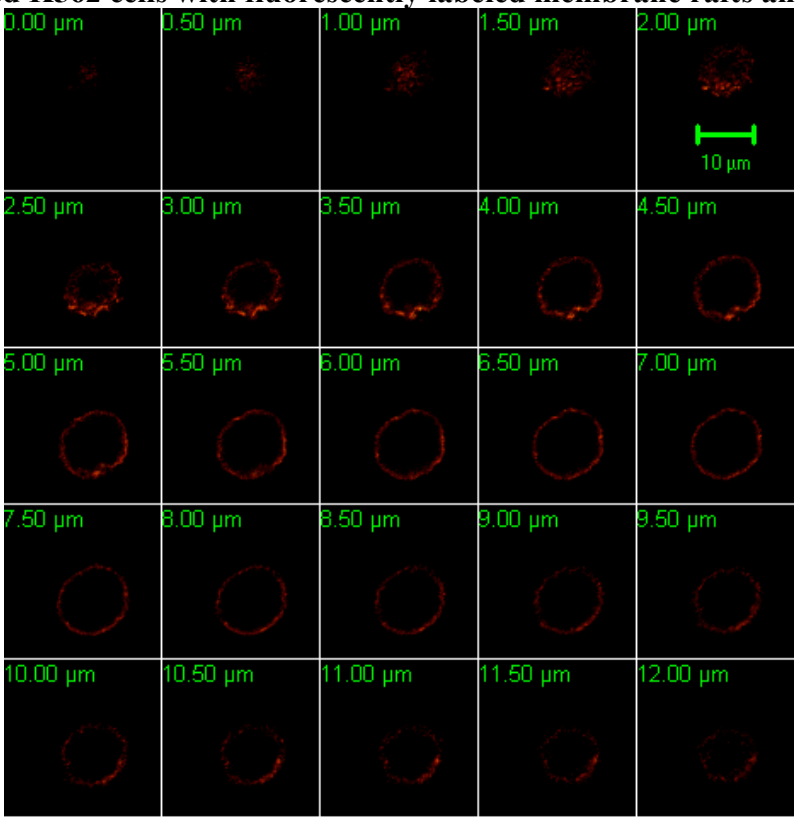

Alexa Fluor 488 goat anti-mouse IgG **Alexa 647 cholera toxin B** **Merged**

Profile View

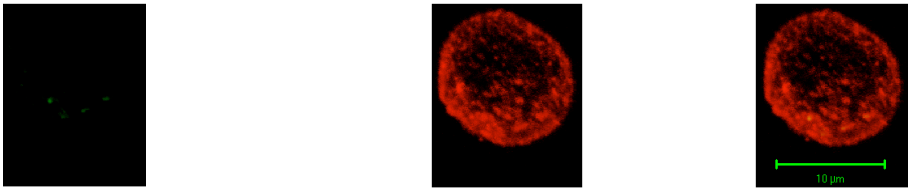

Figure 6 Cholesterol depletion disrupts CD32A clusters and Membrane Rafts

Z-Stack of K562 cells with fluorescently stained after cholesterol oxidation

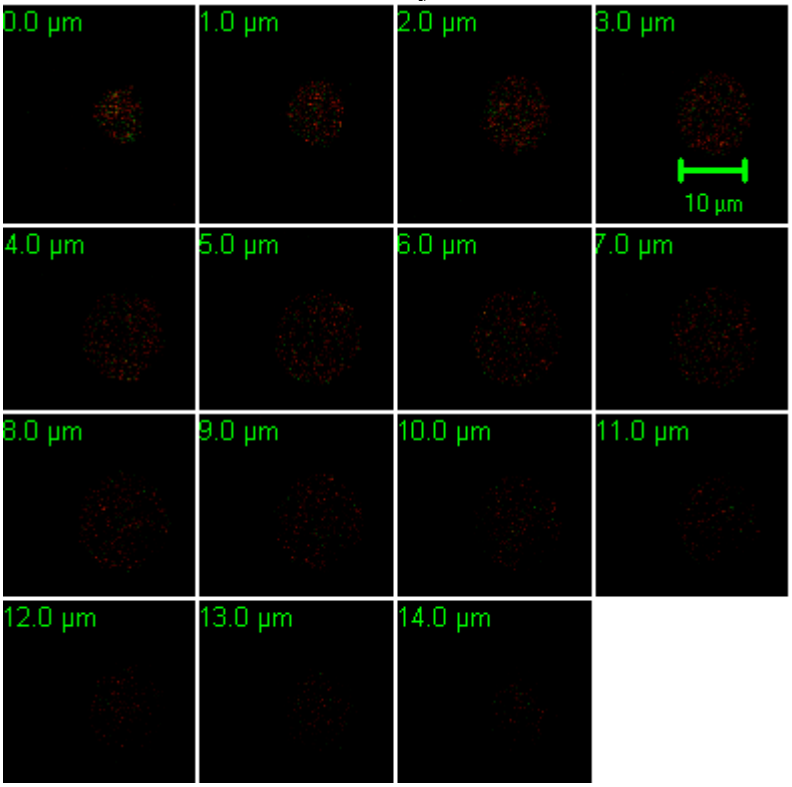

Alexa Fluor 488 goat anti-mouse IgG **Alexa 647 cholera toxin B** **Merged**

Profile view

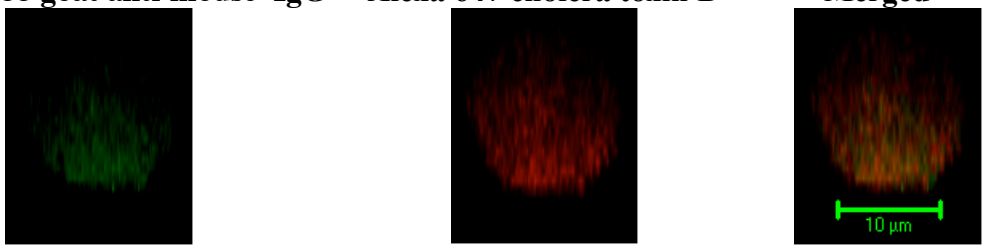

Figure 7 Oxidation of cholesterol disperses CD32A clusters and Membrane Rafts

Z-stack a K562 cell with an established contact area at three minutes

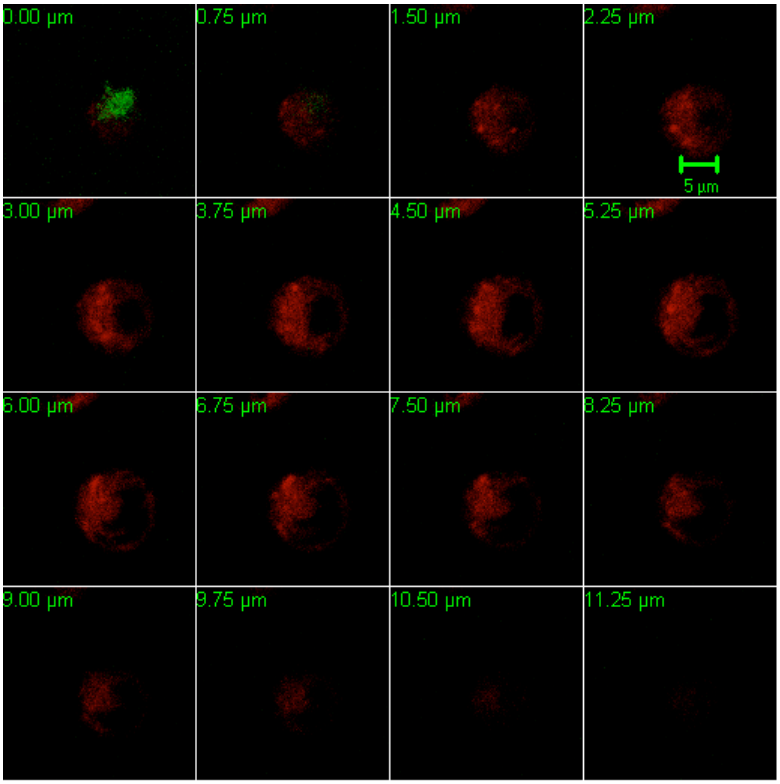

3D Profile View

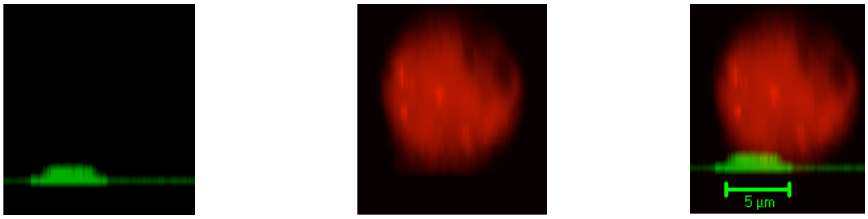

Alexa 488 anti-dnp IgG **Alexa 555 cholera toxin B** **Merged**

Figure 8 Colocalization of membrane rafts and anti-dnp IgG at 3 minutes

Z-stack a K562 cell with an established contact area at three minutes

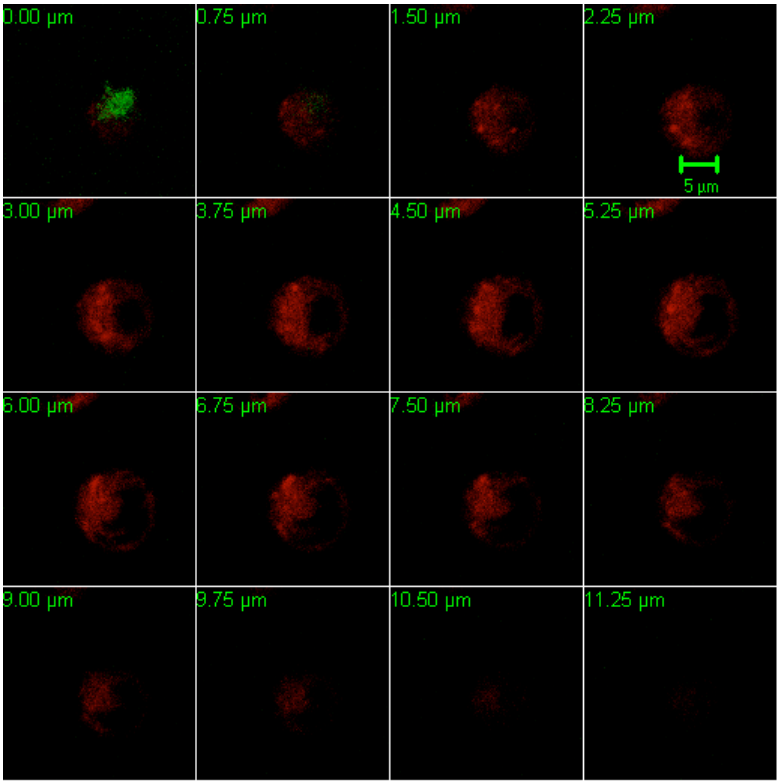

Alexa 488 anti-dnp IgG **Alexa 555 cholera toxin B** **Merged**

3D Adjusted View

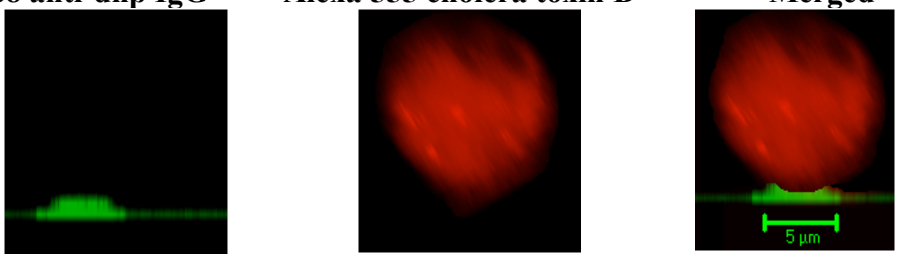

Figure 9 Colocalization of membrane rafts and anti-dnp IgG at 3 minutes

Z-stack a K562 cell with an established contact area at nine to twelve minutes

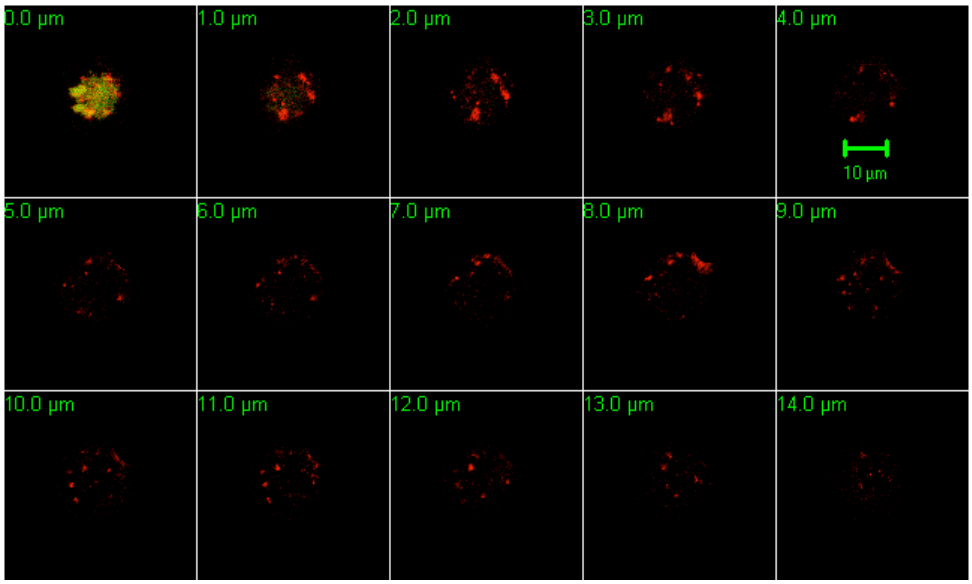

Alexa 488 anti-dnp IgG **Alexa 647 cholera toxin B** **Merged**

3D Profile View

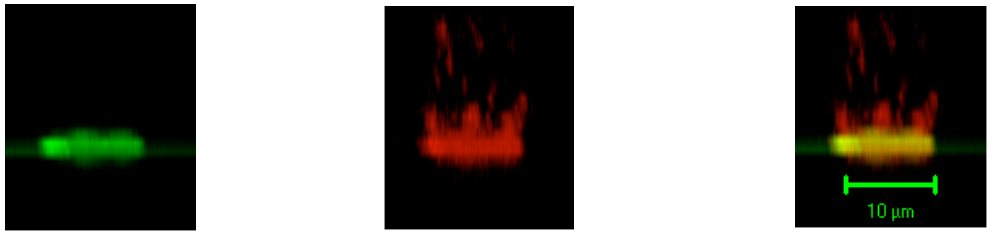

Figure 10 Colocalization of membrane rafts and anti-dnp IgG - 9 to 12 minutes

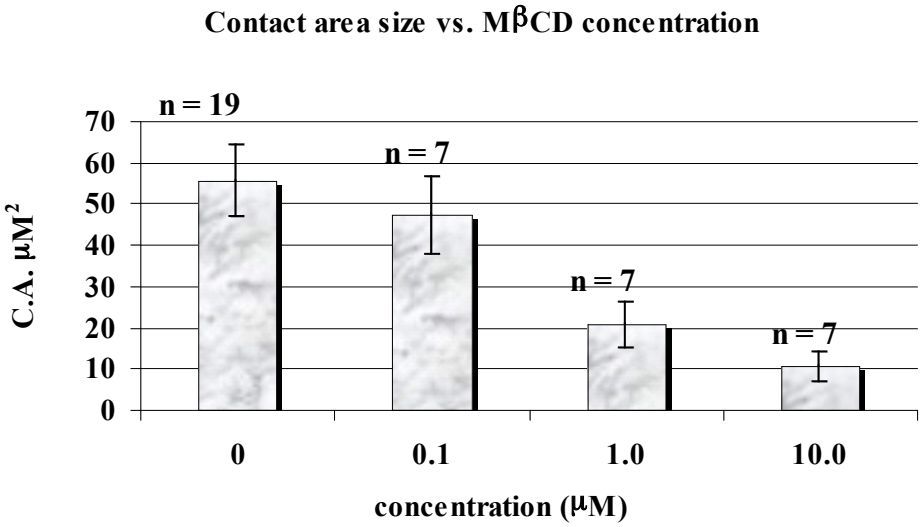

Figure 11 Cholesterol extraction by MβCD treatment affects contact area size.

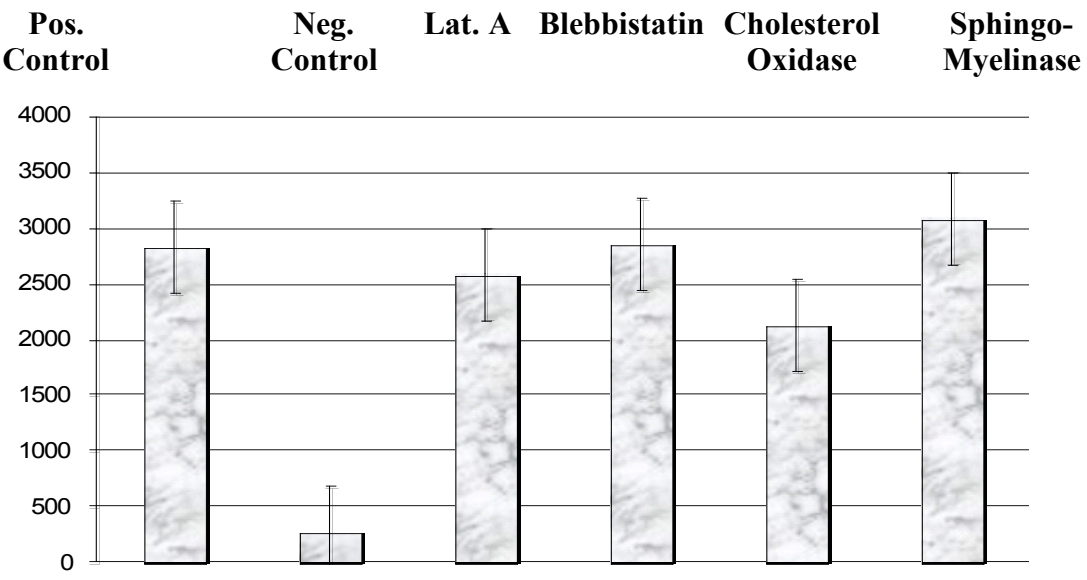

Figure 12 Flow cytometry analysis of chemically treated K562 cells

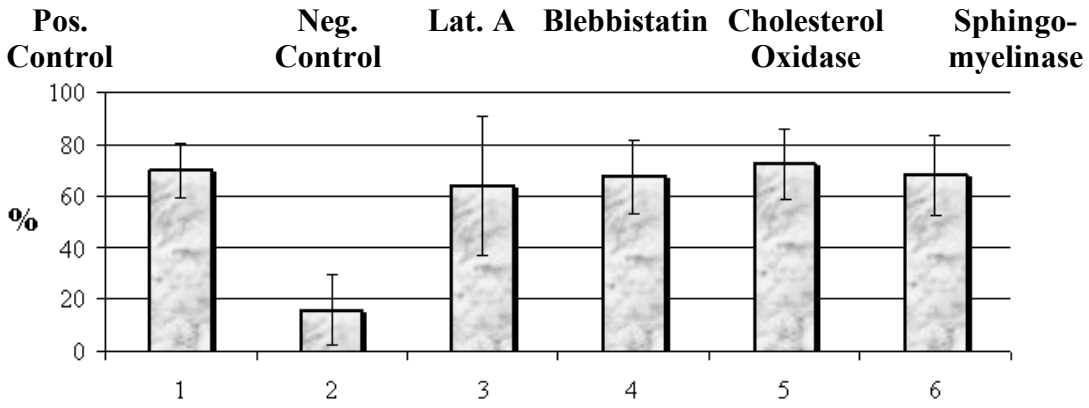

Figure 13 Adhesion frequency of K562 cells to RBCs

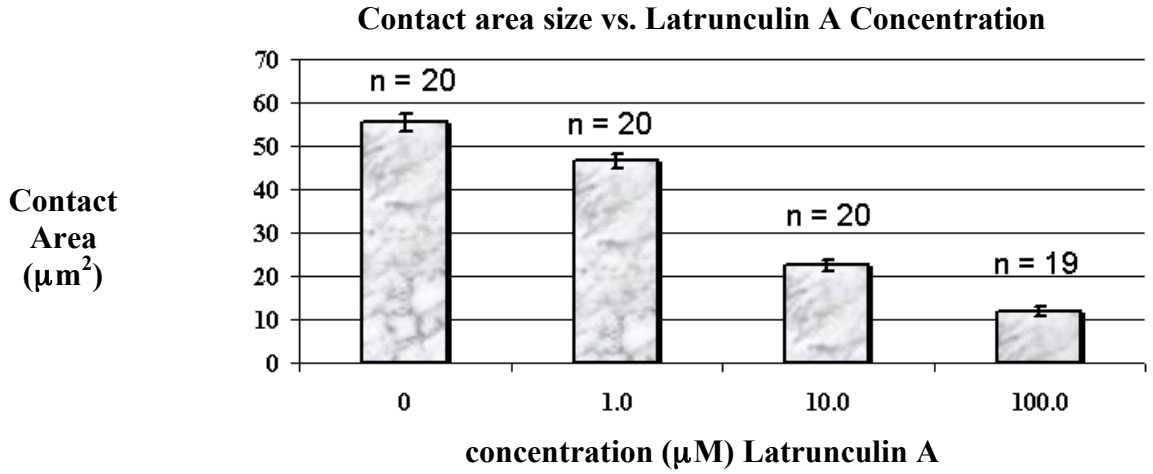

Figure 14 Latrunculin A treatment affects the contact area size

	Contact Area Formation
Positive Control	√
Blebbistatin	X

Figure 15 Blebbistatin inhibition abrogates contact area formation

Z-stack of fluorescently labeled SYK and PO4 three minutes into contact area formation.

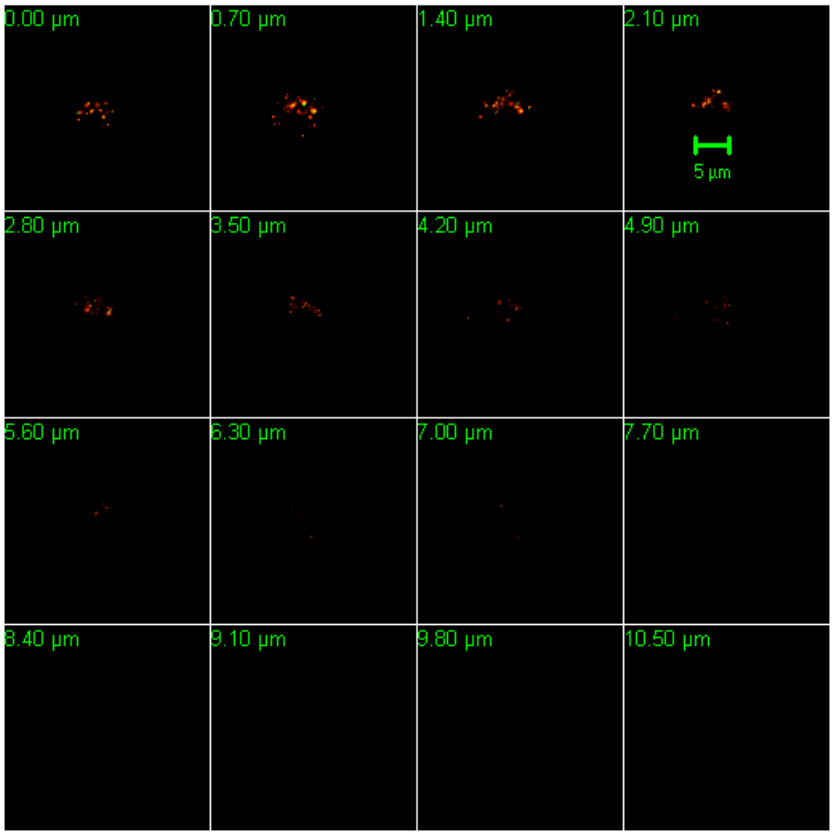

1° donkey anti-SYK IgG
2° FITC anti-donkey

1° mouse anti-PO4-Y
2°Alexa 647 anti-mouse IgG

Merged

3D profile view

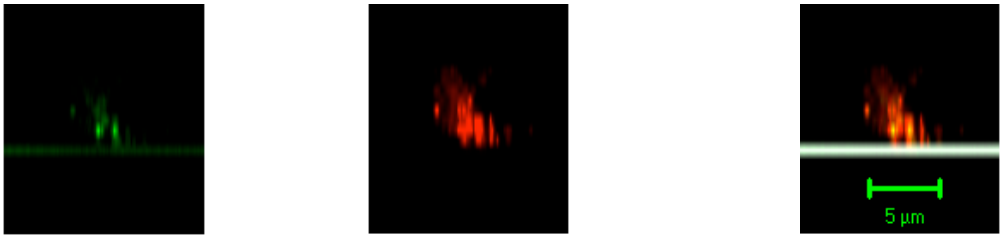

Figure 16 PO_4-Y and SYK three minutes into contact area formation

Z-stack of fluorescently labeled SYK and PO4 nine minutes into contact area formation.

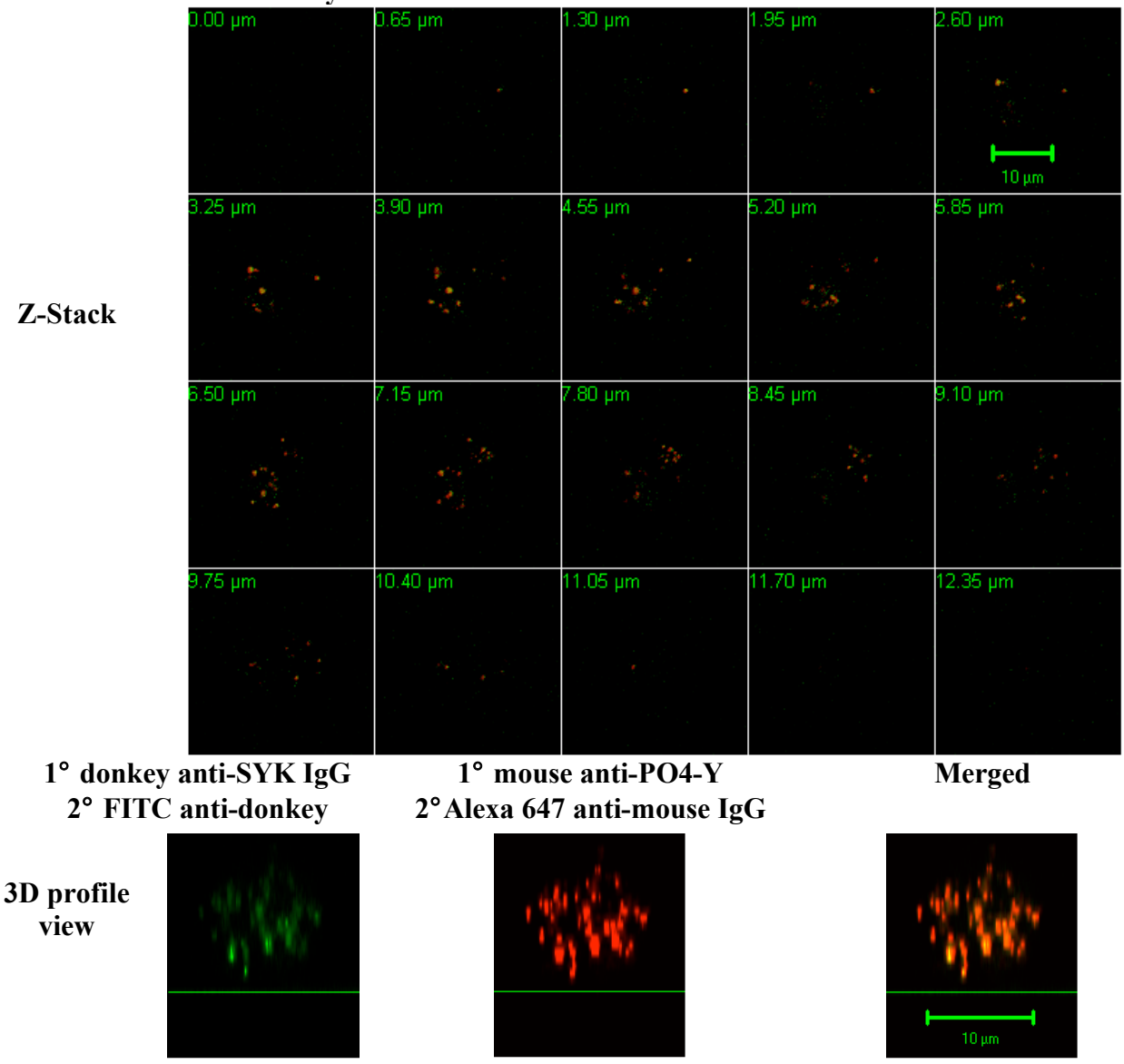

Figure 17 PO_4-Y and SYK nine minutes into contact area formation

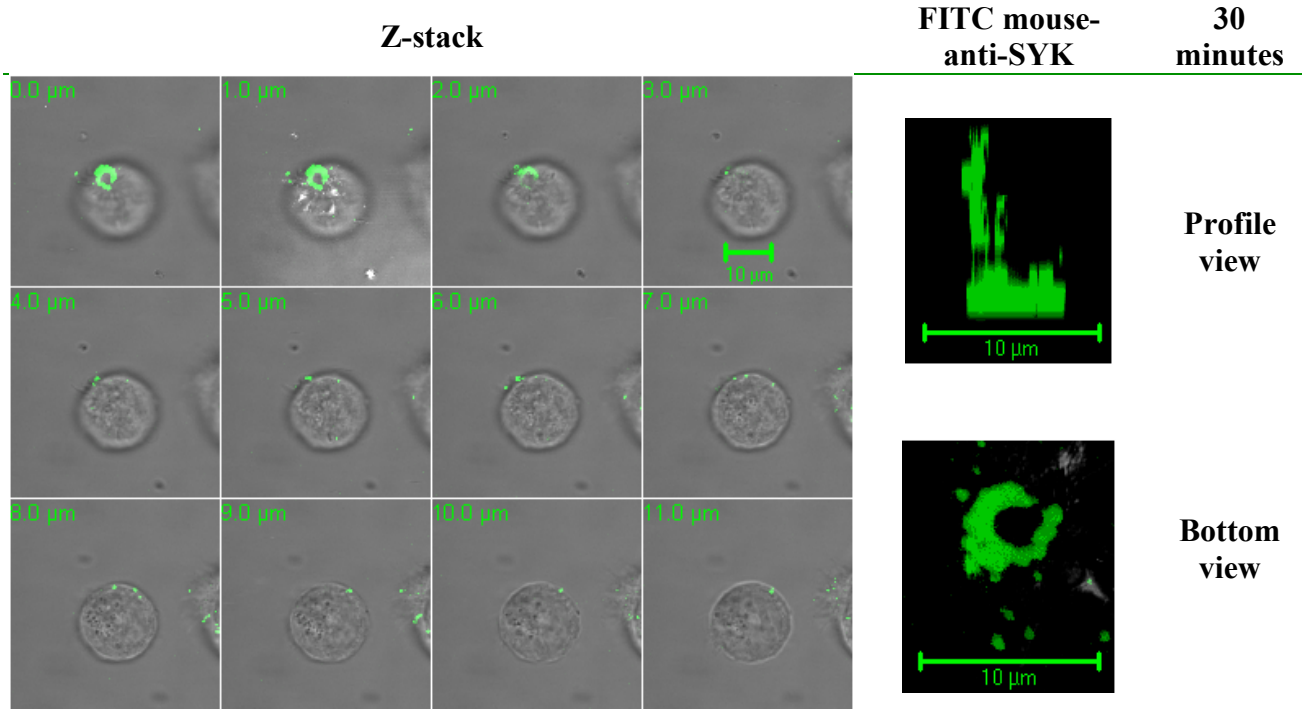

Figure 18 SYK thirty minutes into contact area formation

Z-stack	FITC mouse-anti-SYK	60 minutes
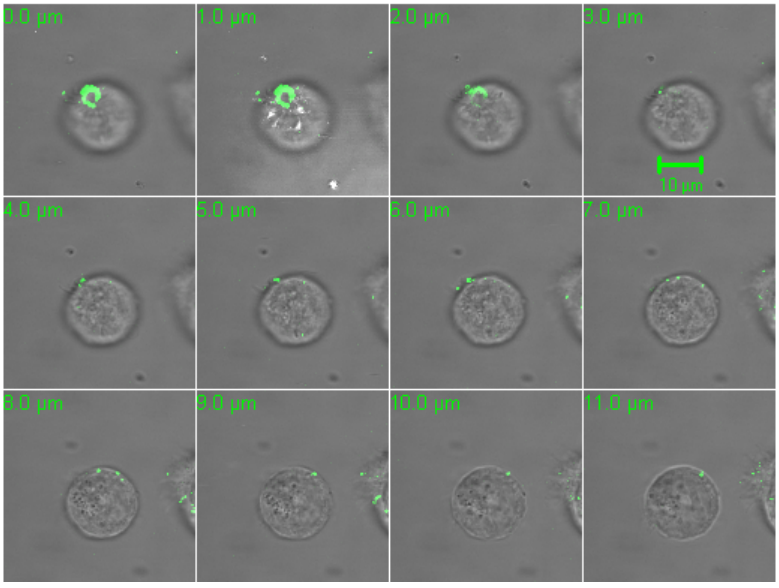	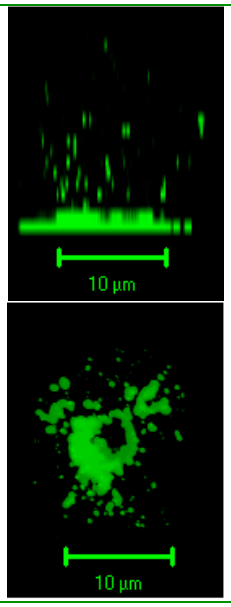	Profile view
		Bottom view

Figure 19 SYK sixty minutes into contact area formation

Z-stack of internalization of membrane rafts between fifteen and thirty minutes

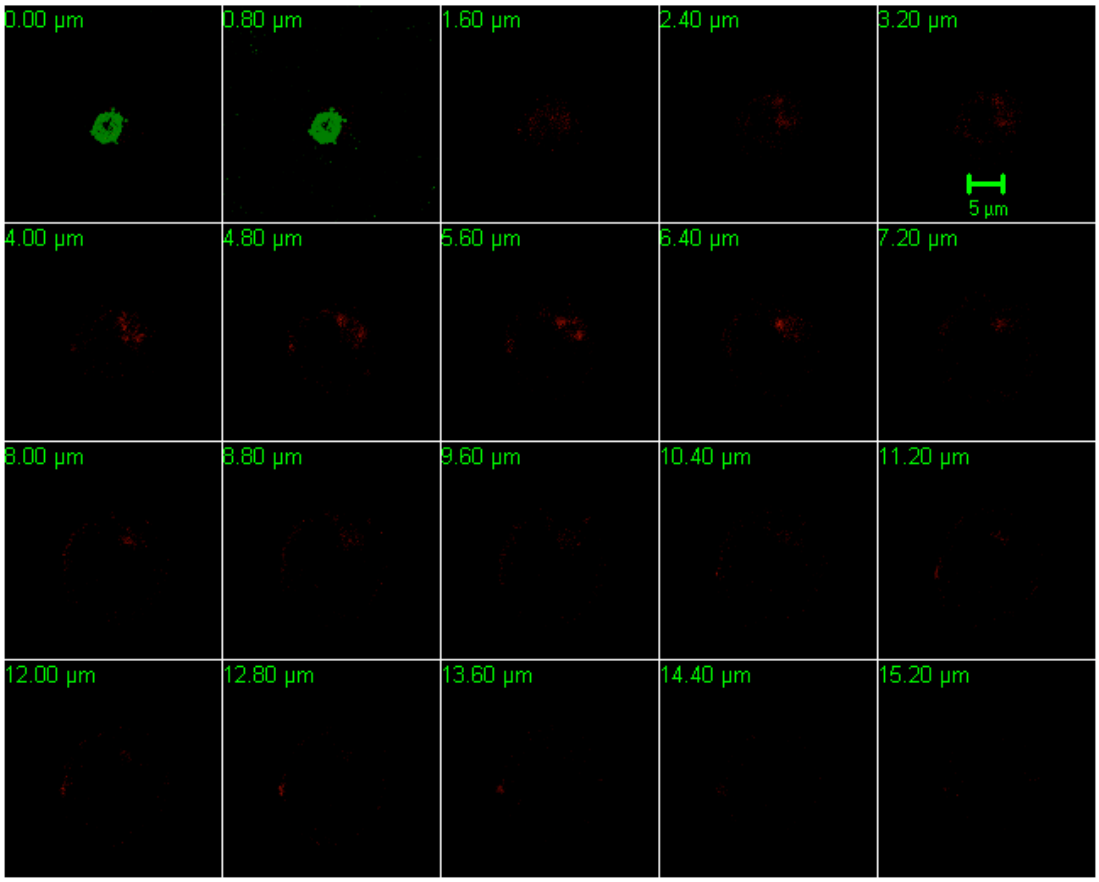

Alexa 488 anti-dnp IgG **Alexa 555 cholera toxin B** **Merged**

3D profile view

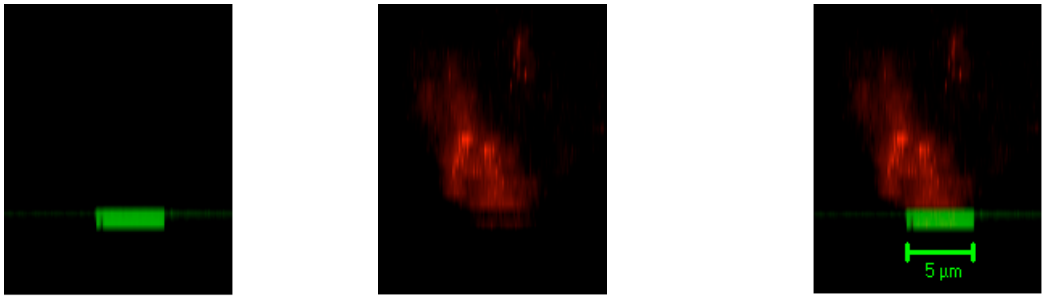

Figure 20 Internalization of membrane rafts between 15 to 30

Z-stack of Alexa 555 internalization of membrane rafts between thirty and sixty minutes

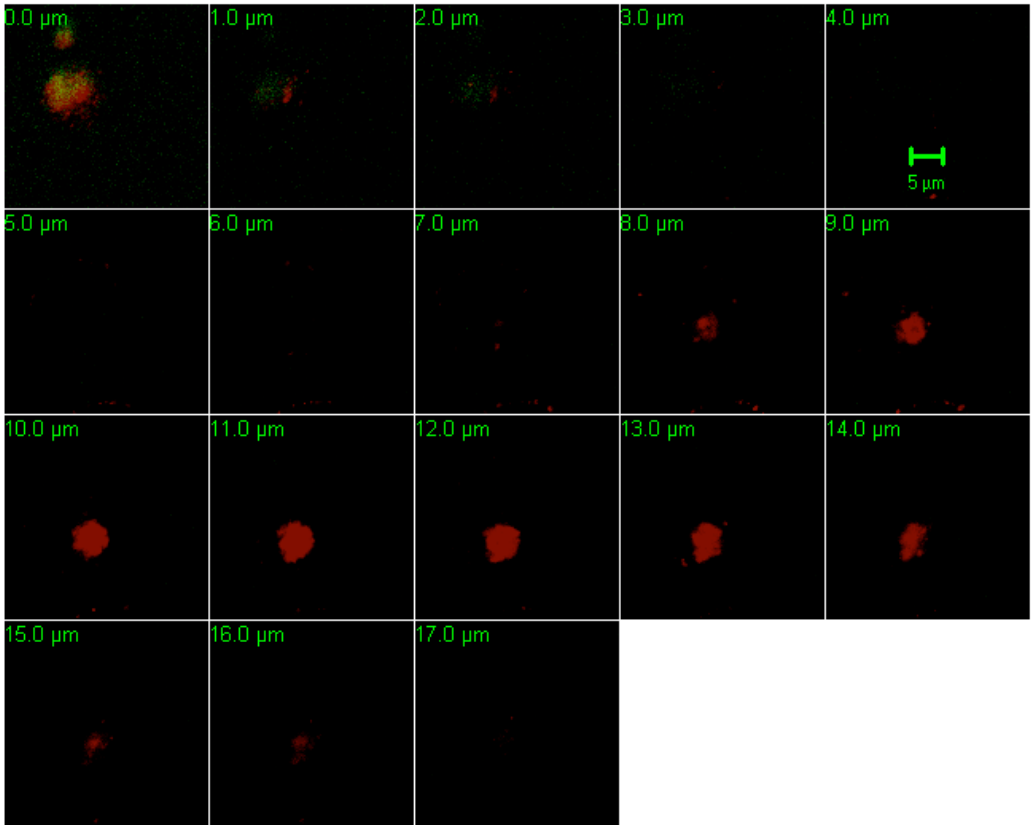

Alexa 488 anti-dnp IgG **Alexa 555 cholera toxin B** **Merged**

3D profile view

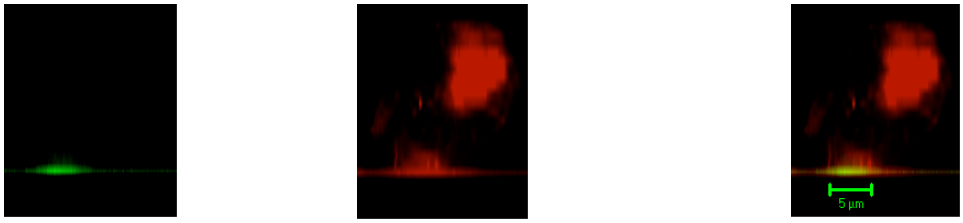

Figure 21 Internalization of membrane rafts between 45 to 60 minutes

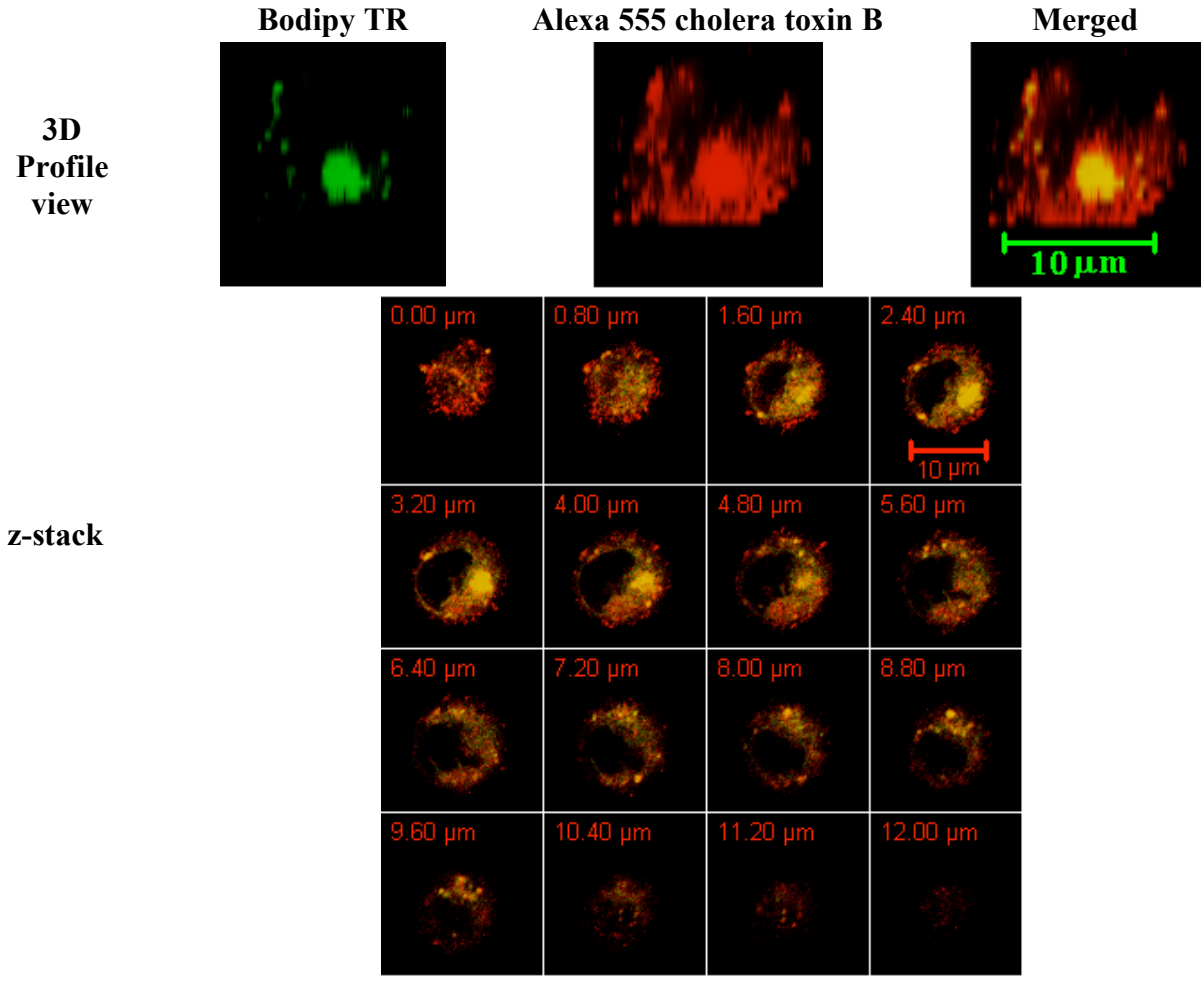

Figure 22 Membrane rafts colocalize with the Golgi complex

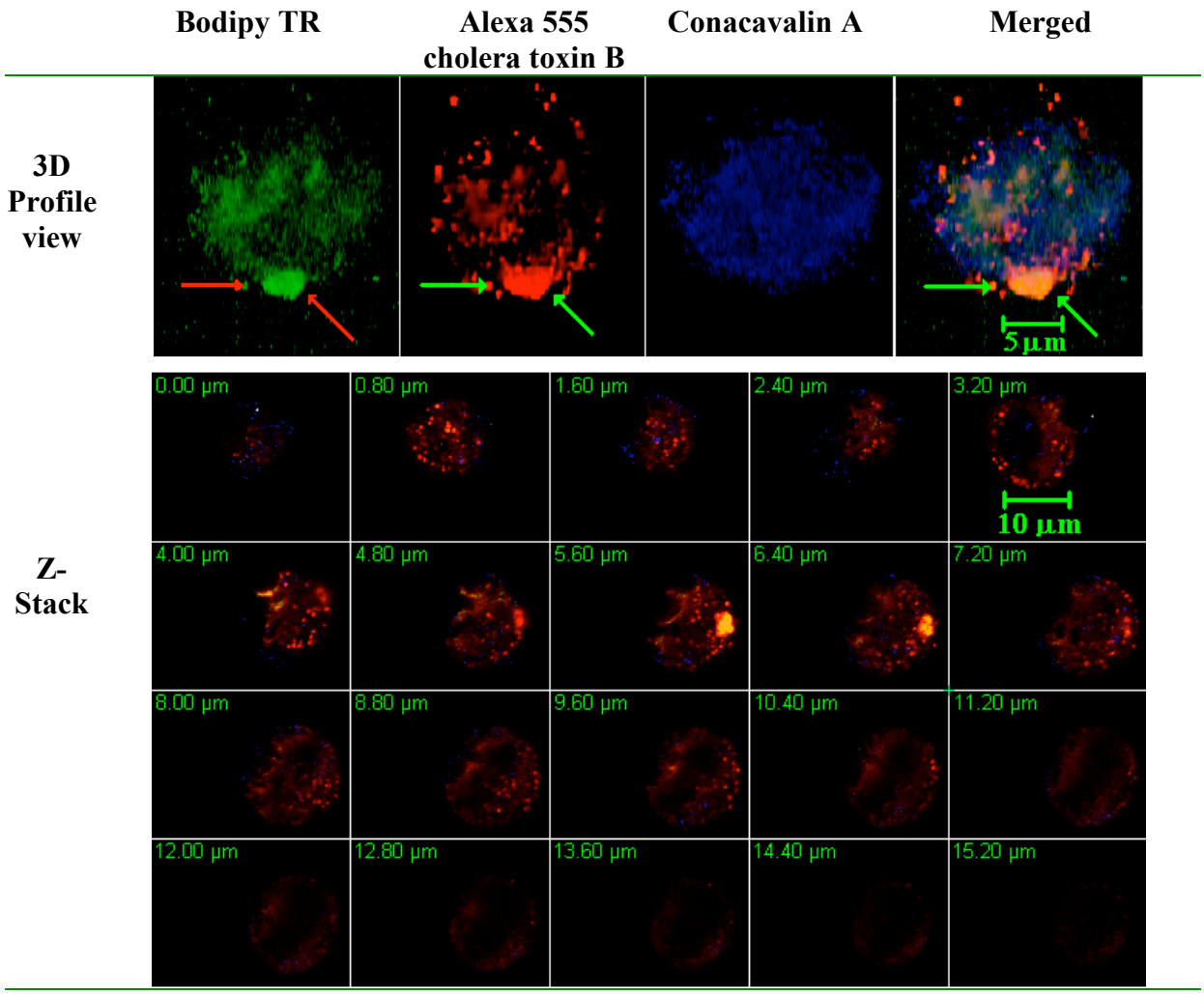

Figure 23 Membrane rafts colocalize with the Golgi but not with the ER

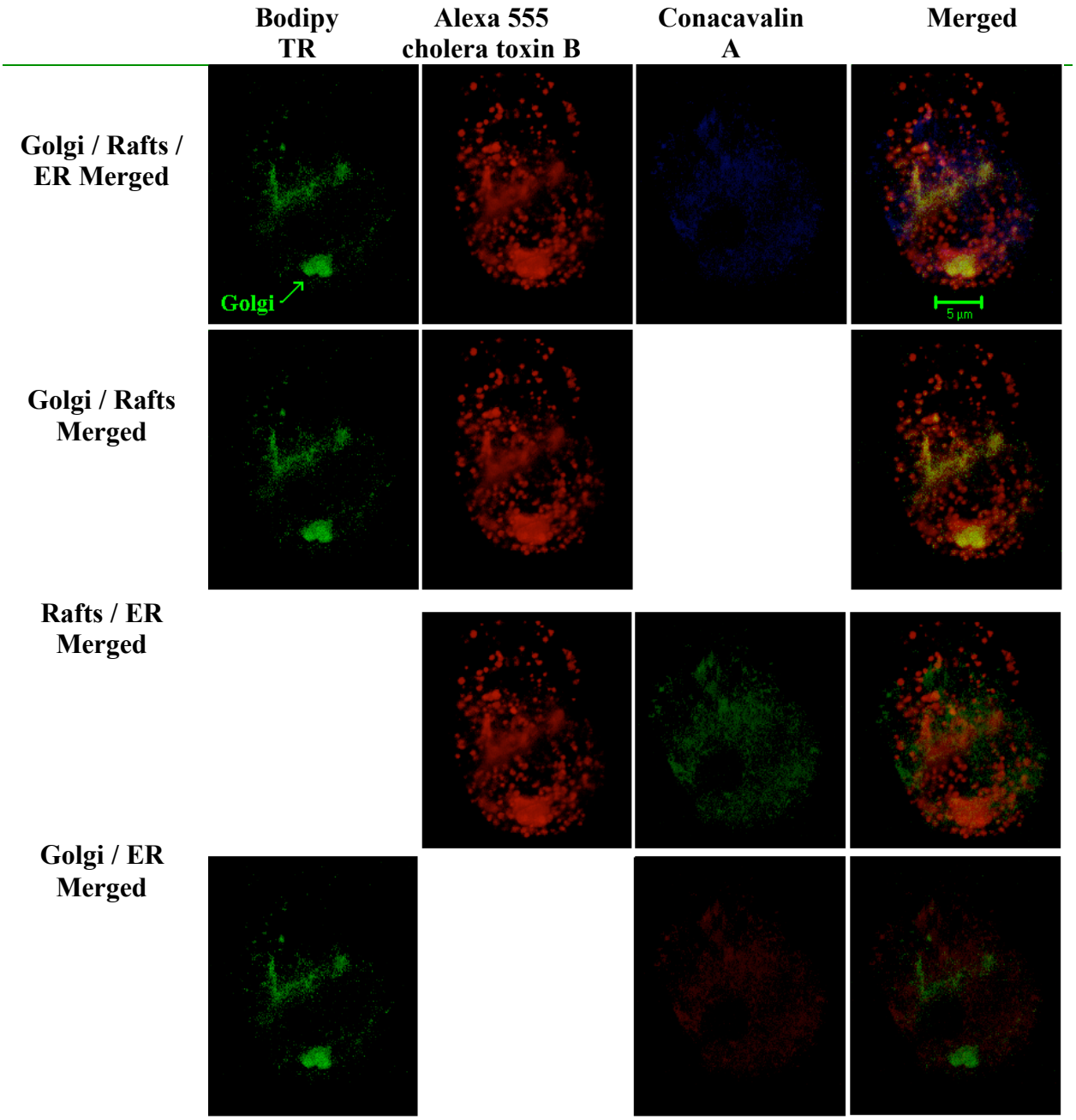

Figure 24 Colocalization exists between membrane rafts and the Golgi

Profile view

fluorescence only

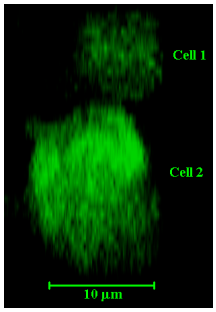

Z-stack of fluorescent and brightfield images

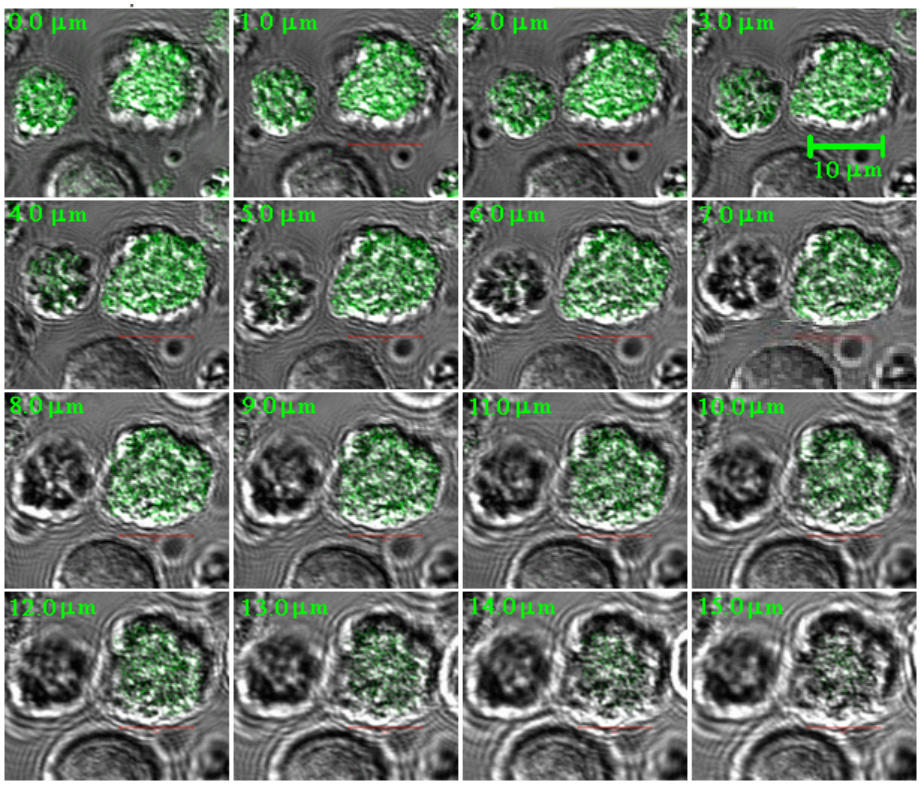

Figure 25 (+) Control – Phagocytosis of opsonized µ-spheres

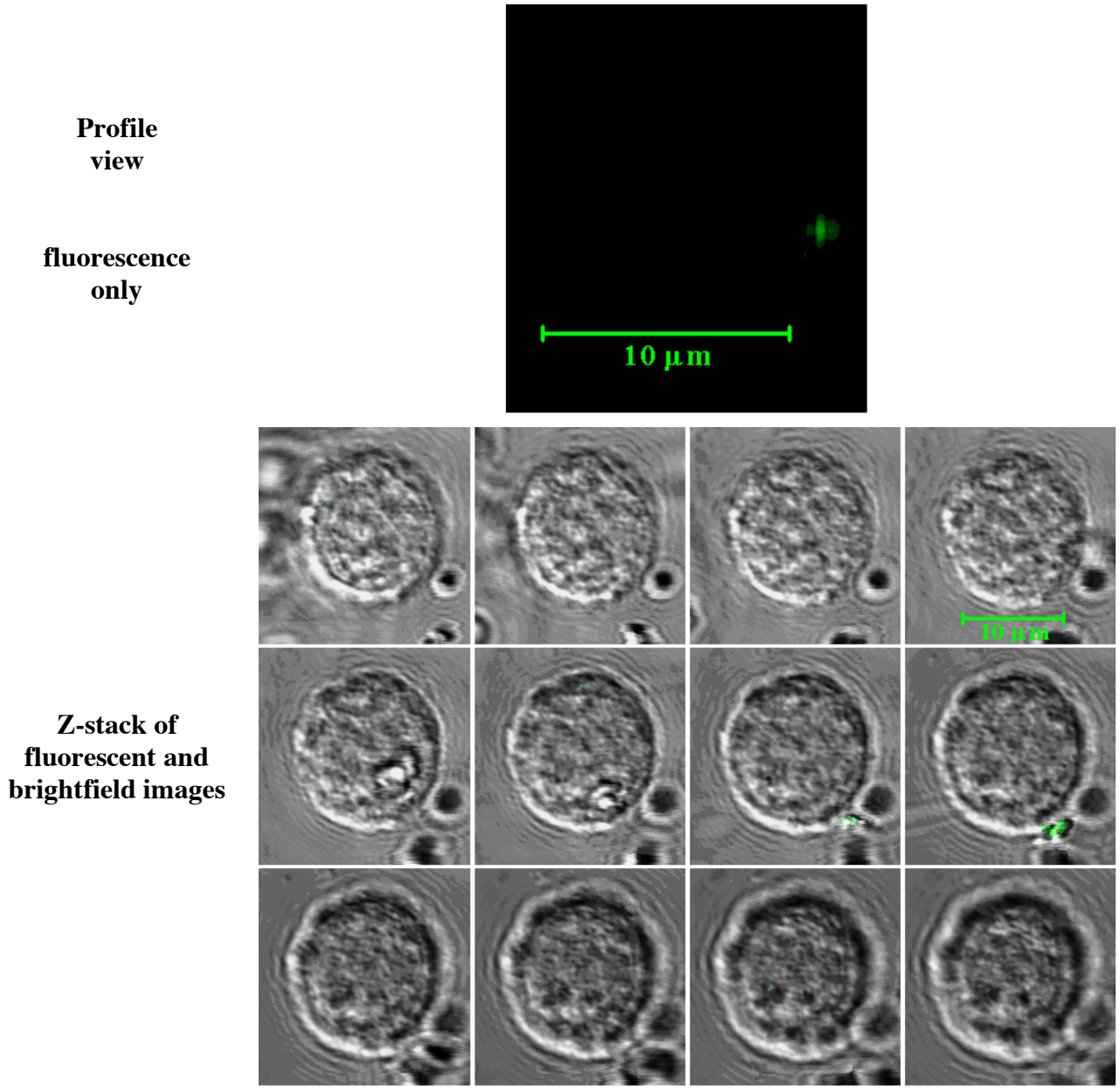

Figure 26 (-) control – Phagocytosis of non-opsonized µ-spheres

Profile view

fluorescence only

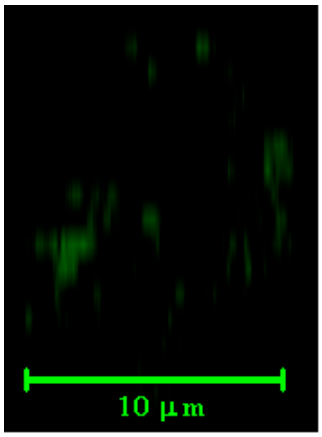

Z-stack of fluorescent and brightfield images

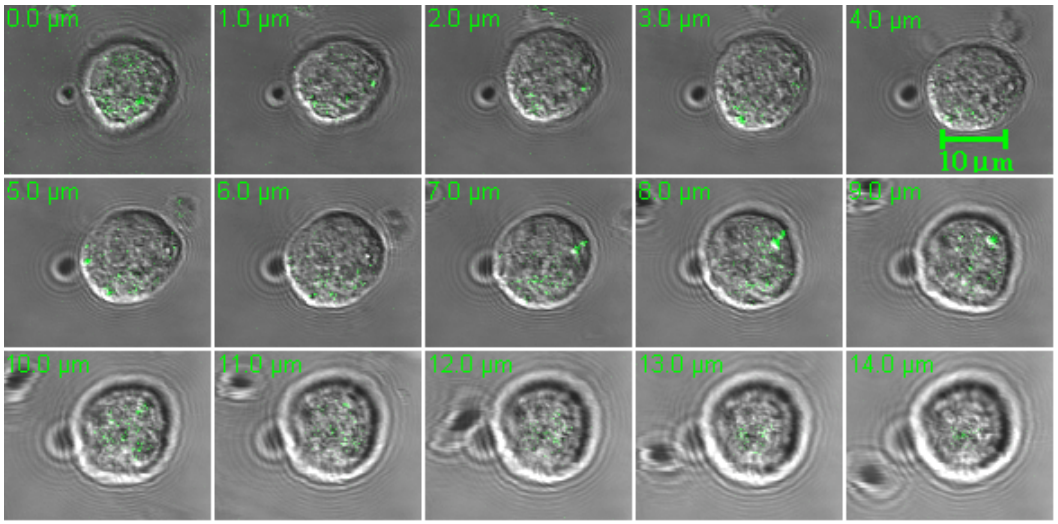

Figure 27 Phagocytosis of opsonized µ-spheres – Latrunculin A

Profile view

fluorescence only

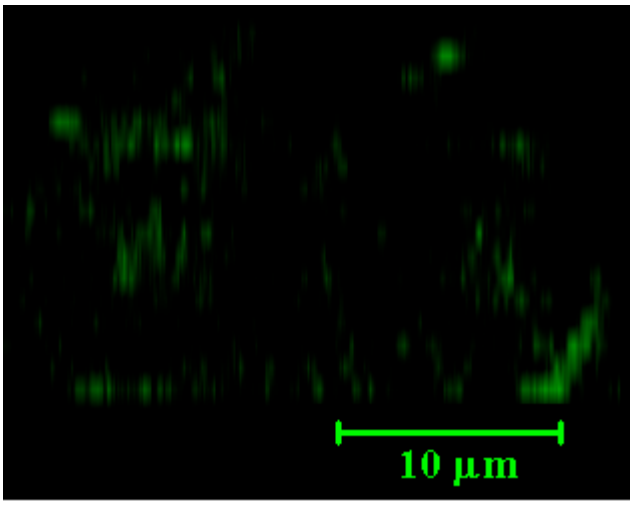

Z-stack of fluorescent and brightfield images

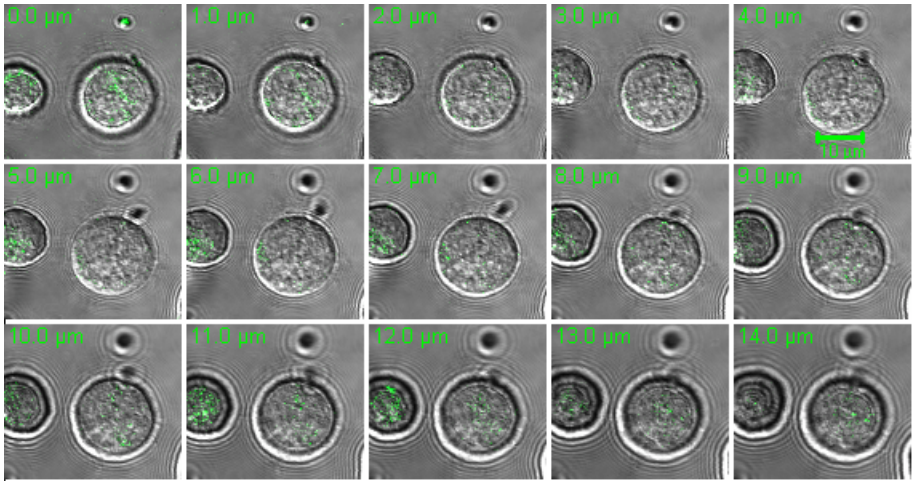

Figure 28 Phagocytosis of opsonized µ-spheres – cholesterol oxidase

Profile view

fluorescence only

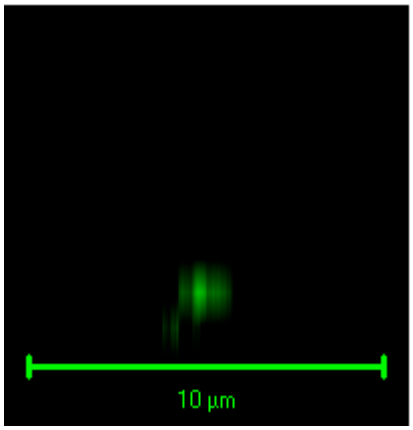

Z-stack

Fluorescence and brightfield

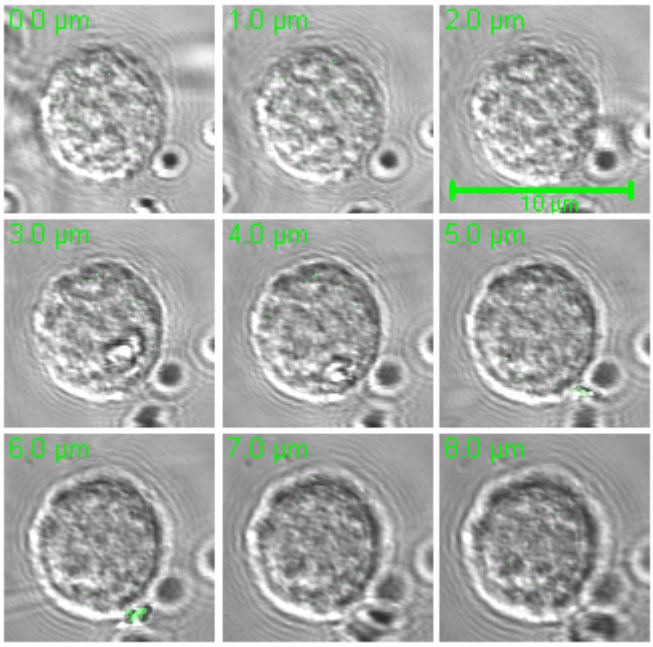

Figure 29 Phagocytosis of opsonized µ-spheres – Sphingomyelinase

Profile view

fluorescence only

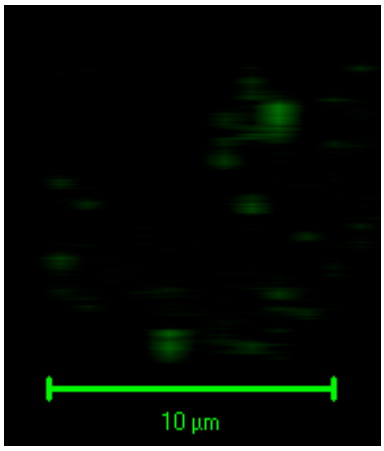

Z-stack

Fluorescence and Brightfield

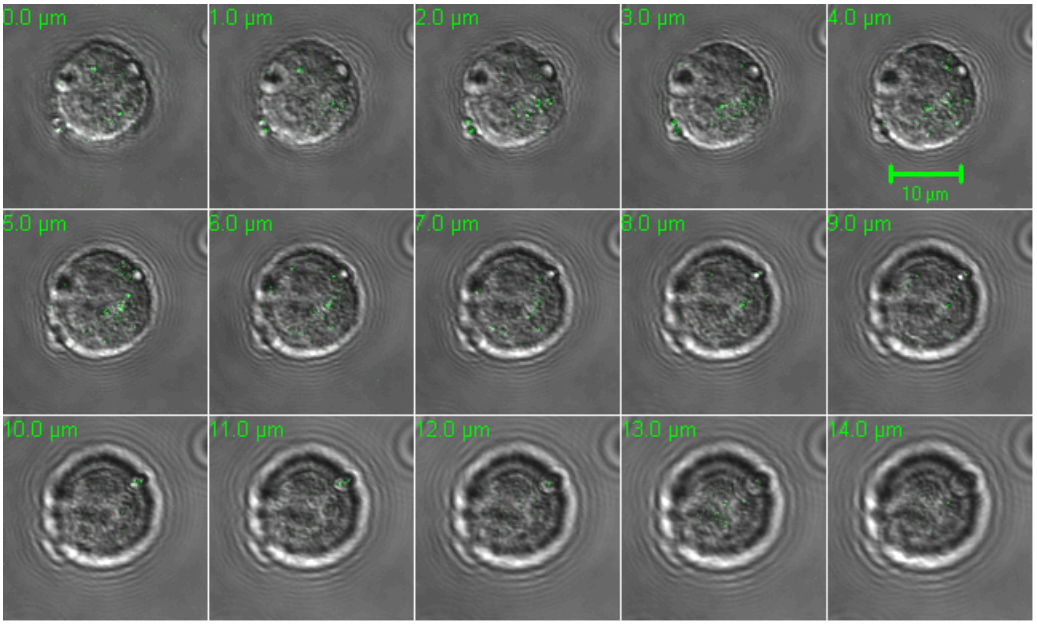

Figure 30 Phagocytosis of opsonized µ-spheres – PTK inhibitor